

DEVELOPMENT OF POLYACRYLAMIDE-CO-  
ACRYLIC ACID/ SODIUM CARBOXY METHYL  
CELLULOSE/ SODIUM SULFIDE POLYMER  
ELECTROLYTE FOR PHOTOVOLTAIC  
APPLICATIONS

BY

IRAJ ALAEI

A thesis submitted in fulfillment of the requirement for the  
degree of Doctor of Philosophy (Engineering)

Kulliyyah of Engineering  
International Islamic University Malaysia

MARCH 2022

## ABSTRACT

Today, the development of photovoltaic (PV) technology based on solar energy is vital to overcome the continuous depletion of fossil fuels which bring various environmental impacts particularly global warming and air pollution. The electrolyte of a PV cell is one of the most essential components. Highly efficient electrolyte is crucial for high-performance photovoltaic cell. Liquid electrolytes have yields to produce high efficiency cell over other types of electrolytes, however, it has drawbacks of leakage and corrosion with low volatility. To overcome these issues, solid electrolytes motivate us to undertake among the most promising candidates due to excellent chemical and physical stability, improved durability with wider operating temperature and stay steady. Therefore, this research was intended to develop a highly efficient solid electrolyte. In this study, a solid polymer electrolyte (P-Na-S) comprising poly(acrylamide-co-acrylic acid), sodium carboxymethylcellulose (Na-CMC), sodium sulfide (Na<sub>2</sub>S) blend has been fabricated by solution casting method. To fabricate solid polymer electrolytes containing of (P-Na-S), with and without ethylene carbonate (EC) as plasticizer. The concentration of Na<sub>2</sub>S was added with varied range from 10 to 50 wt.% salt. Electrochemical Impedance Spectroscopy (EIS) technique, FTIR and XRD were used to characterize electrical and optical properties. Consequently, polymeric plasticizer, ethylene carbonate (EC), was then added to the certain amount of (P-Na-S) to investigate the effect of the plasticizer on the electrolyte performance. The EC concentration was varied from 10 to 50 wt%. Based on the electrical conductivity measurement, the optimum electrolyte composition was found to be 30 wt.% Na<sub>2</sub>S salt and 40wt.% EC plasticizer. The highest conductivity of further salt was  $9.82 \times 10^{-7} \text{ Scm}^{-1}$  achieved at 30 wt.% Na<sub>2</sub>S. The addition of EC from 10 to 50 wt.% caused an increase in the conductivity from  $1.06 \times 10^{-6}$  at 10 wt.% EC to the maximum  $2.74 \pm 2.52 \times 10^{-4} \text{ Scm}^{-1}$  at 40wt% EC which signify (P-Na-S)-EC. From the impedance measurements, the lowest activation energy for the electrolyte without EC was 0.36 eV, which was estimated for the electrolyte of 30wt% Na<sub>2</sub>S. Meanwhile, for the electrolyte with 40wt% EC, a minimum activation energy dropped to 0.16 eV. This study gives a comprehensive description of electron transport through intramolecular circuits of covalent bonds and ionic compound from tunneling to thermally activated hopping. It exhibits that higher conductivity is associated with lower activation energy. FTIR measurements revealed that the peaks of the relevant functional groups shifted when the different concentrations of Na<sub>2</sub>S salt and EC were added, indicating chemical interactions among materials added. XRD analysis showed the polymer electrolyte improved largely the amorphous region when Na<sub>2</sub>S was added. However, the addition of EC increased again crystallinity. This work explores based on ion activities and movement of these electrolyte systems.

## خلاصة البحث

هذه الأيام يعد تطوير تقنيته الخلايا الكهروضوئية (PV) القائمة على الطاقة الشمسية أمراً مهماً للتغلب على لاستهلاك المستمر للوقود الأحفوري الذي يؤدي الى الاحتباس الحراري وتلوث الهواء. ويعتبر الألكتروليت في الخلية الكهروضوئية من المكونات الأساسية، وخاصةً النوعية ذو الكفاءة العالية تعتبر ضرورية للخلية الكهروضوئية عالية الاداء. وتتمتع الألكتروليتات السائلة بمزايا لإنتاج خلايا عالية الكفاءة مقارنةً بالأنواع الأخرى من الألكتروليتات، ولكن عيوبها التسريب والتآكل مع تقلبات منخفضة. للتغلب على هذه العيوب، الإلكتروليتات الصلبة تحفظنا على أخذ أكثر المرشحين الواعدين بناءً الاستقرار الكيميائي والفيزيائي الممتاز، والمتانة المحسنة مع درجة حرارة التشغيل الأوسع. يهدف هذا البحث لتطوير الألكتروليت الصلب ليصبح ذو كفاءة عالية. في هذه الدراسة، تم تصنيع إلكتروليت بوليمر كمادة صلبة (P-Na-S) مكون من البولي (حمض أكريلاميد-أكريليك مشترك)، وكربوكسي ميثيل سلولوز الصوديوم (Na-CMC)، وكبريتيد الصوديوم (Na<sub>2</sub>S)، مزيج تم تصنيعه باستخدام طريقة صب المحلول. لتصنيع إلكتروليتات بوليمر صلبة تحتوي على (P-Na-S)، مع أو بدون كربونات الإيثيلين (EC) كمادة ملدنة. تمت إضافة تركيز Na<sub>2</sub>S بنطاق متنوع من 10 إلى 50٪ من وزن ملح. وقد تم استخدام تقنية التحليل الطيفي للمقاومة الكهروكيميائية (EIS) و FTIR و XRD لتمييز الخواص الكهربائية والبصرية. نتيجة لذلك، قد تم إضافة الملدن البوليمري، كربونات الإيثيلين (EC)، إلى كمية معينة من (P-Na-S) (للتحقق من تأثير الملدن على أداء الإلكتروليت. تفاوت تركيز EC من 10 إلى 50٪ بالوزن. وبحسب قياس الموصلية الكهربائية، وجد أن التركيبة الأمتثل للإلكتروليت هي 30 بالوزن٪ ملح Na<sub>2</sub>S و 40٪ بالوزن من الملدنات EC. أعلى موصلية للملح الإضافي كانت  $9.82 \times 10^{-7} \text{ Scm}^{-1}$  حصلت عند 30 وزن٪ Na<sub>2</sub>S. وقد أدت إضافة EC من 10 إلى 50 بالوزن٪ إلى زيادة الموصلية من  $1.06 \times 10^{-6}$  عند 10 بالوزن٪ EC إلى الحد الأقصى  $2.74 \pm 2.52 \times 10^{-4} \text{ Scm}^{-1}$  عند 40٪ بالوزن EC مما يدل على (P-Na-S)-EC. أما بالنسبة للقياسات الممانعة، كانت أقل طاقة تنشيط للإلكتروليت بدون EC هي 0.36 فولت، والتي تم تقديرها للإلكتروليت بنسبة 30٪ بالوزن من Na<sub>2</sub>S. وفي الوقت نفسه، بالنسبة للإلكتروليت مع 40٪ بالوزن من EC، حيث انخفض الحد الأدنى من طاقة التنشيط إلى 0.16 eV. وتقدم هذه الدراسة وصفاً شاملاً لانتقال الإلكترون عبر الدوائر الجزيئية للروابط التساهمية والمركب الأيوني من النفق إلى التنقل المنشط حرارياً. يُظهر أن الموصلية العالية مرتبطة بانخفاض طاقة التنشيط. كشفت قياسات FTIR أن قمم المجموعات الوظيفية ذات الصلة قد تحولت عند إضافة تركيزات مختلفة من ملح Na<sub>2</sub>S و EC، مما يشير إلى التفاعلات الكيميائية بين المواد المضافة. وفي النهاية أظهر تحليل XRD أن إلكتروليت البوليمر تحسن إلى حد كبير المنطقة غير المتبلورة عند إضافة Na<sub>2</sub>S. ومع ذلك، فإن إضافة EC زادت مرة أخرى من التبلور. يستكشف بأن هذا العمل بناءً على الأنشطة الأيونية وحركة أنظمة الإلكتروليت هذه.

## APPROVAL PAGE

The thesis of Iraj Alaei has been approved by the following:

---

Iis Sopyan  
Supervisor



Mohd Lukman Inche Ibrahim  
Co-Supervisor

**DR. MOHD LUKMAN INCHE IBRAHIM**  
*ASSOC ASSISTANT PROFESSOR*  
Department of Science Engineering  
Kulliyah of Engineering  
International Islamic University Malaysia

---

Mohd Hamdi bin Ali Buraidah  
Field Supervisor 1

---

Yose Fachmi Buys  
Field-Supervisor 2

---

Muhd Zuazhan bin Yahya  
External Examiner



Abdul Maleque  
Internal Examiner

**DR. MD. ABDUL MALEQUE**  
*Professor*  
Department of Manufacturing and Materials Engineering  
Kulliyah of Engineering  
International Islamic University Malaysia

---

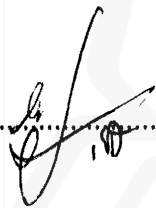
Ismail Hassanien Ahmed  
Chairman

## DECLARATION

I hereby declare that this thesis is the result of my own investigations, except where otherwise stated. I also declare that it has not been previously or concurrently submitted for any other degrees at IIUM or other institutions.

Iraj Alaei

Signature .....



Date .....

22/04/2022

**INTERNATIONAL ISLAMIC UNIVERSITY MALAYSIA**

**DECLARATION OF COPYRIGHT AND AFFIRMATION OF  
FAIR USE OF UNPUBLISHED RESEARCH**

**DEVELOPMENT OF POLYACRYLAMIDE-CO-ACRYLIC  
ACID/ SODIUM CARBOXYL METHYL CELLULOSE (NA-  
CMC)/ SODIUM SULPHIDE (NA<sub>2</sub>S) POLYMER  
ELECTROLYTE FOR PHOTOVOLTAIC APPLICATIONS**

I declare that the copyright holders of this thesis are jointly owned by the student and IIUM.

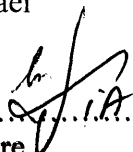
Copyright © 2022 (Iraj Alaei) and International Islamic University Malaysia. All rights reserved.

No part of this unpublished research may be reproduced, stored in a retrieval system, or transmitted, in any form or by any means, electronic, mechanical, photocopying, recording or otherwise without prior written permission of the copyright holder except as provided below.

1. Any material contained in or derived from this unpublished research may be used by others in their writing with due acknowledgement.
2. IIUM or its library will have the right to make and transmit copies (print or electronic) for institutional and academic purposes.
3. The IIUM library will have the right to make, store in a retrieved system and supply copies of this unpublished research if requested by other universities and research libraries.

By signing this form, I acknowledged that I have read and understand the IIUM Intellectual Property Right and Commercialization policy.

Affirmed by Iraj Alaei

.....  
Signature 

.....  
Date 22/04/2022

## ACKNOWLEDGEMENTS

*In the name of Allah, the Most Compassionate, the Most Merciful.*

I would like to express my utmost gratitude and thankfulness to Allah subhanahuta'ala for the shower of his blessing and mercies that I have successfully completed my research work. In particular, sincere appreciation and thanks to my thesis supervisor Professor Dr. Iis Sopyan his persistent guidance, patience and support throughout the project.

I wish to express my appreciation and thanks to my first Field-supervisor Dr. Mohd Hamdi bin Ali Buraidah from University Malaya (UM) who provided his time, effort, and support for this project.

I would be grateful to my second Field-supervisor Dr. Yose Fachmi Buys for his continuous support, encouragement and assistance throughout the project.

I would like also to thank Miss. Lee Yap Chen and Mr. Shahan Shah for their cooperation during experimental work at University Malaya.

Finally, I would like to express my appreciation to my family-members who are always behind the inspiration of my works.

## TABLE OF CONTENTS

Abstract.....	ii
Abstract in Arabic.....	iii
Approval Page.....	iv
Declaration.....	v
Copyright Page.....	vi
Acknowledgements.....	vii
List of Tables .....	x
List of Figures .....	xi
List of Abbreviations .....	xv
List of Symbols .....	xi
<b>CHAPTER ONE: INTRODUCTION.....</b>	<b>1</b>
1.1 Background .....	1
1.1.1 Operating principle of QDSSC .....	2
1.1.2 Electrolyte in QDSSC .....	3
1.2 Statement of The Problem.....	6
1.3 Research Philosophy.....	6
1.4 Research Objectives .....	7
1.5 The Scope of The Research .....	7
1.6 Research Methodology.....	8
1.7 Thesis Organization.....	10
<b>CHAPTER TWO: LITERATURE REVIEW.....</b>	<b>11</b>
2.1 Introduction .....	11
2.2 Quantum Dot Sensitized Solar Cells (QDSSCs).....	12
2.3 The Advantage of QDSSCs.....	13
2.4 The QDSSCs Mechanisim .....	14
2.5 Polymer electrolyte.....	19
2.6. Quantum dot sentisizer .....	24
2.7 Transparent Conducting Films (TCF) .....	24
2.7.1 The Working Electrode.....	25
2.7.2 The Counter Electrode.....	25
2.8 Selection materials for polymer electrolyte.....	25
2.8.1 Poly(acrylic amid- <i>co</i> -acrylic acid).....	26
2.8.2 Sodium Carboxymethyl Cellulose (Na-CMC).....	27
2.8.3 Sodium Sulfide (Na <sub>2</sub> S) Salt .....	28
2.9 Salt Concentration .....	29
2.10 Plasticizer .....	29
2.11 Summary.....	30
<b>CHAPTER THREE: METHODOLOGY.....</b>	<b>31</b>
3.1 Introduction .....	31
3.2 Materials .....	31
3.3 Polymer Electrolytes Preparation.....	32
3.3.1 poly(acrylamide- <i>co</i> -acrylic acid)/NaCMC/Na <sub>2</sub> S electrolyte .....	32



3.3.2 poly(acrylamide-co-acrylic acid)/NaCMC/Na <sub>2</sub> S/EC electrolyte..	33
3.4 Characterizations Polymer Electrolytes.....	35
3.4.1 Electrochemical Impedance Spectroscopy (EIS) .....	35
3.4.1.1 Ionic Conductivity Measurement .....	36
3.4.1.2 Ionic Conduction of Activation Energy Calculation .....	36
3.4.2 Fourier Transform Infrared Spectroscopy (FTIR) .....	36
3.4.3 X-ray diffraction (XRD) .....	37
3.5 Summary.....	43
<b>CHAPTER FOUR: RESULTS AND DISCUSSIONS.....</b>	<b>44</b>
4.1 Introduction .....	44
4.2 FTIR Spectroscopy.....	44
4.2.1 FTIR of poly(acrylamide-co-acrylic acid) Powder and Film .....	44
4.2.2 FTIR of (Na-CMC) Powder and Film .....	47
4.2.3 FTIR of Poly (AM-co-AA) and (Na-CMC) Film Formation .....	49
4.2.4 FTIR of (P-Na-S) with various Na <sub>2</sub> S salt Concentrations .....	50
4.2.5 FTIR of (P-Na-S) with various Na <sub>2</sub> S salt Concentrations .....	53
4.2.6 FTIR of (P-Na-S) with various Na <sub>2</sub> S salt Concentrations .....	55
4.3 Electrochemical Impedance Spectroscopy (EIS) .....	57
4.3.1 Activation Energy Measurement .....	57
4.3.2 FTIR of (P-Na-S) with various Na <sub>2</sub> S salt Concentrations .....	61
4.3.3 FTIR of (P-Na-S) with various Na <sub>2</sub> S salt Concentrations .....	67
4.3.3.1 Ionic Conductivity Measurement .....	67
4.3.3.2 Ionic Conduction of Activation Energy Calculation .....	69
4.4 Dielectric study of (P-Na-S) Electrolyte .....	71
4.4.1 Frequency of Dielectric Constant ( $\epsilon_r$ ) .....	71
4.4.2 Frequency Dependence of Loss Tangent ( $\tan\delta$ ) .....	76
4.4.3 AC Conductivity of Dielectric Properties .....	79
4.5 Dielectric Study Of (P-Na-S)-Ec Electrolyte .....	83
4.5.1 Frequency Dielectric constant ( $\epsilon_r$ ) at Selected Temperatures .....	84
4.5.2 Dielectric Loss Tangent ( $\tan\delta$ ) .....	88
4.5.3 Measurement of AC Conductivity of Dielectric Properties.....	93
4.6 XRD Pattern Without Salt, By Na <sub>2</sub> S And EC Plasticizer .....	97
4.7 Summary.....	100
<b>CHAPTER FIVE: CONCLUSION.....</b>	<b>101</b>
5.1 Conclusions .....	101
5.2 Recommendations .....	102
<b>REFERENCES.....</b>	<b>103</b>
<b>LIST OF PUBLICATIONS .....</b>	<b>119</b>

## LIST OF TABLES

Table 2.1	The polysulfide with different protocols component materials used	20
Table 2.2	Table of liquid electrolyte of QDSSC	21
Table 2.3	Table of solid electrolyte of QDSSC	23
Table 3.1	<b>Chemical structures of materials used in this work</b>	<b>31</b>
Table 3.2	Composition of materials used to prepare polymer electrolyte	33
Table 3.3	Polymer electrolytes prepared with fixed compositions and addition of ethylene carbonate (EC)	34
Table 4.1	poly(AM-co-AA) functional groups powder and film	46
Table 4.2	The functional groups and structural formula of Na-CMC	48
Table 4.3	The functional groups of the Poly (AM-co-AA) and Na-CMC film	50
Table 4.4	Functional groups of (P-Na-S) electrolyte with various Na <sub>2</sub> S	53
Table 4.5	The Functional group through various EC	55
Table 4.6	The conductivity of various salt concentration at room temperature	61
Table 4.7	The conductivity of various EC concentration at room temperature	66
Table 4.8	Activation energy of various salt concentration for the (P-Na-S) electrolyte	<b>68</b>
Table 4.9:	Shows via various EC comparison the conductivity with activation energy	70
Table 4.10	Activation energy and conductivity through of Na <sub>2</sub> S salt and EC plasticizer	70

## LIST OF FIGURES

Figure 1.1	Structure and mechanism of QDSSC	3
Figure 1.2	TiO <sub>2</sub> and CdS with electrolyte and platinum joined between two FTO substrates as a QDSSC cell	5
Figure 1.3	Flowchart of research methodology	9
Figure 2.1	Structure of QDSSC	15
Figure 2.2	The J-V curve plots of QDSSC	17
Figure 2.3	Chemical Formula of Acrylamide (AM) and Acrylic Acid (AA)	26
Figure 2.4	Chemical Formula Sodium Carboxymethyl Cellulose (Na-CMC)	27
Figure 2.5	Chemical Formula of Sodium Sulfide (Na <sub>2</sub> S) salt	28
Figure 3.1	The thin film layers were removed and cut into three sections for conductivity measurements	35
Figure 3.2	The slope gradient with Log $\sigma$ against 1/T	37
Figure 3.3	Definition of transmission	38
Figure 3.4	Construction of Michelson Interferometer	39
Figure 3.5	Relationship Between Spectrum and Interferogram	40
Figure 3.6	Deriving Bragg's Law: $n\lambda = 2d\sin\theta$	41
Figure 4.1	poly(AM-co-AA) powder and film characteristic peaks	45
Figure 4.2	FTIR spectra of Na-CMC powder and film	47
Figure 4.3	poly(AM-co-AA) and Na-CMC film FTIR spectra	49
Figure 4.4	FTIR spectrum of (P-Na-S) with various wt. % salts	52
Figure 4.5	The Cole-Cole plot show the bulk resistance $R_b$ of a 10% Na <sub>2</sub> S salt	55
Figure 4.6	The Cole-Cole plot show the bulk resistance $R_b$ of a 20% Na <sub>2</sub> S salt	57
Figure 4.7	The Cole-Cole plot show the bulk resistance $R_b$ of a 30% Na <sub>2</sub> S salt	58
Figure 4.8	The Cole-Cole plot show the bulk resistance $R_b$ of a 40% Na <sub>2</sub> S salt	58

Figure 4.9	The Cole-Cole plot show the bulk resistance $R_b$ of a 50% $\text{Na}_2\text{S}$ salt	59
Figure 4.10	The different conductivity by various wt.% $\text{Na}_2\text{S}$ salt shown at room temperature	59
Figure 4.11	Arrhenius plot containing various ( $\text{Na}_2\text{S}$ ) via $\ln \sigma$ versus $1000/T$ temperature	60
Figure 4.12	Frequency dependence of the dielectric constant ( $E_r$ ) with 10% salt of the electrolyte at different temperatures	62
Figure 4.13	Frequency dependence of the dielectric constant ( $E_r$ ) with 20% salt of the electrolyte at different temperatures	62
Figure 4.14	Frequency dependence of the dielectric constant ( $E_r$ ) with 30% salt of the electrolyte at different temperatures	63
Figure 4.15	Frequency dependence of the dielectric constant ( $E_r$ ) with 40% salt of the electrolyte at different temperatures	63
Figure 4.16	Frequency dependence of the dielectric constant ( $E_r$ ) with 50% salt of the electrolyte at different temperatures	64
Figure 4.17	Frequency dependence of dielectric constant ( $E_r$ ) via samples of (P-Na-S) polymer electrolyte at room temperature	65
Figure 4.18	The loss tangent ( $\tan \delta$ ) of (P-Na-S) electrolyte at 10 wt.% salt with preferred temperatures	68
Figure 4.19	The loss tangent ( $\tan \delta$ ) of (P-Na-S) electrolyte at 20 wt.% salt with preferred temperatures	69
Figure 4.20	The loss tangent ( $\tan \delta$ ) of (P-Na-S) electrolyte at 30 wt.% salt with preferred temperatures	72
Figure 4.21	The loss tangent ( $\tan \delta$ ) of (P-Na-S) electrolyte at 40 wt.% salt with preferred temperatures	72
Figure 4.22	The loss tangent ( $\tan \delta$ ) of (P-Na-S) electrolyte at 50 wt.% salt with preferred temperatures	73
Figure 4.23	The loss tangents ( $\tan \delta$ ) variation with frequency of (P-Na-S) electrolyte	73
Figure 4.24	Measurement of $\text{Log } \sigma_{a.c}$ by 10 wt.% salt of (P-Na-S) at selected temperature	74
Figure 4.25	Measurement of $\text{Log } \sigma_{a.c}$ by 20 wt.% salt of (P-Na-S) at selected temperature	75

Figure 4.26	Measurement of Log $\sigma_{a.c}$ by 30 wt.% salt of (P-Na-S) at selected temperature	76
Figure 4.27	Measurement of Log $\sigma_{a.c}$ by 40 wt.% salt of (P-Na-S) at selected temperature	77
Figure 4.28	Measurement of Log $\sigma_{a.c}$ by 50 wt.% salt of (P-Na-S) at selected temperature	77
Figure 4.29	Log ( $\omega$ ) conductivity with frequency spectra vs. Variation of log ( $\sigma_{a.c}$ ) of (P-Na-S) electrolyte	78
Figure 4.30	FTIR spectroscopy of (P-Na-S)-EC various plasticizers	78
Figure 4.31	The Cole-Cole plot illustrates the bulk resistance $R_b$ by 10 wt.% EC	79
Figure 4.32	The Cole-Cole plot illustrates the bulk resistance $R_b$ by 20 wt.% EC	80
Figure 4.33	The Cole-Cole plot illustrates the bulk resistance $R_b$ by 30 wt.% EC	80
Figure 4.34	The Cole-Cole plot illustrates the bulk resistance $R_b$ by 40 wt.% EC	81
Figure 4.35	The Cole-Cole plot illustrates the bulk resistance $R_b$ by 50 wt.% EC	81
Figure 4.36	The different conductivity by various wt.% EC shown at room temperature	82
Figure 4.37	Indicates the $\ln \sigma$ versus $1000/T$ graphs for various EC plasticizer	83
Figure 4.38	Dielectric constant's frequency ( $\log E_r$ ) by 10 wt. % EC plasticizers at preferred temperatures	85
Figure 4.39	Dielectric constant's frequency ( $\log E_r$ ) by 20 wt. % EC plasticizers at preferred temperatures	85
Figure 4.40	Dielectric constant's frequency ( $\log E_r$ ) by 30 wt. % EC plasticizers at preferred temperatures	86
Figure 4.41	Dielectric constant's frequency ( $\log E_r$ ) by 40 wt. % EC plasticizers at preferred temperatures	86
Figure 4.42	Dielectric constant's frequency ( $\log E_r$ ) by 50 wt. % EC plasticizers at preferred temperatures	87
Figure 4.43	Dielectric constants of frequency ( $\log E_r$ ) dependence using different EC plasticizers	88

Figure 4.44	The tangent loss's ( $\tan \delta$ ) frequency for polymer blend by 10 wt. % EC plasticizers	89
Figure 4.45	The tangent loss's ( $\tan \delta$ ) frequency for polymer blend by 20 wt. % EC plasticizers	90
Figure 4.46	The tangent loss's ( $\tan \delta$ ) frequency for polymer blend by 30 wt. % EC plasticizers	90
Figure 4.47	The tangent loss's ( $\tan \delta$ ) frequency for polymer blend by 40 wt. % EC plasticizers	91
Figure 4.48	The tangent loss's ( $\tan \delta$ ) frequency for polymer blend by 50 wt. % EC plasticizers	91
Figure 4.49	Frequency dependence of loss tangent ( $\tan \delta$ ) electrolytes membrane at room temperature with various EC	92
Figure 4.50	Spectra conductivity of polymer electrolyte (P-Na-S) by 10 wt. % EC at preferred temperatures	93
Figure 4.51	Spectra conductivity of polymer electrolyte (P-Na-S) by 20 wt. % EC at preferred temperatures	94
Figure 4.52	Spectra conductivity of polymer electrolyte (P-Na-S) by 30 wt. % EC at preferred temperatures	
Figure 4.53	Spectra conductivity of polymer electrolyte (P-Na-S) by 40 wt. % EC at preferred temperatures	94
Figure 4.54	Spectra conductivity of polymer electrolyte (P-Na-S) by 50 wt. % EC at preferred temperatures	95
Figure 4.55	Conductivity spectra of polymer electrolyte by different EC	96
Figure 4.56	Shows polymer with Poly (AM-co-AA) and Na-CMC without $\text{Na}_2\text{S}$ salt	97
Figure 4.57	Shows polymer with Poly (AM-co-AA) and Na-CMC by 30 wt.% $\text{Na}_2\text{S}$ salt	98
Figure 4.58	Indicates XRD diffraction for 40 wt. % EC	99

## LIST OF SYMBOLS

$D_n$	Diffusion coefficient
$E_a$	Activation energy
$e^-$	Electron
$E_f$	Fermi energy
$J_{sc}$	Short-circuit current density
$\eta$	Efficiency
$h\nu$	Photon energy
$I_{MPP}$	Current at the Maximum Power Point
$I_{SC}$	Short-Circuit Current
$P_{light}$	Power of the incident light
$P_{MAX}$	Power at the Maximum Power Point
$R_b$	Bulk resistance
$S$	Sensitizer
$V_{MPP}$	Voltage at the Maximum Power Point
$V_{OC}$	Open-Circuit Voltage

# CHAPTER ONE

## INTRODUCTION

### 1.1 BACKGROUND

Nowadays, the use of non-renewable energy sources of fossil fuel such as oil, coal, and natural gas has led to critical environmental concern worldwide, including greenhouse effect and air pollution. Researchers predicted the primary energy source is facing a rapid depletion. Therefore, an introduction of renewable energy source such as hydroelectric, wind-power, and solar energy became essential. Among renewable energy sources, solar energy has several benefits as it is free, clean, and environment friendly. Solar energy can be converted into electricity using photovoltaic cells.

Photovoltaic system converts light energy directly into electricity by utilizing semiconductor materials. Semiconductors achieved electrical conductivity by combining p-type and n-type semiconductor materials to form a p-n junction. The p-type semiconductor produces holes that can accept electrons, and it is referred as the electron acceptor. Similarly, the n-type semiconductor material doped with an impurity atom to create free negative charge electron is considered as the electron donors. It brought into an interface between the p-type and the n-type regions called as p-n junction semiconductor materials. The semiconductor free charge carrier (electron-hole pairs) generates electrons from the valence band to the conduction band by exciton in a p-n junction.

Solar cells come in three different technical generations. Crystal silicon (c-Si) used in the phase of first generation includes mono-crystalline silicon (mono-Si) and



polycrystalline (multi-Si) materials fabricated in thick and rigid semiconductor devices, making it high cost. Amorphous silicon (a-Si), cadmium Telluride (CdTe), and copper-indium-gallium-di-selenide (CIGS) are the second-generation solar cells and appear as thin film solar cells. Organic photovoltaic cells (OPVs), dye sensitized solar cells (DSSCs), and quantum-dot sensitised solar cells (QDSSCs) are among the third generation low-cost, thin-film solar cells (Semonin et al., 2012).

The advantages of quantum dot sensitized solar cells are light harvesting materials with tuneable structure band gap in QD semiconductors, which can reduce light scattering effect and improve long-term stability through size and composition control (Wu et al., 2019). There are four main features of QDSSC including (i) wide band gap semiconductor of  $\text{TiO}_2$  coat on a glass substrate that act as photo-anode, (ii) QD semiconductor absorbed  $\text{TiO}_2$  to act as a sensitizer, (iii) an electrolyte with (vi) a counter electrode. (Surana & Mehra, 2018).

### **1.1.1 Operating Principle of QDSSC**

When cell illuminated, light is captured by QD semiconductor to create electron-hole pairs (excitons). Excited electron state with superior energy injects into the conduction band of  $\text{TiO}_2$ . Conductor glass that coated by  $\text{TiO}_2$  allows charge transfer to external cell where electron through outer circuit travel to the counter electrode. The counter electrode's function is to make electrons possible to get across the outer circuit to the cell, while the redox couple act as a hole scavenger to regenerate the ground state energy level of QD. Then electrons continue to flow in to the counter electrode in outer circuit (Wu et al., 2015). A general illustration of a QDSSC and its operation mechanism is presented in Figure 1.1.

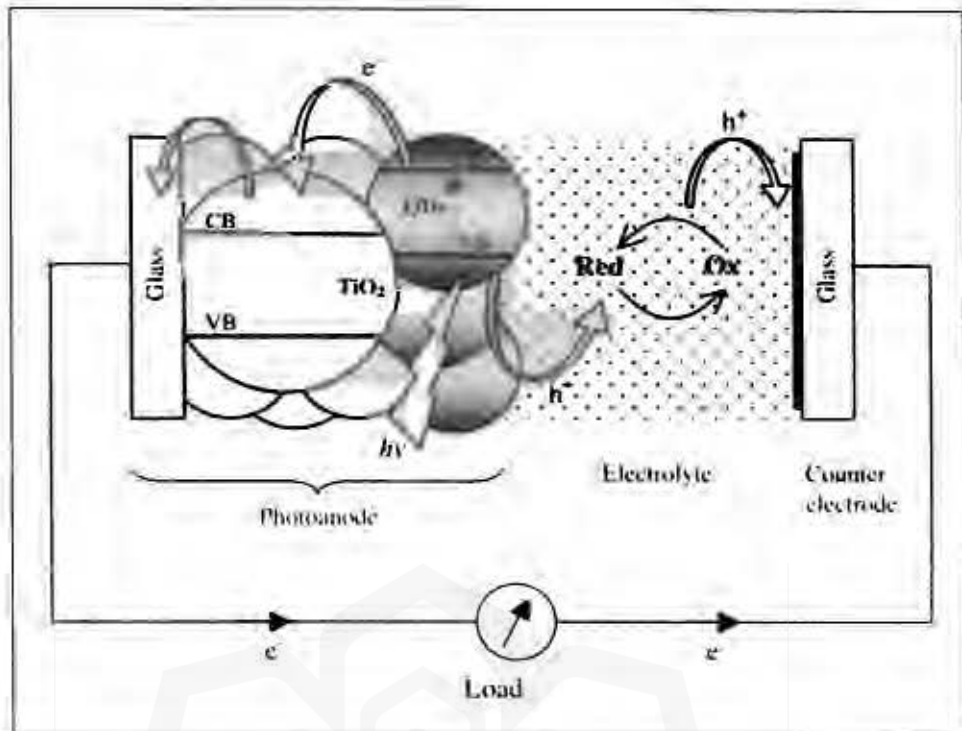


Figure 1.1: Structure and mechanism of QDSSC (Jun, Careem, & Arof, 2013)

### 1.1.2 Electrolyte in QDSSC

A candidate for electrochemical devices is the conductive polymer electrolytes. Studies on development of materials for electrolyte application for high performance QDSSC is essential. Cost-effective polymer electrolyte has been developed to improve QDSSC efficiency (Duan et al., 2015; Duan et al., 2014). Polymers are frequently used as the host in solid polymer electrolytes (SPEs) since they exhibit high room temperature ionic conductivity of approximately  $10^{-3}$  S.cm. Some polymers have been investigated for its applicability in QDSSC, including poly(vinylidene fluoride-co-hexafluoropropylene) (PVdF-co-HFP) (Selvakumar et al., 2016), polyacrylonitrile (PAN) (Sikkanthar et al., 2016), and poly(vinyl chloride) (PVC) (Deraman, Mohamed, & Subban, 2014).

Meanwhile, due to high water absorption and rapid copolymerization, the poly(acrylamide-*co*-acrylic acid) is often selected as the monomer base for polymeric electrolyte materials. It is a water-soluble polymer that can trap large water loads due to its hydrophilic polymer chains (Kumaran et al., 2018), as it displays strong electrical and transport properties, Na-CMC is also used as a host polymer for electrolytes (Mingsukang et al, 2017).

To produce a new material with specific physical properties, researchers are currently focusing not only on one polymer as a host but also two or three blended polymers. In this research, the solid composite polymer electrolyte modifies the polysulphide redox reaction. The electrolyte consists ideally of poly (acrylamide-*co*-acrylic acid) and Sodium-carboxylic-methylcellulose (Na-CMC) mixing ratios according to the optimum Sodium sulfide (Na<sub>2</sub>S) concentrations and compositions of the supporting electrolyte (Trausel et al., 2014). The present challenge, however, is to blend poly(AM-*co*-AA) / Na-CMC/ Na<sub>2</sub>S as a functional unit of ionic conductive electrolytes to investigate electrical and chemical properties for the QDSSC.

While electrolytes as liquids produce high conductivity in many energy devices compared to solids electrolyte (Dissanayake, 2006), solid electrolyte have the benefits of preventing leakage and degradation of electrolyte. Therefore, with a new workable approach for QDSSC, we chose solid polymer electrolyte to make a solid polysulphide redox pair. Chemical symbols or abbreviations used with three letters of (P-Na-S) indicates the electrolyte of the polymer mixture is found as an integral part of the structure formation QDSSC: FTO- (TiO<sub>2</sub>-CdS)/(P-Na-S)-Pt-FTO thin film PV module. The design of the assembled QDSSC cell containing an electrolyte is shown in Figure 1.2. The electrolyte for QDSSC applications, however, is the focus of this work.

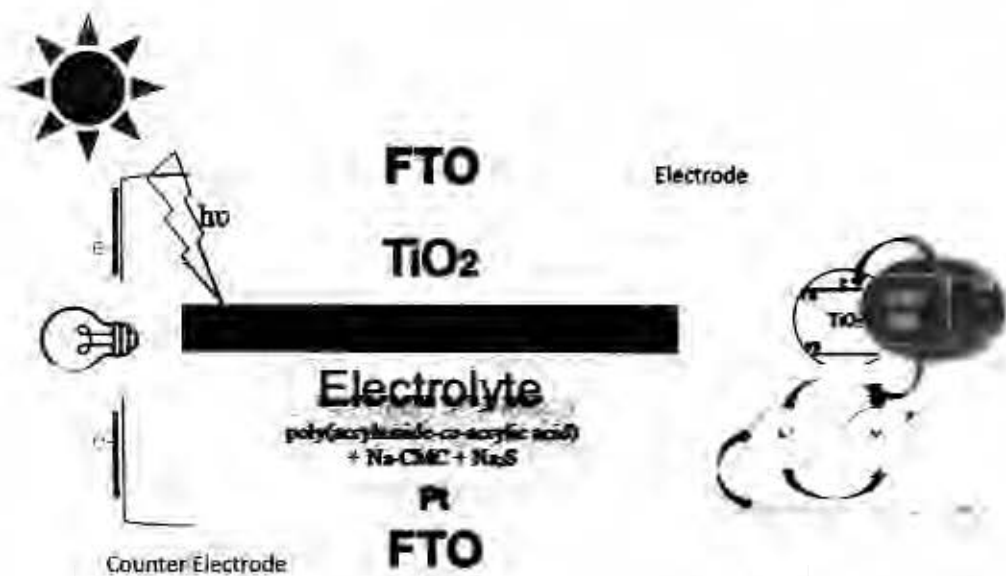


Figure 1.2:  $\text{TiO}_2$  and CdS with electrolyte and platinum joined between two FTO substrates as a QDSSC cell

## 1.2 PROBLEM STATEMENT

Redox electrolytes significantly influence both the efficiency and stability of QDSSCs. It is a medium which transfers charges between counter electrodes and photoanodes for the regeneration of oxidized QDs. QDSSC needs for certain electrolytes with a redox couple. The redox couple stimulate the sensitized oxidation to provide the electron. Unfortunately, materials for electrolyte/ redox system that could be used in QDSSC are limited. The electrolyte plays a key operational efficiency for the QDSSCs performance (Lee & Chang, 2008). The QDSSC based on the iodide electrolyte have been introduced for the first time, but it yields a poor conversion efficiency (Lee & Chang, 2008). Meanwhile, Diguna et al, gained an efficiency of 2.7% only with  $\text{Na}_2\text{S}$  liquid electrolyte (Diguna et al, 2007). However, conventional liquid electrolytes possess several disadvantages such as leakages of corrosive solvent and electrolytic degradation of electrolyte. Poor long-term stability due to the evaporation as well as low safety performance because of using the flammable organic solvent (Ramesh et al., 2011 and

Yang et al., 2008). Other drawbacks are low operating temperature range (-15 to 60), difficulty in handling and manufacturing due to the presence of liquid phase in the electrolytes. Therefore, the researchers came up with a brilliant idea to replace the conventional liquid electrolytes that is solid state electrolytes. Conductive solid polymer electrolytes (SPEs) were firstly prepared by Wright (1975). Apart from high safety performances, solid electrolytes possess some other advantages. These advantages are negligible vapor pressure, high energy density and operating temperature range (-40 to 150), photochemical and chemical stabilities. The most promising candidates are solid electrolyte. The major downside, however, is less effective due to charge transfer, hindering suitable application. The solid polymer electrolyte based on sodium sulfide ( $\text{Na}_2\text{S}$ ) with its ionic properties introduced by (Friedrich, 1914) inspires us to embark on a systematic study of how to make an electrolyte function properly in this project. This sodium sulfide salt is then blended with poly(acrylamide-*co*-acrylic acid) and sodium-carboxy methyl cellulose (Na-CMC) to make an electrolyte. The electrolyte composition play an important role on the efficiency of QDSSC cells. There is no study reported in the literature on this kind of electrolyte.

### **1.3 RESEARCH PHILOSOPHY**

The solar cell mechanism can be divided into three processes: charge generation, charge separation, and charge transportation. Charge separation and charge transportation efficiencies need to be improved to enhance the solar cell performances. The aim of this research is to build a thin-film solid polymer electrolyte for QDSSC. This cell has the same working principle as dye sensitized solar cell (DSSC). The dye component of DSSC is replaced by cadmium sulfide (CdS) sensitized into titanium dioxide ( $\text{TiO}_2$ ) in QDSSC system. The objective of the research is to fabricate a polymer blend with new

technique to enhance the photovoltaic performance of QDSSC. Thus, the present approach is used to study the effect of various amounts of the salt on the ionic conductivity of the solid composite polymer electrolyte comprising poly(acrylamide-*co*-acrylic acid) and sodium carboxy methyl cellulose (Na-CMC) based sodium sulfide ( $\text{Na}_2\text{S}$ ). As a result, we adopt the novel approach and method with different blend materials to develop a redox couple of polysulfide to improve the conductivity of electrolyte into the QDSSC applications.

#### **1.4 RESEARCH OBJECTIVES**

The following are the research objectives:

- i. To fabricate solid polymer electrolytes consisting of poly(AM-*co*-AA), Na-CMC, and sodium sulfide ( $\text{Na}_2\text{S}$ ), with and without ethylene carbonate (EC) as plasticizer.
- ii. To characterize the optical and electrical properties of poly(AM-*co*-AA)/Na-CMC based electrolyte.
- iii. Analysis the ionic conductivity of both electrolytes.

#### **1.5 THE SCOPE OF THE STUDY**

Fabrication of ionic solid polymer electrolyte using poly(acrylamide-*co*-acrylic acid) and sodium carboxy methyl cellulous (Na-CMC) based on sodium sulfide ( $\text{Na}_2\text{S}$ ) blends, as well as electrical conductivity optimization, is the focus of this research project. Then, various amount of ethylene carbonate (EC) additive is added to increase the conductivity of polymer composites. Lastly, characterize with Electrochemical Impedance Spectroscopy (EIS), Frontier Transform Infrared (FTIR), and X-Ray diffraction (XRD).

## 1.6 RESEARCH METHODOLOGY

The developments of solid polymer electrolytes (SPE) makes with poly(acrylamide-*co*-acrylic acid) and sodium carboxy methyl cellulous (Na-CMC) with ratio 1:9 and various sodium sulfides ( $\text{Na}_2\text{S}$ ) salt from 10 to 50 % which represents with (P-Na-S) at the beginning and characterize by EIS, FTIR and XRD to optimize through ionic electrical conductivity measurements and evaluations. Then, enhance the improved electrolyte with variation of Ethylene carbonate (EC) plasticizer from 10 to 50 % which represents with (P-Na-S)-EC to increase the conductivity and elucidate with identical equipment's to appraise of ionic electrical conductivity measurements. Ultimately, explore the values for both solid polymer electrolytes conductivity with and without plasticizers. The details are shown step by step in two main divisions with flow diagram in Figure 1.3.

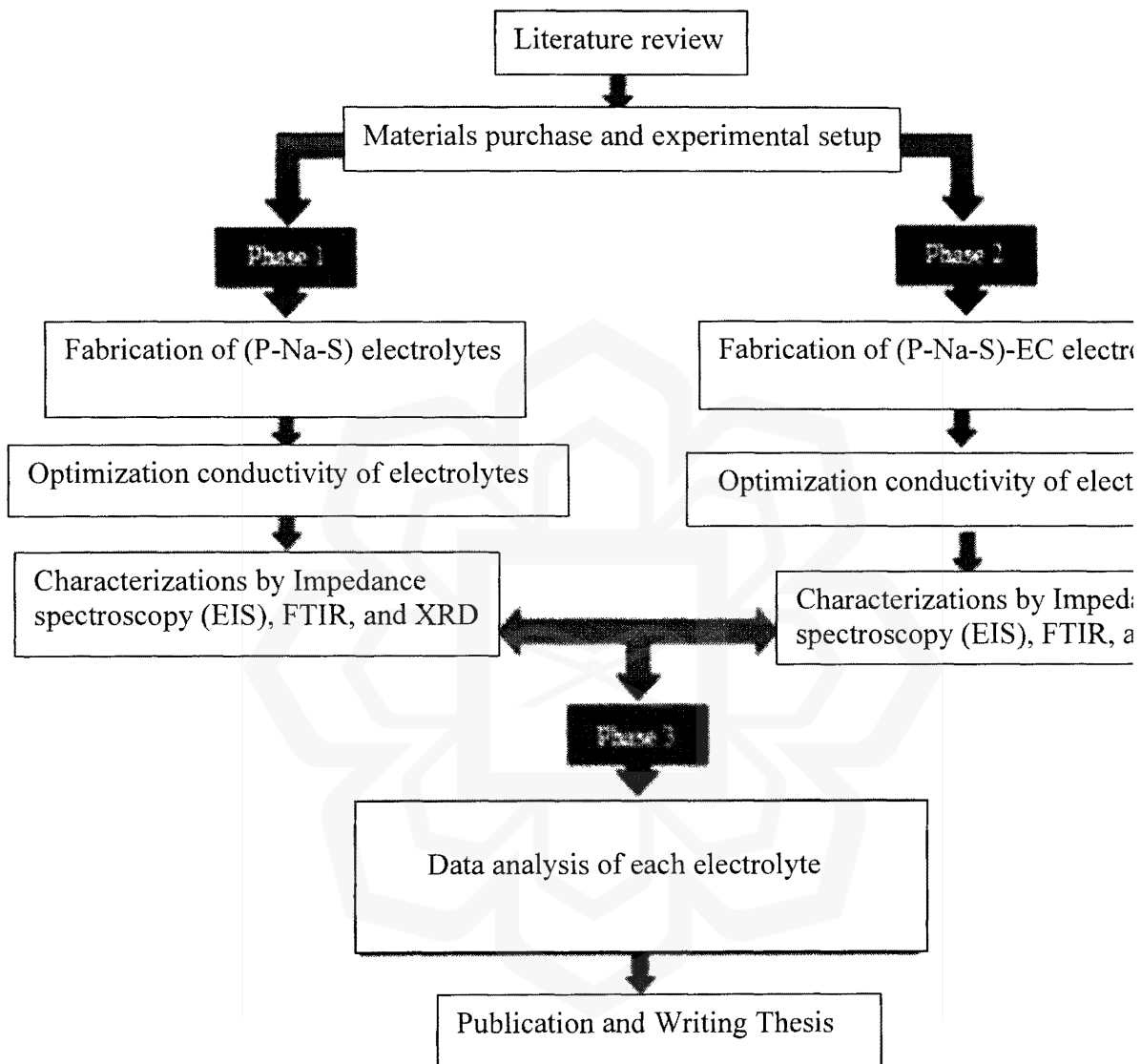


Figure 1.3: Diagram of Methodology



## **1.7 ORGANIZATION OF THE THESIS**

Chapter One presents an overview the energy sources and further alternatives of the renewable energy source, which leads research to the solar energy consumption that came to the photovoltaic technology. Chapter Two present of the literature review through mechanism and advantages principles of QDSSCs with the solid polymer electrolyte (SPE). Chapter Three explained the research method with materials selection for electrolytes and characterization technique with the Fourier transform infrared spectroscopy (FTIR), X-ray diffraction spectroscopy, and Electrochemical impedance spectroscopy (EIS). Chapter Four contains the results and discussion on synthesis and characterization of SPE polymer (P-Na-S) electrolyte base on Na<sub>2</sub>S. Chapter Five presents the effects of the addition EC plasticizer on electrolyte based on ethylene carbonate (EC) on the performance of electrolyte. Chapter Six presents the overall results and discussions on both the electrolytes with and without EC. Finally, Chapter Seven present the conclusion.

# **CHAPTER TWO**

## **LITERATURE REVIEW**

### **2.1 INTRODUCTION**

A major part of the green living society involves the use of alternative energy sources to replace our consumption of traditional fossil-fuel generated electricity. One of alternative energy can be generated by solar cell, which has become an increasingly popular way to power residential and commercial structures. Solar cell is derived directly from the sun's natural light and its use is both environmentally friendly and cost effective over the long term. Scientists believe one year energy of the sun onto our planet earth is ten thousand time more than the universal energy consumed in the year. Moreover, 1% of the sun merely produces energy from solar cells, which can be sufficient for the energy supply of the universal population. The conversion of solar light into electricity is currently a promising renewable source potential that has been established by photovoltaic (PV) technology. It converts visible light (photons) into electricity (voltage) that is direct current (DC). Photovoltaic cells are an integral part of solar electric energy systems, which are becoming increasingly significant as alternative sources of utility power.

For the first time, in 1839, French scientist Alexander Becquerel explored a PV system. Ten decades later, however, researchers understand the actual method of using sunlight to create an electrical voltage with PV materials (Grätzel, 2001). Through the light radiation, the electron in the solar cell absorbs energy from the doped semiconductor molecules, extracting it to create electron-hole pairs and transfer electron (B. Li, Wang, Kang, Wang, & Qiu, 2006). PV cell is a system that transfer light into electricity when exposed to light by generating current at the inner combination of two semiconductor materials.

Meanwhile, PV has been furniture for powering satellites in galaxy in the mid-twentieth century (Bosi & Pelosi, 2007), cathode shield (Kharzi, Haddadi, & Malek, 2006), telecommunications (Johnson, Billigmeier, & Lieb, 2005), motioning systems (Al-Busaidi, 2005), distant utility-connection, housing and industrial construction (Chow, He, & Ji, 2006). As the price of tools decreases and the cost of fossil fuels is rising, PV use is increasing worldwide (Nguyen & Lehman, 2008).

Three generations of solar cell devices exist in the market. The first generation is crystalline silicon. The second generation is called thin-coating inorganic layers, which is made of low-cost materials, namely crystal, stainless steel, and polymers; the examples of these substances are copper indium selenide ( $\text{CuInSe}_2$ ), cadmium telluride ( $\text{CdTe}$ ), amorphous silicon (a-Si) and copper indium gallium selenide (CIGS). The third generation is known as Dye-sensitized solar cell (DSSC), Quantum dot solar cells (QDSSC), and PV polymers. The great competition in photovoltaic equipment generates novel materials to improve optical and electrical production features in high-performance and low-cost PV cells.

Our main research work is focused on the development of materials and their successful application on Quantum dot sensitized solar cells (QDSSC). For the operation of a QDSSC, a good electrolyte with a redox mediator is required. Therefore, the electrolyte chosen has played a major role in determining the QDSSCs' performance.

## **2.2 QUANTUM DOT SENSITISED SOLAR CELL (QDSSC)**

The dye-sensitized solar cells with inorganic ruthenium known as a dye developed in 1990 were initially cheap and the most compatible solar cells offered (M. Wang et al., 2010). Then, from DSSC, numerous studies have moved on to the development of different dyes for PV cells. These studies apply organic and inorganic dyes for DSSC (Buraidah et

al., 2011; Hagberg et al., 2008). Due to its important Opto-electronics properties, investigators moved the application of DSSC to the quantum dot (QD) by modifying the dye (R Vogel, Hoyer, & Weller, 2002; Ralf Vogel, Pohl, & Weller, 1990). Quantum dot sensitized solar cells (QDSSC) are fabricated via following four steps - a mesoporous  $\text{TiO}_2$  layer upon supporting substrate acting as a photoanode, Quantum dots attached upon  $\text{TiO}_2$  layer playing role of sensitizer, an electrolyte with redox couple and a platinum coated counter electrode. QDs are nano-scale semiconductors based on physical and chemical properties that are not independent of size in characteristics materials. QDs are remarkably, such as energy spectrum tenability, small radiation scale, proper photo-stabilization, wide-range excitation scale, and high co-efficient of absorption with multiple excitations (González-Pedro et al., 2010; Kamat, 2008).

Cadmium chalcogenide from  $\text{Cd}_x$  ( $x = \text{S, Se or Te}$ ) QDs concentrated more on QDSSC research many years ago. This identifies  $\text{Cd}_x$  capable of absorbing an effective photon including a large energy gap of roughly 1.3 eV with an energy gap range of 2.25 eV, 1.73 eV and 1.49 for CdS, CdSe and CdTe, respectively (Peter, 2011). With QD altering scale, and band gap can be better tuned to a preferred option of energy gap. As a result, the physical and chemical dimensions of  $\text{Cd}_x$  QD for research applications need to be comprehend.

### **2.3 ADVANTAGES OF QDSSC**

The quantum dot solar cell (QDSSC) is absorber material is quantum dots. The QD hybrid polymer QD, Schottky junction cell, hetero-junction QD, rainbow solar cell-based, QD solar cell co-sensitized QD and dye, and solar cell sensitized QD (QDSSC) are all example of QD process-based structures (Kamat, 2008).

Meanwhile, the QDSSC configuration approach has recently emerged as a significant PV cell effect. The fundamental working principle of QDs as sensitizers is

like that of DSSC dye particles (Kamat, 2008), which can absorb a broad range of wavelengths in electromagnetic (EM) waves. QDs have a unique mechanism that allows for easy material processing (Loiudice et al., 2014), inexpensive (Tang et al., 2011), elasticity and high absorption in the making of the cell. Increases quantum performance by wide intrinsic dipole moments account for quick and efficient charge separation to add their coefficients, band gap tenability via size power, and multiple exciton generation (MEG) (Cheng et al., 2016) could be a promising option for Si cells.

## 2.4 THE QDSSC MECHANISM

Process and operational for potential efficient applications can be given to clarify the mechanisms of different photo-sensitization processes. Dyes and quantum dots (QDs) are sensitized to two kinds of photovoltaic (PV) cells third generation, the former being the abbreviated (DSSC) dye-sensitized solar cell. The latter is known as the quantum dot sensitized (QDSSC). The DSSC and QDSSC have three main components.

The photo-anode is the part where either the dye's molecules or the quantum dots (QDs) absorb light. The sensitizers are connected to the surface of the semiconductor (usually  $\text{TiO}_2$ ) surface. For fast electron transfer, the conduction band (CB) of the semiconducting material should be at a lower level than the lowest unoccupied molecular orbital (LUMO) of the dye molecules or QDs conduction band.

With a similar framework, QDSSC's working mechanism is like DSSC, as shown in Figure 2.1. Electrons are moved from the working electrode to the counter electrode through an external circuit. As the charge carrier mediator, the electrolyte, most commonly a solution of redox couples or a hole conductor. Electrolyte electron donation produces the ground state of QDs, which is usually sodium sulfide ( $\text{Na}_2\text{S}$ ) and elemental Sulphur (S) used to acquire redox polysulfide ( $\text{S}_x^{2-}/\text{S}_x^{2-}$ ) pairs, which can

prevent chalcogenide QDs from degrading electrolyte. Another oxidation then occurs in the electrolyte interface of the photo-anode, in the electrolyte (Kouhnavard et al., 2014).

Reduced species ( $S^{2-}$ ) form holes at the photo-electrode ( $TiO_2/QDs$ ) and, more specifically, at the photo-anode/electrolyte interface is the redox couples working mechanism (2.1 & 2.2 reactions).

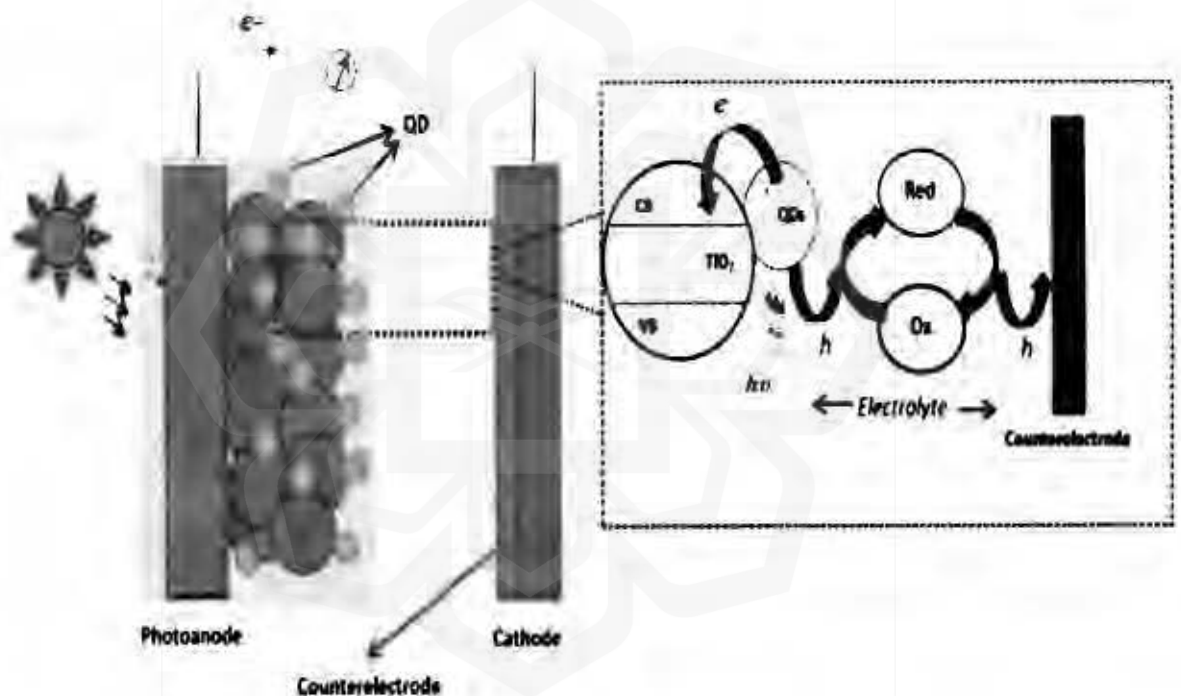


Figure 2.1: Structure of QDSSC

The oxidized species ( $S_x^{2-}$  ions) are transformed to  $S^{2-}$  by trapping electrons at the electrolyte on counter electrode interface after the ion diffusing step in the polysulfide redox couple electrolyte. Electrons thus migrate to complete the circuit through the external load (Ren, Li, & He, 2015) (2.3 reaction).



The  $S^{2-}/ S_x^{2-}$  redox pair will effectively mediate the carrier for cadmium chalcogenide QDSSC. Consequently, there are some variations in levels of Fermi between the redox potential in the electrolyte and the electron in the photo-electrode, which produces voltage. The outcome of QDSSC devices produce electricity from sunlight, and the cell efficiency is determined using the equation below (Fukui et al., 2009).

$$\eta = \frac{J_m V_m}{P} \quad (2.4)$$

$J_m$  and  $V_m$  stand for voltage and density on the real maximum power density at the operating level, where  $P$  representing the power density. The fill factor (FF) can calculate efficiency as follows (Ye et al., 2016).

$$\eta(\%) = \frac{J_{sc} \times V_{oc} \times FF}{P} \times 100 \quad (2.5)$$

$V_{oc}$  and  $J_{sc}$ , respectively represent open circuit voltage and short current density (mA/cm<sup>2</sup>). The direct density-voltage current (J-V) curve has been depicted in Figure 2.2. Light intensity, absorption, inject efficacy, and the production of oxidized dye are all effects in  $J_{sc}$ . Both the semiconductor Fermi level and the dark current level are dependent on  $V_{oc}$ .

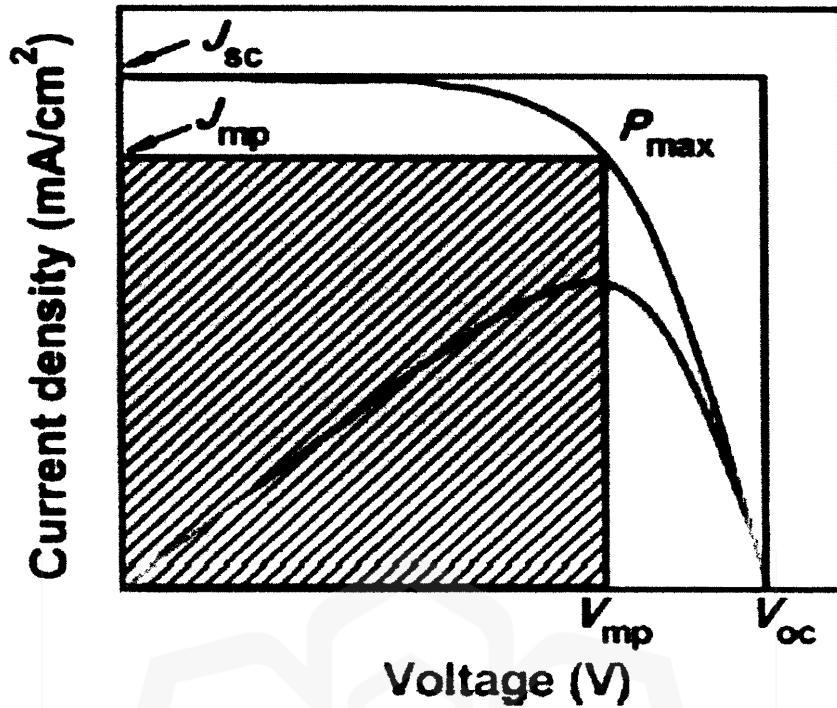


Figure 2.2: The J-V curve plots of QDSSC (Pan, et al. 2018)

Differences between the semiconductor Fermi level and the redox potential of the hole conductor determine the maximum value of the open-circuit voltage. The proportion of the inner ( $J_m \times V_m$ ) to outer rectangular ( $J_{sc} \times V_{oc}$ ) fields determines by FF at the ideal and real PV cell.

$$FF = \frac{J_m \times V_m}{J_{sc} \times V_{oc}} \quad (2.6)$$

While the J-V curve touches the outer rectangular field, evaluating that FF is equal to one. FF is affected by various factors. One of these variables (a band counter electrode, for example) is high inner resistance, which reduces the fill factor (FF) and overall efficacy. An electron could be carried to the outer circuit by an incident photon.



Short-circuit photocurrent ( $I_{sc}$ ) at different wavelengths of excitation ( $\lambda$ ) can be used to measure the potential of an incident photon delivering an electron to the outer circuit. We can measure the by:

$$IPCE (\%) = [1240 \times I_{sc} (A/cm^2)] / [\lambda (nm)] \times I_{inc} (W/m^2)] \times 100\% \quad (2.7)$$

where  $I_{inc}$  represents the incident of light power.  $J_{sc}$  is attained through combining IPCE ( $\lambda$ ) and the photon flux density  $F(\lambda)$  output into the incident light wavelength spectrum ( $\lambda$ ). It represents  $J_{sc}$  as follows (Grinis et al., 2010):

$$J_{sc} = \int qf(\lambda)IPCE(\lambda)d\lambda \quad (2.8)$$

(q) stands for an electron charge. We can employ the following equation to calculate IPCE:

$$IPCE(\lambda) = LHE(\lambda) \times \varphi_{ing} \times \eta_c \quad (2.9)$$

That  $\varphi_{ing}$  represents the quantum production of electron injection,  $\eta_c$  represents the efficiency level of electrons injected at the back touch collection, and LHE shows the light-harvesting efficiency (Luque & Hegedus, 2011). The LHE wavelength could be achieved as follows:

$$LHE = 1 - T = 1 - 10^{-Absorbance} \quad (2.10)$$

QDs absorb light, which is called absorbance. The injected electron numbers are equivalent to stored electron numbers on the TCO; thus, the loss of an electron is attributed exclusively to charge recombination. Consequently,  $\eta_c$  it is measured as:

$$\eta_c = \frac{J_{sc}}{J_{inj}} = \frac{J_{sc}}{[J_{sc} + J_r]} = 1 - \left[ \frac{\tau_{sc}}{\tau_{oc}} \right] \quad (2.11)$$

$J_{inj}$  refers to the current of electron injection from QDs to the anode, then  $J_r$  refers to current density recombination.  $\tau_{sc}$  stands for the time of electron transit.  $\tau_{oc}$  refers to the recombination period, and  $J_{sc}$  is current density of the short circuit. A striking feature of a solar cell considers as internal quantum efficiency (IQE), which illustrates how absorbed photons' efficiency in the external circuit is turned into the current.

We can measure the solar cell of IQE at a given wavelength (IQE-1) by utilizing IPCE and LHE for a perfect solar cell after calculating light absorption by the TCO substrate ( $\%T_{TCO}$ ) calculated as follow: (Fuke et al., 2010)

$$IQE = \frac{IPEC}{[\% T_{TCO} \times LHE]} = \varphi_{inj} \times \eta_c \quad (2.12)$$

A typical solar spectrum of 1.5G (global) air mass (AM) is utilized for cell structure derived from the direction length of light, which requires entering the surface through the atmosphere. Then the spectrum is generally normalized to a  $1000W/m^2$  standardized irradiance or ( $100mW/m^2$ ) (Fuke et al., 2010).

## 2.5 ELECTROLYTE

Our current research focuses on electrolytes, which play a critical role in sustaining photovoltaic action in QDSSC through a regeneration mechanism involving redox species. A redox couple in the electrolyte for regenerating QD and hole transport to the counter electrode is one of the essential components of QDSSC (Zhu, Song, & Lian, 2013). Even though polyiodide is utilized and acts as an electrolyte in DSSC, the most desirable and appropriate electrolyte in QDSSC is polysulfide (Bhambhani, 2018). Electrolyte conductivity and electron mobility in  $TiO_2$  layer affect the energy conversion efficiency of the QDSSC cell. (Lee et al., 2008). An effective system is defined primarily through the density of current short-circuit ( $J_{sc}$ ), fill-factor (FF), and

open-circuit voltage ( $V_{oc}$ ). These critical variables can be affected by electrolytes and have influenced the counter electrode of QDSSC efficiency.

The value of  $J_{sc}$ , for example, is influenced by transporting of the redox couple in electrolytes (Sun et al., 2017). The fill factor (FF) could also affect catalyst potential of counter electrode for redox reaction (Du et al., 2016; Jiao et al., 2017). The value of  $V_{oc}$  directly affected by redox electrolyte pairs (Kouhnavard et al., 2014). The  $V_{oc}$  is a potential difference between the Fermi level of  $TiO_2$  and the redox potential presented in the electrolyte.

The major reason for employing polysulfide in the QDSSC because it has chemical compatibility and stability with the metal chalcogenides. Polysulfide solid polymer electrolyte made better photoconversion efficiencies for QDSSC (Baharun et al., 2020). In the literature, a range of procedures of making electrolyte have been used with various combinations of components such as methanol, ethanol, water, and some ionic additives in various concentrations as shown in Table 2.1.

Table 2.1: The type of liquid polysulfide electrolyte in QDSSC

<b>Na<sub>2</sub>S M</b>	<b>S M</b>	<b>Methanol (ml)</b>	<b>Additive</b>	<b>Ethanol (ml)</b>	<b>Water (ml)</b>	<b>References</b>
0.5	0.1	-	0.1M NaOH	-	25	(Mora-Seró & Bisquert, 2010)
0.5	0.1	-	-	20	5	(Mora-Seró & Bisquert, 2010)
0.5	2	17.5	0.2 M KCl	-	7.5	(Chakrapani et al., 2011)
0.5	0.1	5	-	17.5	2.5	(Prasad et al., 2018)

According to Ingle et al., 2020, the distilled water-based polysulfide electrolyte ( $\text{Na}_2\text{S} + \text{S}$ ) has a significant impact on the overall efficiency of QDSSCs compared to the methanol-based polysulfide electrolytes ( $\text{NaOH} + \text{Na}_2\text{S} + \text{S}$ ). Jiao and co-worker reported that co-solvents polysulfide electrolytes have a greater cell efficiency (Jiao et al., 2017). Water and ethanol has been found as the perfect solvent for preparing liquid electrolytes (Jun et al., 2013).

Many experiments have been conducted to improve the polysulfide electrolyte, such as controlling the redox mediator concentration (Liao et al., 2015) and using a solvent modification (Li et al., 2011).

Jovanovski and co-worker presented the opportunity of using a pyrrolidinium ionic liquid electrolyte that comprises  $\text{S}^{2-}/\text{S}_x^{2-}$  (Jovanovski et al., 2011). Table 2.2 show the QDSSC performance having liquid polysulfide electrolytes.

Table 2.2. Liquid electrolyte for QDSSCs

QDs	Electrolyte	CE	Jsc ( $\text{mA.cm}^{-2}$ )	Voc V	FF	$\eta$ %	References
CdS/CdSe	$\text{Na}_2\text{S} / \text{S} + \text{KCl}$ Methanol/Water	Au	17.30	0.63	38.0	4.15	(Seol et al., 2010)
HTS/CdS	$\text{Cd} (\text{CH}_3\text{COOH})_2 +$ ethylene diamine tetra acetic acid disodium salt (EDTA) + $\text{Na}_2\text{SeSO}_3$ +Se powder + $\text{Na}_2\text{SO}_3$ +water	Pt	7.53	0.49	27.0	1.01	(Yu et al., 2011)
CdTe/CdSe	$\text{Na}_2\text{S} / \text{S}$	$\text{Cu}_2\text{S}$	19.6	0.61	57.0	6.76	(Wang et al., 2013)

	Water/HCl						
CIS/ZnS	Na <sub>2</sub> S +S Polysulfide/KCl	Cu <sub>2</sub> S	20.7	0.59	58.0	7.04	(Pan et al., 2014)
CdSe/Te	Na <sub>2</sub> S /S Water	Cu <sub>2</sub> S	20.8	0.65	60.5	8.21	(Zhao et al., 2015)
CdSe	Na <sub>2</sub> S /S methanol/deionized water/KCl	Cu <sub>2</sub> S	15.65	0.74	51.0	5.92	(Zhao et al., 2016)
ZnSe/CdS/CdSe	Na <sub>2</sub> S /S Deionized water	Cu <sub>2</sub> S	20.8	0.71	64.0	9.48	(Yang et al., 2015)
CdS	Na <sub>2</sub> S /S/ GPE	Cu <sub>2</sub> S	12.40	0.55	0.41	2.77	(Raphael, Jara & Schiavon, 2017)
CdS	Na <sub>2</sub> S/S polysulfide/glycerol/PEG /Pt	CZTS /Pt	11.47	0.59	60.5	4.09	Patel & Gohel, 2019)
PbS	Na <sub>2</sub> S/S /cellulose acetate nanofibers	Pt	9.95	0.46	34.75	1.51	(Dissanayake et al., 2020)
CdS/CdSe	Na <sub>2</sub> S /S Polyvinylpyrrolidone /Deionized water	Cu <sub>2</sub> S	9.82	0.57	68.0	3.82	(Ma F et al. (2021)

Although liquid electrolyte exhibited higher efficiency, there are some disadvantages such as leakage and corrosion. New materials have been developed to replace conventional liquid electrolytes (Mingsukang et al., 2017).

In addition, a quantum dot-sensitized solar cell is fabricated by sandwiching a solid electrolyte between distinct alloy counter electrodes, most commonly a CdS-sensitized anode. The use of solid electrolytes and various hole conductors for researchers tend to replace the liquid electrolyte in QDSSCs to improve their stability. The composition and performance of selected solid electrolytes is shown in Table 2.3.

Table 2.3. Solid electrolyte for QDSSCs

QDs	Electrolytes	CE	Jsc (mA.cm <sup>-2</sup> )	Voc V	FF	η %	References
CdS	poly(ethylene oxide) /succinonitrile /Na <sub>2</sub> S	-	-	-	-	-	(Fan & Maier, 2006)
CdS	PVP/ Na <sub>2</sub> S/ S	CoSe	2.84	0.67	28.9	0.55	(Duan et al., 2014)
CdSe	PEO-PVDF with S/TMAS and S/Na <sub>2</sub> S	-	-	-	-	-	(Yang & Wang, 2015).
CdS	Plastic crystal /succinonitrile /Na <sub>2</sub> S	CoSe	3.65	0.67	52.7	1.29	Duan et al., 2015)
-	PEO-NaPF <sub>6</sub> +SN	-	-	-	-	-	(Arya & Sharma, 2018)
-	PVC/PMMA/LiCF <sub>3</sub> SO <sub>3</sub> /EC	-	-	-	-	-	Aziz et al.,2018)
-	NaCMC/EC/polysulfide	-	-	-	-	-	(Baharun et al., 2018)
CdS/ZnS	Na-CMC/Na <sub>2</sub> S/S	Pt	4.92	0.41	0.45	0.9	(Baharun et al., 2020)

CoSe: cobalt selenide, CuS:copper sulfide, TMAS: tetramethylammonium sulfate

## **2.6 QUANTUM DOTS (QDs) SENSITIZERS**

Quantum dots have a greater extinction coefficient than traditional dyes, which might result in lower dark current and improved solar cell efficiency. Furthermore, using hot electrons transfer (HET) from QDs to create numerous electron–hole pairs per photon is conceivable due to the impact ionization effect. Hishikawa (2005) explains that QD semiconductors are considered spherical nanomaterials with special optical features. There are some advantages of using QDs: the first advantage is that hot carrier injection (HCI) forms the highly excited state to the TiO<sub>2</sub> of CB by irradiating light (Williams et al., 2013). The second advantage refers to carrier multiple exciton generation (MEG) (Semonin et al., 2011). Thirdly, as quantum confinement outcome, the band gap and properties are tunable and size dependent which enhances the separation of the charge and absorption of solar cells (Laban & Etgar, 2013). Due to their unique photosensitization properties, the researcher studied different QD materials for QDSSCs application. These materials are PbS, CdS, CdSe, CdHgTe, ZnSe, Ag<sub>2</sub>S, CdTe, and InP. Because of their ease of preparation and characterization, CdS and CdSe are commonly used as QD materials (Jun et al., 2013). Much research has been conducted in recent years to enhance the absorption range of light in the solar spectrum through tuning the photoelectrode by using different QDs with various bandgaps. Using integrated QD systems, conversion efficiencies were significantly improved.

## **2.7. TRANSPARENT CONDUCTING FILMS (TCFs)**

A very significant element of QDSSCs is transparency conducting films or TCF. They are thin films of materials covered on certain substrates that conduct materials. Two well-known substrates are indium tin oxide (ITO) and fluorine-doped tin oxide (FTO).

In visible light, the ITO layer exhibits a higher transparency (80-90%) and poor thermal stability compared to transparency (80.786%) of FTO glass. The optical band gap energy of ITO and FTO glass projected 3.75 eV and 3.65 eV, respectively.

### **2.7.1 The Working Electrode**

CdS as quantum dot (QD) embedded in a TiO<sub>2</sub> layer coated on FTO glass. The photogenerated electrons are transferred to an electron-transport layer by the QD active layer, which absorbs sunlight. As working electrodes of QDSSC, a semiconductor coated on fluorine doped tin oxide (FTO) typically consists of TiO<sub>2</sub> with a wide band gap of 3.2 eV and QD adsorbed onto the semiconductor sheet. When exposed to light, QD acts as a sensitizer, forming electron-hole pairs. Due to these intriguing characteristics, semiconductor QDs with a relatively small band gap have been identified as candidates for the performance of QDSSC cell.

### **2.7.2 The Counter Electrode**

Counter Electrode (CE) is another vital component of QDSSCs which accepts electrons of the external circuit. The CE performs as an electro-catalyst for redox species and transferring electrons to the sensitizer for regenerating the electrons. The most widely used element for preparing good CE is platinum (Pt). In the QDSSCs, a thin film of Pt is coated on FTO glass layer and used as a CE.

## **2.8 ELECTROLYTE MATERIAL SELECTION FOR QDSSC**

In this research, we have chosen poly(acrylamide-*co*-acrylic acid) and sodium carboxymethyl cellulose (Na-CMC) with sodium sulfide (Na<sub>2</sub>S) as competent electrolyte for QDSSC. We have chosen polymer blend based on acrylic acid and



acrylamide as monomers to enhance the electrolyte features because of the fast co-polymerization velocity and high water affinity (K. Park, Chen, & Park, 2001). The host polymer was sodium carboxymethyl cellulose (Na-CMC). Polymer electrolytes based on Na-CMC have shown good performance with ionic conductivity (Zhang et al., 2016). Also, used sodium sulfide ( $\text{Na}_2\text{S}$ ) as a charge carriers in the electrolyte (Ahmed, 2016). The advantages of polymer blend is thermal stability, higher mechanical strength and salt provide ionic charge carrier to enhance the conductivity of electrolyte.

### 2.8.1 Poly(Acrylic Amid- Co-Acrylic Acid)

As monomers acrylic acid (AA) and acrylamide (AM) are two important water-soluble. Polyacrylic acid (PAA) is a polymer produced from acrylic acid, which is a monomer. The polymer has some cross linking between the chains, and the large chains contain thousands of monomer units. Polyacrylic acid, on the other hand, is extremely hydrophilic, as carboxylic acid groups are the only polymer that can form hydrogen bonds with water molecules. Because of its benefits as a conductivity improver and filler, as well as its good electrical-thermal characteristics. It is ideal for a variety of electrochemical device applications (Wieczorek et al., 1995). Figure 2.3 illustrates the chemical formula for poly(acrylamide-co-acrylic acid).

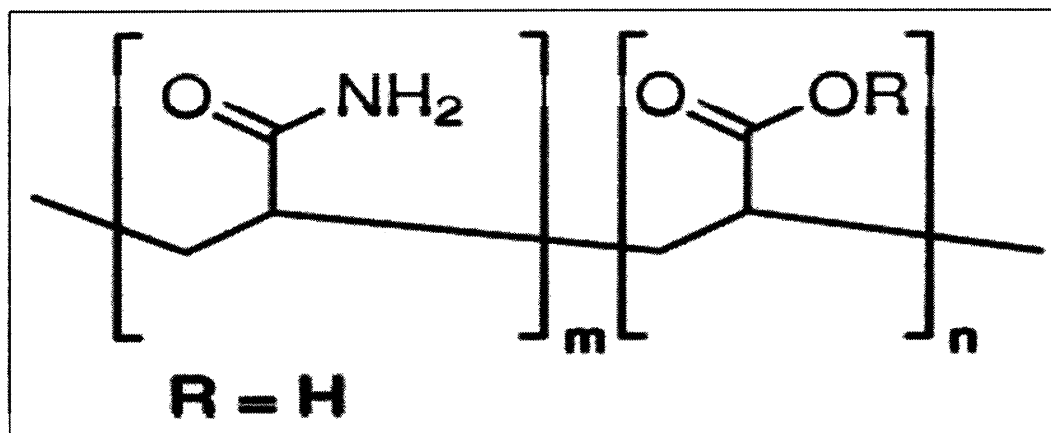
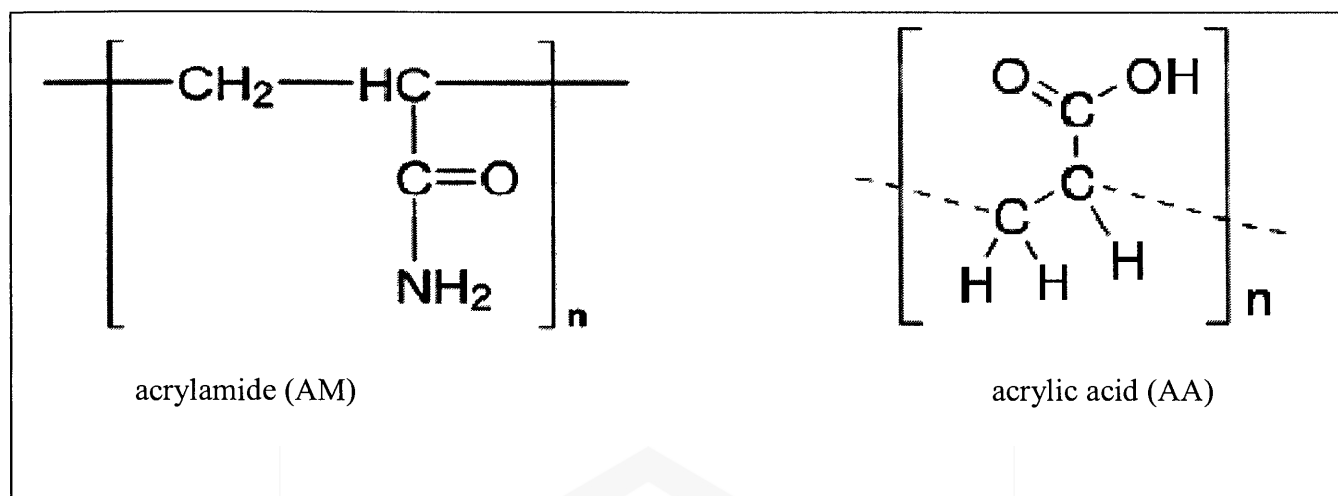


Figure.2:3 Compound formulation of poly(acrylamide-co-acrylic acid)

The structure of polyacrylamide and polyacrylic acid are illustrious below:



### 2.8.2 Sodium Carboxymethyl Cellulose (Na-CMC)

The sodium salt of carboxymethyl cellulose is sodium carboxymethyl cellulose (Na-CMC). Na-CMC considered a linear polymeric cellulose derivative with varying rate of carboxymethyl substitution. Na-CMC is a polyelectrolyte that is anionic and water soluble. Besides, it was indicated that homogeneous solution with Na-CMC would be beneficial in stabilizing electrochemical output, resulting in better conductivity of electrolyte in comparison with poly (vinylidene fluoride) (PVdF) (Dahbi et al., 2014).

Figure 2.4 shows the chemical formula for Na-CMC.

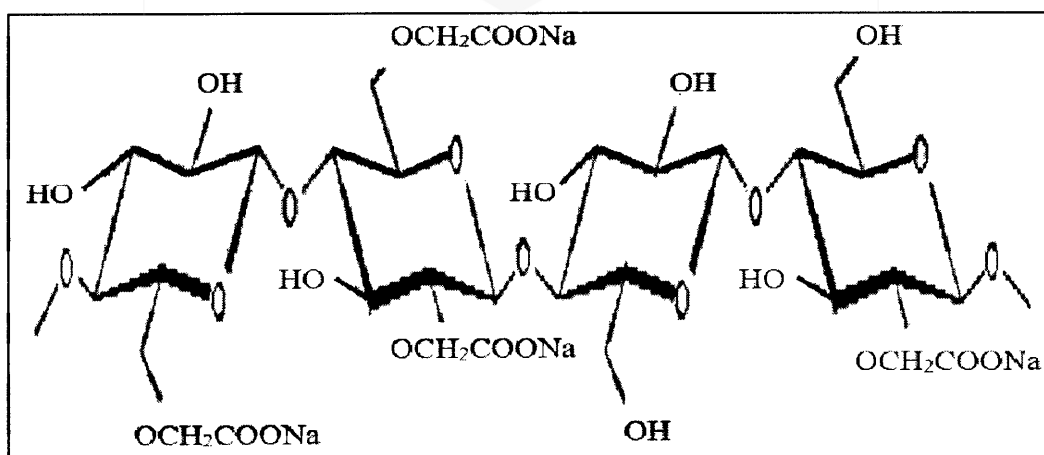


Figure 2.4: Compound formulation of sodium carboxymethyl cellulose (Na-CMC)

### 2.8.3 Sodium Sulfide (Na<sub>2</sub>S) Salt

The sodium sulfide salt is extremely favorable due to having a high energy density in operating conditions. Also, it is easily available and economically inexpensive. In addition, sodium sulfide hydrate salts (Na<sub>2</sub>S.nH<sub>2</sub>O) have a high energy density of 2.66 GJ/m<sup>3</sup> when changing from pent-hydrate to hemihydrate at the right temperature and pressure (Trausel et al., 2014) system. The chemical reactivity of sodium sulfide (Na<sub>2</sub>S) salt has been recognized, and stabilized salt with cellulose is advantageous because it improves mechanical properties. Figure 2.5 shows the chemical formula for Na<sub>2</sub>S.

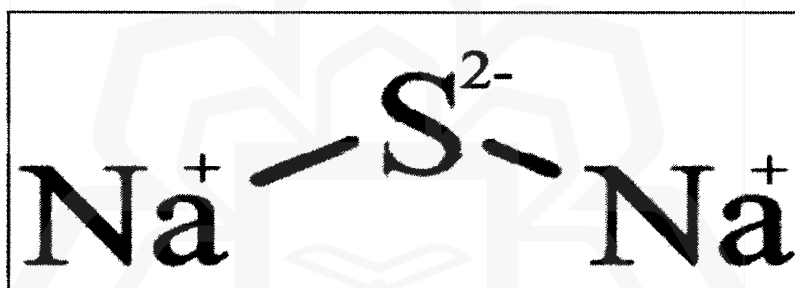


Figure 2.5: Compound formulation of Sodium Sulfide (Na<sub>2</sub>S) salt

The reason to select poly(AM-*co*-AA) is that it often acts as the monomer base because of fast copolymerization and high-water modality. It is a water-soluble polymer and able to entrap massive loading of water due to its hydrophilic polymer chains (Kumaran et al., 2018). The effect of salt concentration Na<sub>2</sub>S on poly(AM-*co*-AA) has not to be explored yet. Also, the Na-CMC is often used as a host polymer for electrolytes as it shows good electrical and transport ionic properties (Samsudin et al., 2014). It is a low-cost natural polymer with good filming ability, good adhesion, and high hygroscopicity. It has a three-dimensional network and polymer chains with presence of both hydroxyl and carboxylate groups on which exhibits characteristics of excellent stability in alkaline solution, superabsorbent, and strong coordination with metal ions (Feng et al., 2016).

## 2.9 SALT CONCENTRATION EFFECT

There are three main factors that affect the conductivity of a solution are the concentrations of ions, the type of ions, and the temperature of the solution. The development of the mixing of several solvents to achieve the desired properties is a more practical key. It is noteworthy that since electrolytes react with active materials such Na<sub>2</sub>S salt, the surface chemistry at the anode and cathode is also central to cell performance. Therefore, the design of new electrolyte systems should also consider the properties of the solid electrolyte interphase at the electrodes. The ionic conductivity of the Na<sub>2</sub>S will increase in the (P-Na-S) electrolyte as the content of polymer and high viscosity decreases at a fixed salt concentration. The level of ionic conductivity increased as the polymer concentration decreased in the Na<sub>2</sub>S conditions, since solubility decreases with polymer concentration. The reasons are: (i) At the same salt concentration, the Na<sub>2</sub>S salt complex has a higher level of conductivity than of the poly(AM-co-AA)/Na-CMC composite.

(ii) The viscosity of the (P-Na-S) blends electrolyte decreases as the amount of Na<sub>2</sub>S increased.

This linear correlation indicated that, the conductivity value is strongly affected by solubility, and thus the salts with low viscosity showed high ionic conductivities. This may be due to an increase in the ion mobility of the salts. When the solvent's solubility is high, the conductivity undergoes as a result of the lower conductance. The capacity of water to conduct an electrical current is measured by its conductivity. Because dissolved salts and other inorganic compounds carry electrical current, conductivity rises as the salt concentration rises, and electrical conductivity in materials is caused by the movement of electrically charged particles.

## **2.10 PLASTICIZER**

One of the methods for enhancing the efficiency of the electrolyte is to plasticize polymer electrolytes by adding chemical additives. Plasticizers, for instance, ethylene carbonate (EC), propylene carbonate (PC), diethyl carbonate (DEC), and dimethyl carbonate (DMC) often enhance polymer electrolyte performance (K. H. Lee, Park, & Kim, 1999). In this work is incorporated ethylene carbonate (EC) into Na-CMC and poly(AM-co-AA) to augment the thin film's conductivity. By complexing polysulfide ions with the functional group of ECs, the amount of polysulfide ions in the electrolyte increased within the presence of poly(AM-co-AA) and Na-CMC films. As a result, ionic conductivity increases. The rise of ionic conductivity caused by the adding of EC due to either ion mobility or number density of ions (M. Park et al., 2010).

## **2.11 SUMMARY**

The focus of literate review was electrolyte integrated with quantum dot synthesized solar cells QDSSC. The process of QDSSC and mechanism with various electrolytes, includes liquid and solid electrolyte functions in QDSSC discussed. Over several years extensive research has been conducted in electrolyte areas to enhance the QDSSC performance with different electrolytes. The development of electrolytes for QDSSC applications was also addressed with liquid and solid function. There are several parameters for improve the electrolyte conductivity includes plasticizer and salt concentrations. The chapter discussed the selected materials to develop an electrolyte for the photovoltaic efficiency of QDSSC. Finally, the material choices are explained in this study to apply for a new polymer blend electrolyte.

## CHAPTER THREE

### METHODOLOGY

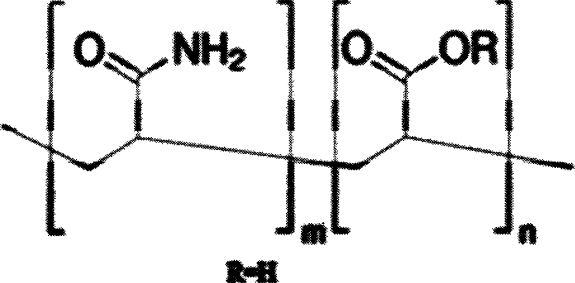
#### 3.1 INTRODUCTION

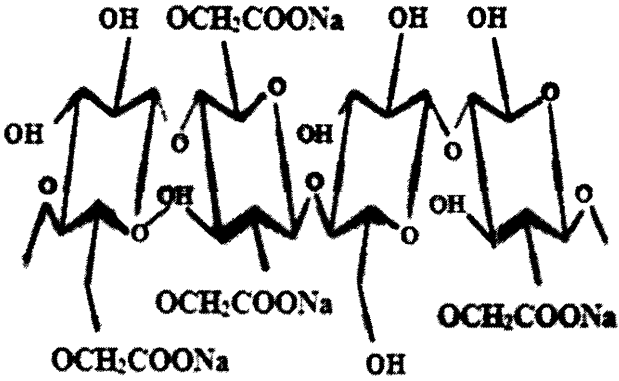

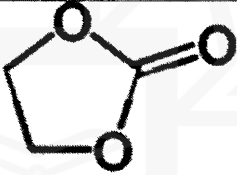
The flow chart of experimental works performed in this project has been described in Figure 1.3. In this chapter, the details of the materials used, the preparation of polymer electrolytes (without and with ethylene carbonate (EC)), and their characterizations, which comprise of Electrochemical Impedance Spectroscopy (EIS), Fourier transform infrared spectroscopy (FTIR), X-ray Diffraction Spectroscopy (XRD) are explained.

#### 3.2 MATERIALS

The essential parts of the electrolytes (P-Na-S) consist of poly(acrylamide-*co*-acrylic acid) (abbreviated as poly(AM-*co*-AA)) and sodium-carboxy methyl cellulose (Na-CMC) as the polymer hosts, sodium sulfide (Na<sub>2</sub>S) as the salt, and ethylene carbonate (EC) as the plasticizer. The materials used in this study are tabularised in Table 3.1.

Table 3.1: Chemical structures of materials used in this work.

Material	Chemical structure	Manufacturer
Poly(acrylamide- <i>co</i> -acrylic acid)	 <p>The chemical structure shows a polymer backbone with two repeating units. The first unit is an acrylamide unit with a carbonyl group (C=O) and an amide group (-NH<sub>2</sub>). The second unit is an acrylic acid unit with a carbonyl group (C=O) and an ester group (-OR). The units are labeled with 'm' and 'n' respectively. A label 'R-H' is placed below the structure.</p>	Sigma Aldrich

<p><b>Sodium carboxy methyl celluloses (Na-CMC)</b></p>		<p><b>Sigma Aldrich</b></p>
<p><b>Sodium sulfide</b></p>		<p><b>Asia pacific specialty chemicals</b></p>
<p><b>Ethylene carbonate</b></p>		<p><b>Merck</b></p>

Using the chemicals presented in the Table 3.1, the following two types of polymer electrolyte with and without EC were prepared:

- Poly (AM-co-AA)/ Na-CMC/ Na<sub>2</sub>S
- Poly (AM-co-AA)/ Na-CMC/ Na<sub>2</sub>S/ EC

### 3.3. POLYMER ELECTROLYTE PREPARATION

#### 3.3.1 Poly(AM-co-AA)/ Na-CMC/ Na<sub>2</sub>S Electrolytes

Solid poly(AM-co-AA)/ Na-CMC/ Na<sub>2</sub>S electrolyte or (P-Na-S) blends with and without EC plasticizer were produced using the solution cast technique.

0.05-gram poly(AM-co-AA) powder and 0.45-gram sodium carboxy methyl cellulose (Na-CMC) powder were mixed at 1:9 ratio and dissolved in 15 mL purified distilled water at room temperature for one hour in this process. The fixed amount ratio

of poly(acrylamide-*co*-acrylic acid) based on pervious works give the highest dielectric constant.

After that, a variable amount of sodium sulfide ( $\text{Na}_2\text{S}$ ) by (10, 20, 30, 40, and 50 wt. %) was added while stirring and continuously mixed for another two hours to create a homogeneous solution.

Subsequently, the solution was poured into a clean glass petri dish, and the solvent was allowed to gradually evaporate in the vacuum oven at  $40\text{ }^\circ\text{C}$  for seven days. To remove all traces of water, the film was dried in a desiccator. Table 3.2 shows the detailed composition of the samples used in this research.

Table 3.2: Composition of materials used to prepare polymer electrolyte

Sample	P(AM- <i>co</i> -AA) (g)	Na-CMC (g)	Na <sub>2</sub> S salt	
			(%)	(g)
A	0.05	0.45	10	0.05
B	0.05	0.45	20	0.125
C	0.05	0.45	30	0.176
D	0.05	0.45	40	0.33
E	0.05	0.45	50	0.5

### 3.3.2 Poly(AM-*co*-AA)/ Na-CMC/ Na<sub>2</sub>S/ EC Electrolytes

In this study, ethylene carbonate (EC) is used as a plasticizer to improve the conductivity of the thin film, leading to increased ionic conductivity. Various amount of ethylene carbonate (EC) by (10, 20, 30, 40, and 50 wt.%) were added and continuously stirred to



obtain (P-Na-S)-EC with the highest conductivity. The solution was then casted onto a glass petri dish and kept at 40°C for seven days in the vacuum oven to get thin film formation. The concentration of poly(AM-co-AA), Na-CMC and Na<sub>2</sub>S are fixed at 0.05 g, 0.45 g, and 0.176 g respectively. The detailed composition of polymer electrolyte with addition of EC used in this research is shown in Table 3.3.

Table 3.3: Polymer electrolytes prepared with and addition of ethylene carbonate (EC)

Sample	EC	
	(%)	(g)
C1	10	0.075
C2	20	0.169
C3	30	0.289
C4	40	0.45
C5	50	0.676

Subsequently, the fresh thin layer formation after seven days, the film layer was removed from the petri dish. Three circular specimens with diameter of 2 cm were cut from the thin film for electrochemical impedance spectroscopy (EIS) measurement. Figure 3.1 shows the produced thin film and how the specimens for EIS characterizations are prepared.

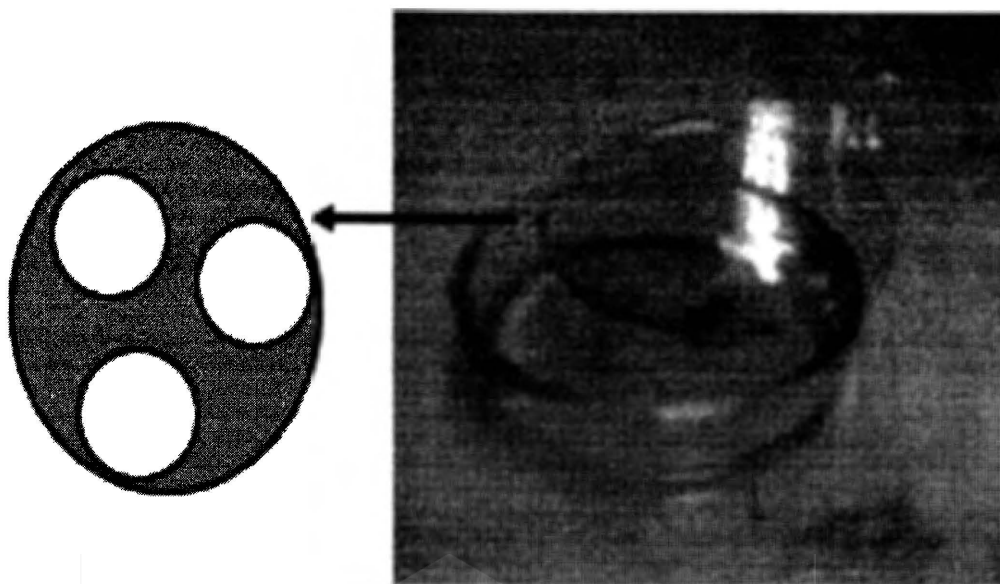


Figure 3.1: The thin film layers was removed and cut into three sections for EIS measurements

### 3.4 CHARACTERIZATIONS OF POLYMER ELECTROLYTES

#### 3.4.1 Electrochemical Impedance Spectroscopy (EIS)

A tiny sinusoidal potential was applied across the samples to measure the current. The voltage was as low as 10 mV. Between two stainless-steel blocking electrodes, solid polymer electrolytes were arranged. In a Cole-Cole plot diagram, negative imaginary impedance was plotted against real impedance. A range of complex impedance values, known as  $Z^*$  values, was measured in the range of 50 Hz – 1 MHz.

Real impedance ( $Z_r$ ) and imaginary impedance ( $Z_i$ ) were calculated to obtain the values of  $Z^*$ .

The equation below was applied to measure the  $Z_r$  and  $Z_i$  values.

$$Z_r = |\omega| \cos \theta \quad (3.1)$$

$$Z_i = |\omega| \sin \theta \quad (3.2)$$

In complex impedance data,  $Z^*$  is characterized by its real ( $Z_r$ ), and imaginary ( $Z_i$ ) part utilizing the equation below:

$$Z^* = Z_r - iZ_i \quad (3.3)$$

where,  $i = \sqrt{-1}$ .

#### **3.4.1.1 Ionic Conductivity Measurement**

$R_b$ , the bulk resistance was measured from the Cole-Cole plot intercept to the real impedance axis. The electrical conductivity of the samples ( $\sigma$ ) was calculated using the following equation (Cao et al., 2010):

$$\sigma = \frac{t}{A.R_b} \quad (3.4)$$

Where, (t) represents the section thickness, and (A) represents solid electrolyte of lateral surface area.

The Electrochemical Impedance spectroscopy (EIS) was measured by HIOKI 3532-50 LCR Hi-Tester device from 50 Hz to 1 MHz between 30°C to 100°C, at Center for Ionic University of Malaya (CIUM).

#### **3.4.1.2 Calculation of Activation Energy ( $E_a$ ) for Ion Conduction**

The increase in free volume and polymer segmental motion may be responsible for the enhanced ionic conductivity at higher temperatures (Moniha et al., 2018). The polymer chain segment receives adequate energy to vibrate and produce a larger free volume surrounding the polymer when the SPE is subjected to higher temperatures. (Hafiza & Isa, 2018). As a result, mobile ion migration across the polymer matrix is increased. The nature of ion transport in Arrhenius type films at elevated temperatures is nearly identical to that in ionic crystals, where ions can hop onto neighboring empty sites, resulting in enhanced ionic conductivity (Kumar et al., 2012). When an ionic mobility requires intermolecular ion hopping, the conductivity changes as a function of the ions thermal hopping frequency (Baskaran et al., 2006). The relationship (P-Na-S) of conductivity-temperature is also influenced by the free-volume model, which indicates

that the polymer matrix contains large amorphous phase free-volume cages. It is observed that more spaces are formed at higher temperatures because of accumulated kinetic motion, resulting in more movable ions and higher ionic conductivity in the (P-Na-S) electrolyte.

The activation energy is calculated using the Arrhenius equation, which considers the temperature dependency of the rate constant.

$$\sigma = \sigma_0 \exp\left(-\frac{E_a}{RT}\right) \quad (3.5)$$

$$\log \sigma = \log \sigma_0 - \frac{E_a}{RT} (0.4343) \quad (3.6)$$

$E_a$  = Activation energy,  $\sigma$  = Ionic conductivity,  $R$  = Gas constant ( $8.31 \text{ J}\cdot\text{mol}^{-1}\cdot\text{K}^{-1}$ ),  $T$  = Absolute temperature, and  $\sigma_0$  = Pre-exponential factor. Figure 3.2 illustrates a straight-line based on Equation (3.6)

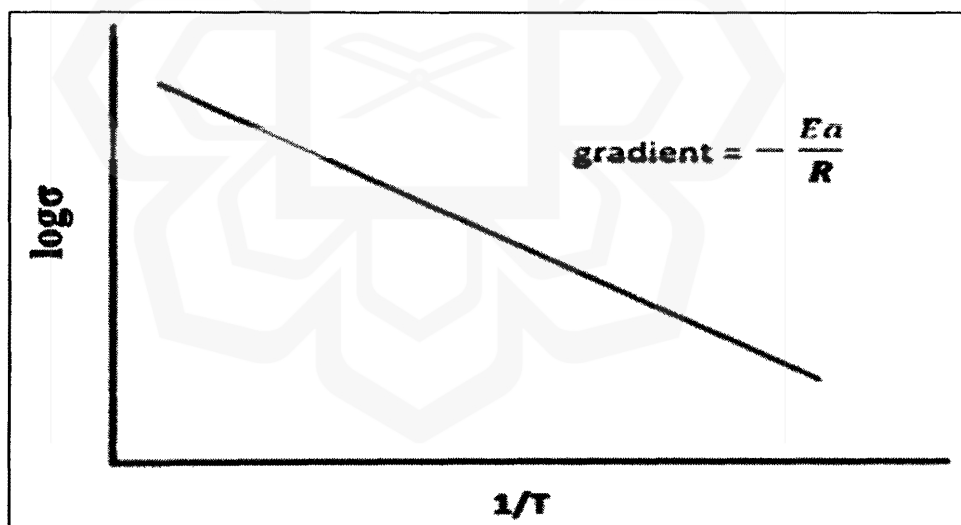


Figure 3.2: The slope gradient with Log  $\sigma$  against  $1/T$

### 3.4.2 Fourier Transform Infrared Spectroscopy (FTIR)

The FTIR method of analysis employs infrared light to scan samples and monitor chemical features as a frequency function, wavelength, and wavenumber (Shen et al., 2011).

The relationship between electromagnetic energy  $E$  (J), frequency  $f$  (Hz), wavelength  $\lambda$  ( $\mu\text{m}$ ), wavenumber  $\nu$  ( $\text{cm}^{-1}$ ) can be expressed as follow:

$$E = h \cdot f = \frac{h \cdot c}{\lambda} = h \cdot c \cdot \nu \quad (3.7)$$

Where  $h$  represents Plank's constant ( $6.63 \times 10^{-34}$  J·s), " $c$ " represents the light velocity in vacuum ( $2.9979 \times 10^8$   $\text{ms}^{-1}$ ). Infrared energy is defined as electromagnetic radiation containing the wavenumbers ( $\nu$ ) between  $13300 \text{ cm}^{-1}$  and  $3.3 \text{ cm}^{-1}$ . There are typically three areas in the infrared area: far-infrared ( $200$ - $3.3 \text{ cm}^{-1}$ ) areas, middle-infrared ( $4000$ - $200 \text{ cm}^{-1}$ ) and near-infrared ( $13300$  -  $4000 \text{ cm}^{-1}$ ). The mid-infrared region corresponds to the energy of fundamental vibration bands of organic compounds. Therefore, FTIR is broadly employed in characterization of organic materials. An infrared spectrum considered to be exclusive to each material.

Once radiation is transferred through a specimen, the radiation portion may be absorbed by the specimen if a change occurred in the dipole moment through the vibration. The transmission  $T$  related with the intensity of the transmitted beam  $I$  to that of the incident beam  $I_0$ , as revealed in Figure 3.3 and Equation 3.8.

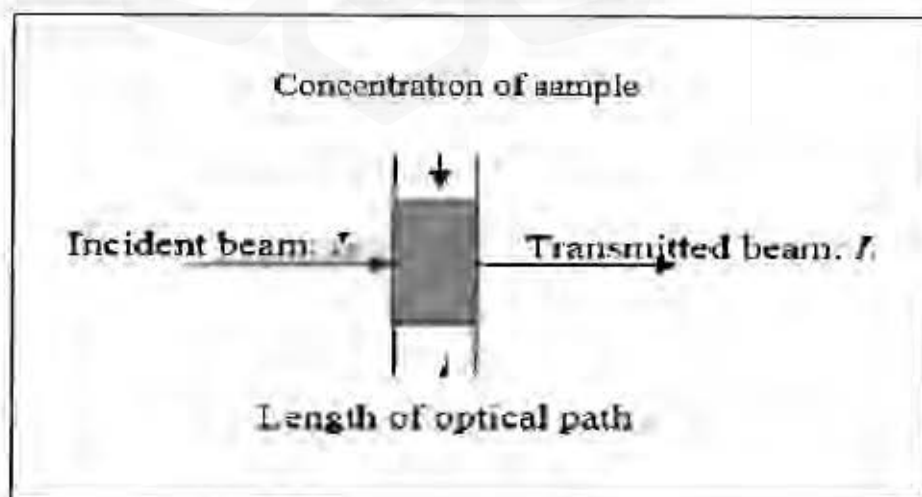


Figure 3.3: Definition of transmission

$$T = \frac{I}{I_0} \times 100 \% \quad (3.8)$$

The IR spectrometers can be separated into two collections: Fourier transform infrared spectrometers (FTIR) and diffusing infrared spectrometer (IR). In an IR spectrometer, a grating monochromator is used to scatter a polychromatic radiation source into diverse spectral basics. An interferometer is employed to produce an interferogram in an FTIR spectrometer in which all wavelengths are gauged simultaneously, resulting in quicker selection and better signal compared to noise ratio dispersive devices. The Michelson interferometer is the most widely used, as shown in Figure 3.4. The interferogram is formerly Fourier transformed, yielding the spectrum, as shown in Figure 3.5. (Bykov, 2008).

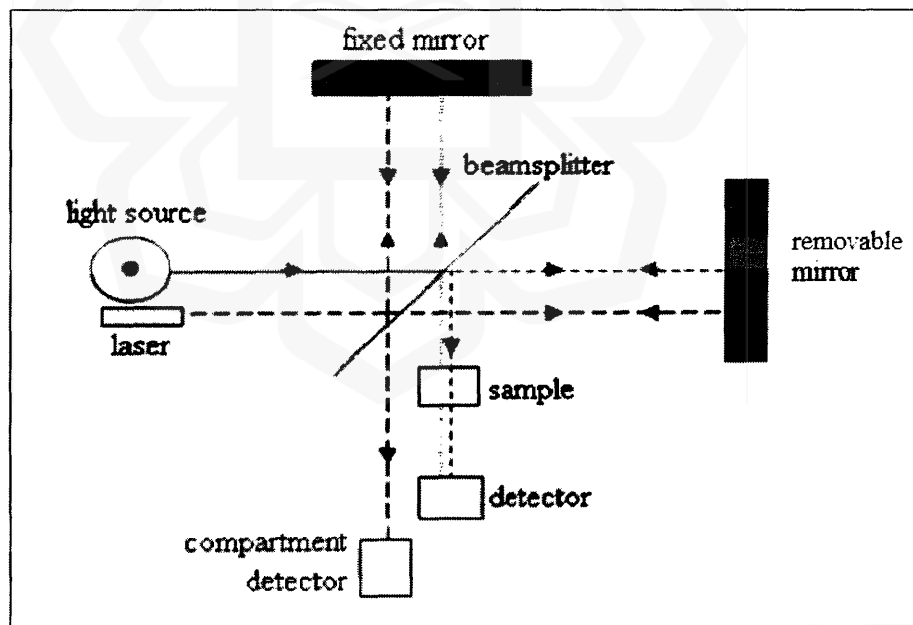


Figure 3.4: Construction of Michelson Interferometer

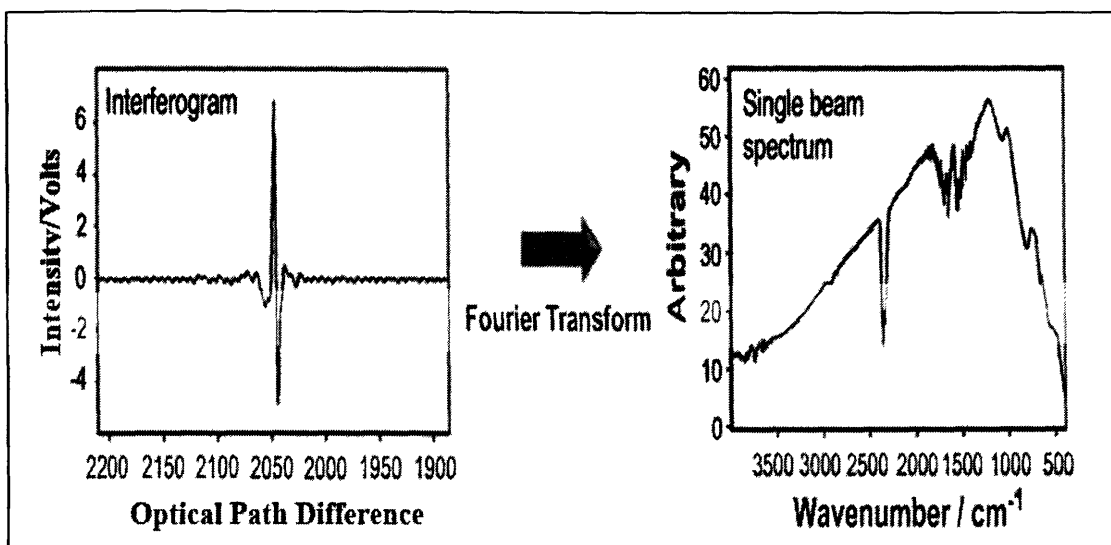


Figure 3.5: Relationship Between Spectrum and Interferogram

Interferogram referred to the signal format gained through an FTIR spectrometer. Different wavelengths will produce peak readings at various regions for a broadband signal if the optical path difference (OPD) is augmented. However, the interferogram improves a complicated oscillatory signal with falling amplitude.

In this project, Perkin Elmer Spectrum 100 Fourier Transform Infrared Spectroscopy (FTIR) spectrometer at Polymer Laboratory, International Islamic University Malaysia (IIUM) was used, with the wave number range 400 to 4000 $\text{cm}^{-1}$ .

### 3.4.3 X-ray Diffraction (XRD)

The X-ray diffraction technique is a non-destructive analytical method for identifying chemical composition, crystal structure, thin films, and physical materials' features. It can measure the X-ray beam's scattered intensity of a sample by adjusting the incidents angle and radiation wavelength.

The X-rays are produced by using a cathode ray tube which is filtered to generate monochromatic radiation, collimated to concentrate, and fixed to the specimen.

Constructive interference (or diffracted ray) is produced by interacting the incident rays with the specimen when circumstances fulfilled the Bragg's Law ( $n\lambda=2d \sin \theta$ ). This law connects the wavelength ( $\lambda$ ) of electromagnetic radiation to the lattice spacing ( $d$ ) in a crystalline sample and the diffraction angle ( $\theta$ ). The transformation of the diffraction peaks to d-spacings permits the materials identification since each crystalline material own a range of specific d-spacings. This is typically obtained by comparing d-spacings with standard reference patterns.

Figure 3.6 illustrates the constructive interference that occurs according to the Bragg's Law:

$$n \lambda = AB + BC,$$

$$AB=BC$$

$$n \lambda = 2AB,$$

$$\sin \theta = AB/d$$

$$AB = d \sin \theta,$$

$$n \lambda = 2d \sin \theta$$

$$\lambda = 2d_{hkl} \cdot \sin \theta_{hkl}$$

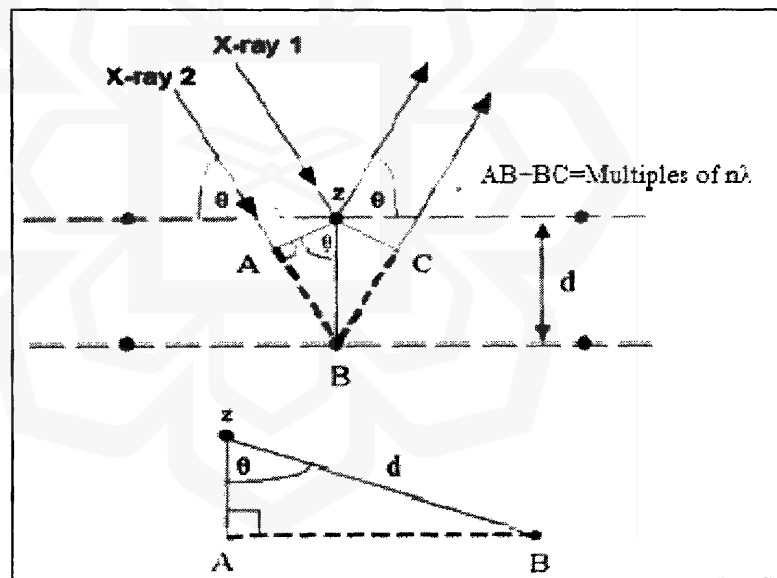


Figure 3.6: Deriving Bragg's Law:  $n\lambda = 2d \sin \theta$



A sample holder, an X-ray detector, and an X-ray tube are the three primary elements of an X-ray diffractometer. These spectra include various elements,  $K_{\alpha 1}$  and  $K_{\alpha 2}$ .  $K_{\alpha 1}$  with shorter wavelength which has twice the intensity as  $K_{\alpha 2}$ . The wavelengths used are unique to the target material (Cu, Fe, Mo, Cr).

It is important to achieve monochromatic X-rays required for diffraction by filtering using foils or crystal monochrometers. The frequently used material for single-crystal diffraction is copper, with  $CuK_{\alpha}$  radiation =  $1.5418\text{\AA}$ . These X-rays are well collimated and centrally directed onto the sample. When the detector and sample are revolved, the intensity of X-rays is subsequently recorded.

As the geometry of the incident X-rays affects the sample meeting the Bragg equation requirement, a peak in intensity and constructive interference happen. This X-ray signal is recorded by a detector that processed and transformed the signal to a count rate yielding to a printer or computer monitor. By scanning the sample within a space of  $2\theta$  angles, all relevant lattice diffraction directions of the specimen can be gained. By passing the diffraction peak to d-spacing, the material can be noticed since every material has a unique d-spacing array as compared to standard reference patterns.

In this study the X-ray Diffraction spectroscopy (XRD) was measured with Bruker, D2 Phaser equipment at Surface Engineering Laboratory, International Islamic University Malaysia (IIUM) with  $CuK_{\alpha}$  radiation.

### 3.5 SUMMARY

The materials selection for electrolytes was poly(acrylamide-*co*-acrylic acid), sodium carboxymethyl cellulose (Na-CMC) and sodium sulfide (Na<sub>2</sub>S). Also, EC plasticizer was used to improve the conductivity. The chapter presents the preparation method of the electrolyte in details, as well as characterization techniques for the specimens through EIS, FTIR, and XRD.



# CHAPTER FOUR

## RESULTS AND DISCUSSIONS

### 4.1 INTRODUCTION

The outcomes of characterization (P-Na-S) and (P-Na-S)-EC electrolyte films as an ionic conductive polymer explained in this chapter. FTIR spectroscopy, Impedance spectroscopy (EIS), and XRD characterization are the three main phases to identify the experiments. The results of each sample characterizations were addressed during this investigation at each phase.

### 4.2 FTIR CHARACTERIZATIONS OF (P-NA-S) POLYME

The presence of common functional groups in the polymeric chains was distinguished by FTIR characterization. The functional group of individual and mixed materials was measured in four steps. These steps are described in detail in the following sequence.

#### 4.2.1 FTIR of Poly (Acrylamide-*co*-Acrylic Acid) Powder and Film Formation

The FTIR spectra in Figure 4.1 were used to interpret functional groups of poly(acrylamide-*co*-acrylic acid) powder and film formation. The FTIR spectra of poly(AM-*co*-AA) powder and film were measured at a wavenumber between 4000 to 400  $\text{cm}^{-1}$ .

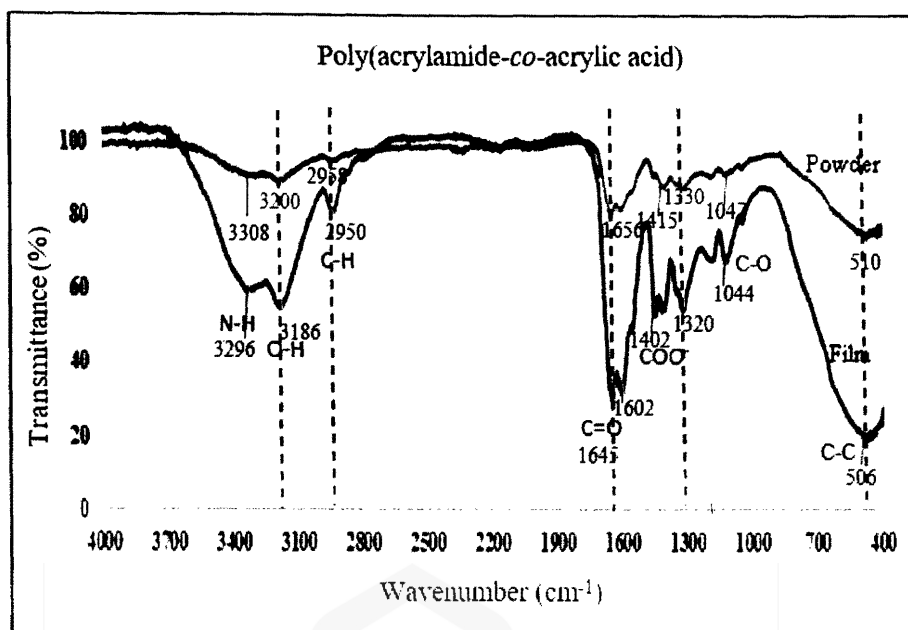


Figure 4.1: Poly (AM-co-AA) powder and film characteristic peaks

The FTIR spectra of poly(acrylamide-co-acrylic acid) powder and film formation presented in Figure 4.1. In the spectra of FTIR powder, the peaks observed were at  $3308\text{ cm}^{-1}$  corresponding to N-H stretching of acrylamide. The peaks at  $2200\text{ cm}^{-1}$ ,  $2958\text{ cm}^{-1}$ ,  $1656\text{ cm}^{-1}$ ,  $1415\text{ cm}^{-1}$ ,  $1047\text{ cm}^{-1}$  are assigned to C-H, C=O, COO, and C-O stretching, respectively. The band association affecting the vibration groups of polymeric segments by FTIR spectra. The formation of a co-polymer of acrylamide and acrylic acid is shown with the wavenumber. The broad bands that appeared indicate the formation of acrylamide and acrylic acid co-polymer. Due to N-H and O-H stretching peaks in the range of  $3296\text{--}3186\text{ cm}^{-1}$  belong to polyacrylamide and poly(acrylic acid) respectively.

1. Asymmetrical and symmetrical stretching of C-H band was found in the symmetric group dipole moment changes considerably are going in and out at the same time and asymmetric stretch going in opposite directions at  $2927$  and  $2950\text{ cm}^{-1}$ , respectively.

2. Carbonyl stretching vibration C=O connected to the carboxyl group gives an absorption peak at  $1678\text{ cm}^{-1}$  in poly(AM-co-AA). This peak C=O group connected to the amide group gives absorption peak at  $1602\text{ cm}^{-1}$  in poly (AM).
3. Symmetric and asymmetric COO<sup>-</sup> stretching, found in poly(AM-co-AA) spectra at  $11405\text{ cm}^{-1}$  and  $1402\text{ cm}^{-1}$  respectively.
4. The peak at  $506\text{ cm}^{-1}$  belong to C-C of amid group.

Table 4.1 FTIR spectra of poly(AM-co-AA) by wavenumbers powder and film formation.

Table 4.1: poly(AM-co-AA) functional groups powder and film

Functional group	Powder Wavenumber ( $\text{cm}^{-1}$ )	Film formation Wavenumber( $\text{cm}^{-1}$ )	References
N-H	3308	3296	Nesrinne & Djamel, 2017)
O-H	3200	3186	
C-H	2958	2950	
C=O	1656	1645	(Erizal, 2012)
COO	1415	1402	(Şolpan et al., 2003)
C-O	1047	1044	
C-C	510	506	

These results indicate that during the polymerization process, the carboxylic groups of poly (AA) are dissociated into COO<sup>-</sup>, which then forms co-polymer complexes with the cationic groups of poly (AM) through electrostatic interaction (Solpan et al., 2003).

#### 4.2.2 FTIR of Powder and Film Formation Sodium Cellulose Carboxylic (Na-CMC)

The following FTIR phase, initiated by Na-CMC powder and film to distinguish the functional group which can be seen in Figure 4.2.

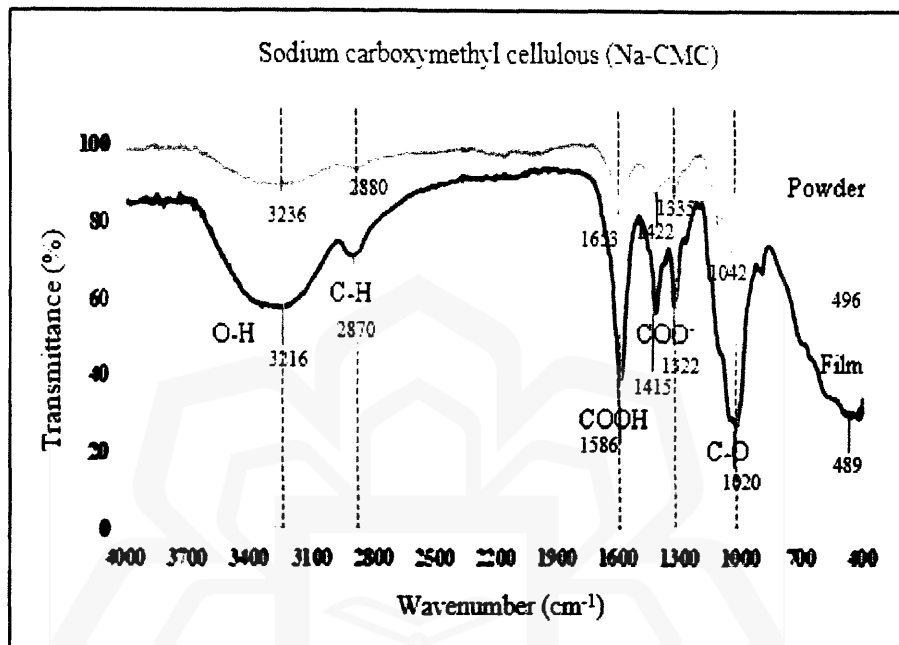


Figure 4.2: FTIR spectra of Na-CMC powder and film

The FTIR spectra of Na-CMC powder presents in Figure 4.2. The band at  $3236\text{ cm}^{-1}$  appear due to the O-H group. The band at  $2880\text{ cm}^{-1}$  assigned to C-H group. The peak at  $1653\text{ cm}^{-1}$  shows carboxymethyl ether group. The band about  $1422\text{ cm}^{-1}$  and  $1335\text{ cm}^{-1}$  assigned to  $\text{CH}_2$  group. The band at  $1042\text{ cm}^{-1}$  is due to COO group.

Also, in Figure 4.2 illustrates the FTIR spectra of Na-CMC film as follow:

1. The broad band at  $3216\text{ cm}^{-1}$  assigned to the hydroxide layer O-H stretch. Assigned to band interaction of hydrogen bonding for hydroxyl stretching.
2. At  $2870\text{ cm}^{-1}$ , the C-H bound stretching to the ring carbon hydrogen atoms appeared.

3. vibration of COOH of carboxylate groups take the lead at  $1586\text{ cm}^{-1}$ .
4. In addition, the symmetric and asymmetric bands are assigned to -COO- stretching in carbonyl groups at  $1322$  and  $1020\text{ cm}^{-1}$  region (Luna-Martinez et al., 2011).
5. The band  $489\text{ cm}^{-1}$  belong to nanocomposite material carbon base with multiphase solid film of Na-CMC.

The IR spectra of functional groups shown the founding of the peaks for powder and film formation of Sodium carboxy methyl Cellulose. The various FTIR functional groups with different wavenumber shown in Table 4.2.

Table 4.2: The functional groups and structural formula of Na-CMC

Functional group	Powder Wavenumber ( $\text{cm}^{-1}$ )	Film formation Wavenumber ( $\text{cm}^{-1}$ )	References
O-H	3236	3216	(Sunardi, 2017)
C-H	2880	2870	(Lopez et al., 2015)
COOH	1653	1586	(Luna-Martinez et al., 2011)
CH <sub>2</sub>	1422	1415	
CO	1335	1415	
COO	1042	1020	(Bertuzzi & Gottifredi, 2007)
C-C	496	489	

### 4.2.3 The Film Formation of Poly(Acrylamide-*co*-Acrylic Acid) and (Na-CMC) by FTIR Study

The FTIR spectra was used to characterize a film created by mixing poly(AM-*co*-AA) and Na-CMC. The IR spectra confirm the formation of poly(acrylamide-*co*-acrylic acid) and sodium cellulose carboxylic (Na-CMC).

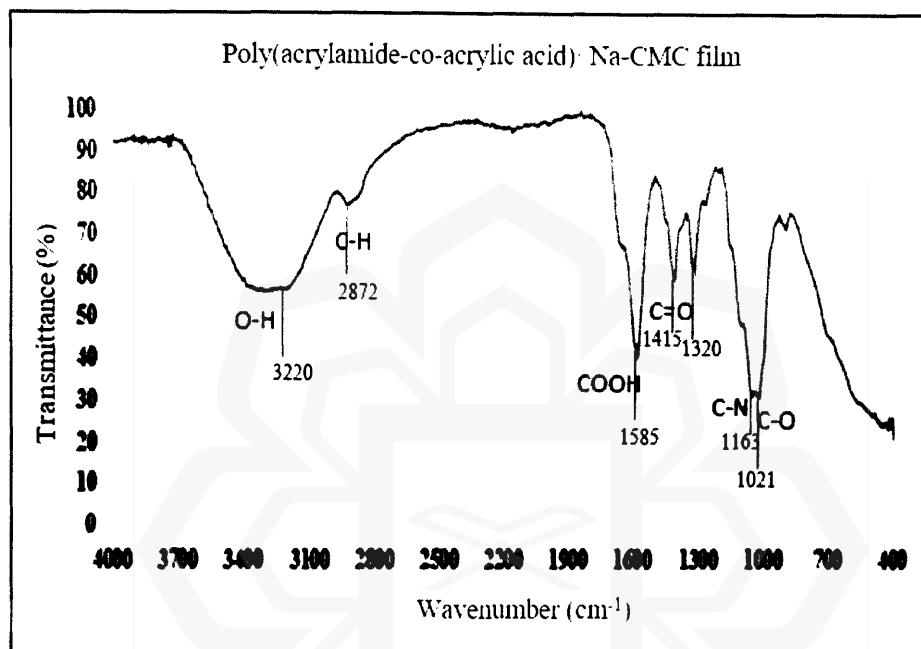


Figure 4.3: poly(AM-*co*-AA) and Na-CMC film by FTIR spectra

In Figure 4.3 shows the functional group of two blend materials with film formation.

1. FTIR spectra measurement of O-H hydroxide group assigned to broad band stretching region at about 3220 cm<sup>-1</sup>.
2. The C-H attached stretching to the circle carbon hydrogen group approximately at 2872 cm<sup>-1</sup>.
3. The stretching vibration of COOH of carboxylate assigned at 1585 cm<sup>-1</sup>.
4. The band is assigned to C=O asymmetric stretching of carboxylate anion at 1415 cm<sup>-1</sup> and another sharp peak is associated with the symmetric



stretching mode of carboxylate anion at  $1321\text{ cm}^{-1}$  (Suo et al., 2007), in the same direction of the  $\text{-C=O}$  group of acrylic acid.

The FTIR spectrum of the absorbent polymer reveals new characteristic absorption bands which stretching in carbonyl groups at  $1021\text{ cm}^{-1}$  attributed to C-O stretching. Furthermore, the band observed at  $1163\text{ cm}^{-1}$  assigned to C-N Carbon nitride stretching. Detailed that polyacrylate has carboxylic acid sources related to CMC, it could have chemical association with components of alloy materials that normally have hydroxyl groups on the surface, resulting in improved capacity retention (Masiak et al., 2007). The Table of 4.3 shown the poly(AM-co-AA) and Na-CMC functional groups by FTIR spectra.

Table 4.3: The functional groups of the Poly (AM-co-AA) and Na-CMC film

Functional group	Film formation Wavenumber ( $\text{cm}^{-1}$ )	References
O-H	3220	(Magalhães et al., 2012)
C-H	2872	
COOH	1585	(Suo et al., 2007)
COO	1415-1320	
C-N	1163	(Pourjavadi et al., 2003)
C-O	1021	

#### 4.2.4 FTIR of (P-Na-S) with Different $\text{Na}_2\text{S}$ Concentrations

The changes on vibrational modes of Na-CMC and poly(AM-co-AA) were investigated with interaction of  $\text{Na}_2\text{S}$  by comparing the samples with different  $\text{Na}_2\text{S}$  addition.

1. At this range, stretching approaches for  $\text{-CH}$  are moderately weak, the more relevant band occurs between  $1653$  to  $1394\text{ cm}^{-1}$  in samples B and C respectively

due to the uneven and concurrent stretching of the polymer correspondence COO- group.

2. The presence of the interaction band hydrogen structure was confirmed by the minimal wavelength peak in poly (AM-*co*-AA). Typical points for -C-N are set at about 1428 cm<sup>-1</sup> in sample A, for acrylamide. In sample C, the peak showing at about 1394 cm<sup>-1</sup> is due to acrylic acid by -NH<sub>2</sub> groups.
3. Next, on the Figure 4.4, the fingerprint area from sample A to D at 542 to 699 cm<sup>-1</sup> shows the probability of the -C-C-groups with a larger peak round of 617 cm<sup>-1</sup>, which is 30% salt of (P-Na-S) electrolyte.
4. For pure poly(AM-*co*-AA), the characteristic peak for sample A, B, C, D, and E are at 3325, 3272, 3435, 3175, 2969 cm<sup>-1</sup> attributed to -NH stretch acrylamide overlapped with O-H stretch acrylate with C-H and amide group C=O stretch asymmetric and symmetric COO- stretch, respectively (Nesrinne, et al., 2017; Jing et al., 2019).
5. The characteristic peaks of pure Na-CMC due to the hydroxyl group (O-H stretch), carboxylic group (C=O stretch) and ether group (C-OH stretch) are observed at 3272, 1653 and 1394 cm<sup>-1</sup> (Lin et al., 2005; Bao et al., 2011) from sample B to C, respectively.

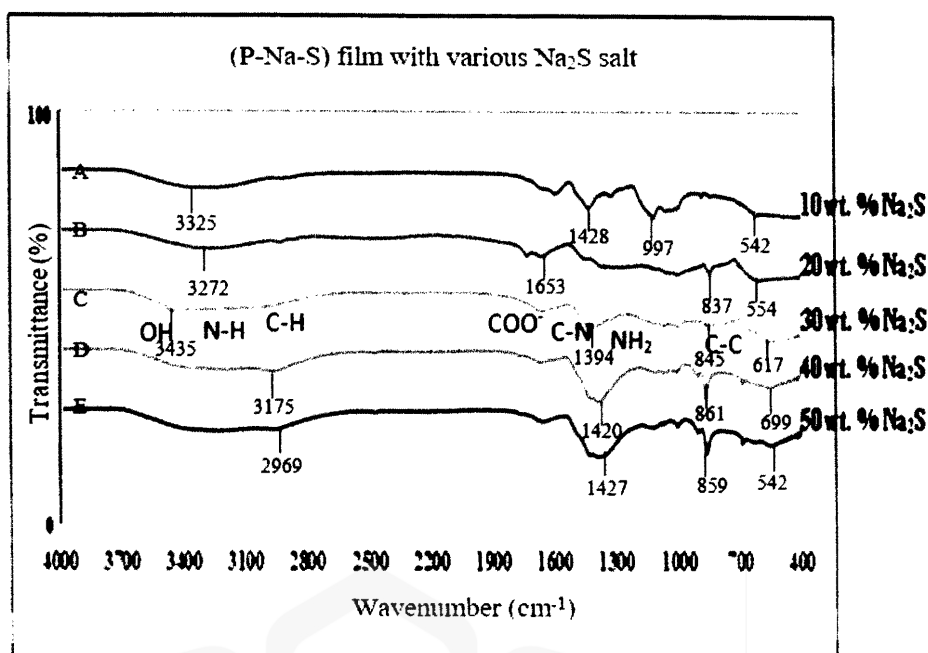


Figure 4.4: FTIR spectrum of (P-Na-S) with various wt. % salt

6. After incorporation of Na<sub>2</sub>S salt into polymer blend thin film, the O-H stretch of hydroxyl group for sample A, C and D are observed that have been shifted to higher wavenumber which is from 3325 cm<sup>-1</sup> to 3435 and 3175 cm<sup>-1</sup>, respectively.
7. In addition, the peak at O-H stretch is remain the same 3272 cm<sup>-1</sup> for sample B while shifted to lower wavenumber at 2969 cm<sup>-1</sup> to sample E. Besides, the C=O stretch of carbonyl group for sample C to E are observed that have been shifted to higher wavenumber which is from 1394 cm<sup>-1</sup> to 1427cm<sup>-1</sup>, respectively.
8. Furthermore, the C-OH stretch of ether group for sample B, C, and D, are observed that have been shifted to higher wavenumber which is from 837cm<sup>-1</sup> to 845, 861 cm<sup>-1</sup>, respectively.

A carboxyl group (C-OH) is considered a functional group that includes a hydroxyl group (O-H). carbonyl group (C=O) attached to a similar carbon atom. Since most of the peaks for all samples containing Na<sub>2</sub>S have been shifted, it can be

deduced that there is an interaction between pure polymer blend thin film based on Na-CMC and poly(AM-co-AA) and Na<sub>2</sub>S salt. These peaks showed homogeneous electrolytes of polymer salt made over all the compositions of materials. As evident from the bands labelled, the IR spectra confirm the forming of carboxylic sodium cellulose. Table 4.4 show the functional groups with wavenumbers.

Table 4.4: Functional groups of (P-Na-S) electrolyte with various Na<sub>2</sub>S

Functional group	Wavenumber (cm <sup>-1</sup> )					References
	Sample	A	B	C	D	
N-H O-H	3325	3272	3435	3175	2969	(Deka & Kumar, 2013)
C=O	1428	1653	1394	1420	1427	(Vlachy et al., 2009)
C-OH	997	837	845	861	859	(Suo et al., 2007)
C-C	542	554	617	699	542	(Suo et al., 2007)

Lastly, in Figure 4.4, the absorption range increases from 542 cm<sup>-1</sup> sample A till 617 cm<sup>-1</sup> to sample C, when added the salt from 10 to 30 wt.% Na<sub>2</sub>S. Furthermore, by adding more salt, the peak shifted from 617 cm<sup>-1</sup> to 699 cm<sup>-1</sup> wavelengths to the solid surface with more salt concentrations from sample C to D, respectively.

#### 4.2.5 FTIR Characterizations of (P-Na-S)-EC Plasticizer

The plasticizing of the (P-Na-S) electrolyte by Ethylene carbonate (EC) to improve electrolyte conductivity. FTIR spectroscopy, used for the experimental research and functional groups of (P-Na-S)-EC.

Figure 4.5 shows the FTIR spectra of (P-Na-S)-EC polymer plasticizer complexes. The various EC concentrations by (10, 20, 30, 40, and 50 wt.%) shows the FTIR peaks of factional group in polymeric chains through different ethylene carbonate (EC) addition.

To check the interaction among poly(acrylamide-*co*-acrylic acid) and sodium carboxylic callous (Na-CMC) with Na<sub>2</sub>S and EC plasticizer, the FTIR spectra of the samples studied. The absorption spectra confirm the formation of (P-Na-S) -(EC) as an evident from bands that listed in the Table 4.5.

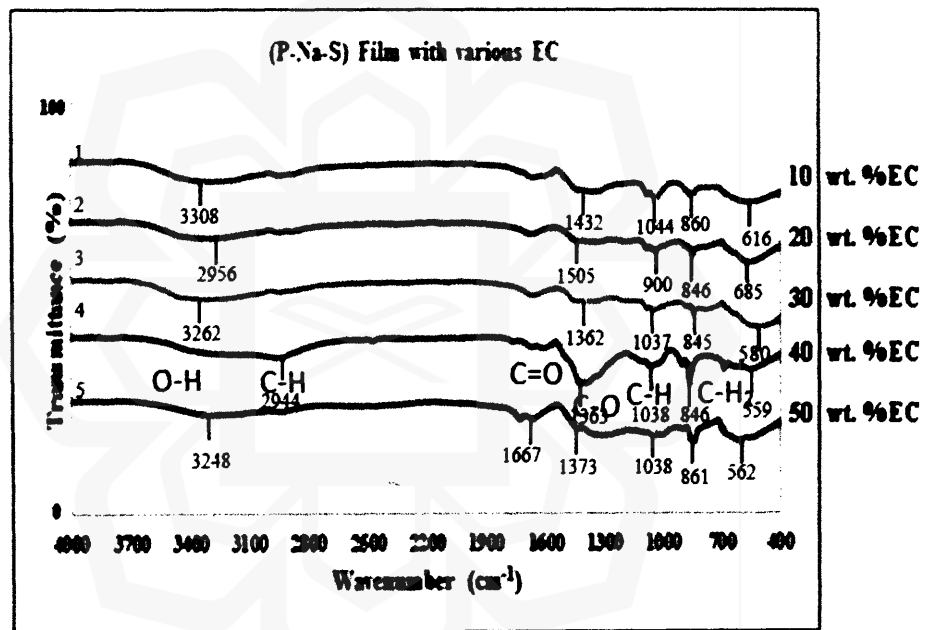


Figure 4.5: FTIR spectroscopy of (P-Na-S)-EC various plasticizers

1. In the polymer electrolytes, the C-O stretching vibration of the plasticizer took place at 1363 cm<sup>-1</sup> appear at 40 wt. % EC sample (4).
2. Also, the highest peak at 2944 cm<sup>-1</sup> closely comes next by peaks at 1363 and 1038 cm<sup>-1</sup> attributed to the C-O stretching and C-H of (P-Na-S)-EC (Balan et al., 2019) from the sample (4).

3. The  $580\text{ cm}^{-1}$  band belong to EC, and  $559\text{ cm}^{-1}$  has changed to  $562$  upon addition plasticizer assigned to C-H<sub>2</sub> (from sample 4 to 5) due to the rise of EC from 40 to 50 wt. %.

This shows occurred the polymer plasticizer complexation. The chemical formula of all materials and the functional groups are presented in Table 4.5.

Table 4.5: Functional group through various EC

Functional group	Wavenumber ( $\text{cm}^{-1}$ )					References
	1	2	3	4	5	
Sample	1	2	3	4	5	(Balan et al., 2019)
OH	3308	2956	3265	2944	3248	(Rahmani et al., 2011)
C=O	1432	1505	1362	1363	1373	(Ramesh & Ling, 2010)
C-H	1044	900	1037	1038	1038	
C-O	860	846	845	846	861	
CH <sub>2</sub>	616	685	580	559	562	

#### 4.2.6 The Comparison of FTIR Results for Both Electrolytes

- (i) The Figure 4.4 illustrates the FTIR spectra of (P-Na-S) by various Na<sub>2</sub>S salts:
- 1- Spreading of the O-H group and NH group indicates the possibility of - NH existence and - OH on sulphonic acid around the range.
  - 2- The stretching of -CH moderately is weak, which is shown decrease the polymer to stretch the dangling chain slightly.

3- The group of  $\text{COO}^-$  reveals irregular movement and simultaneously stretches around the range. The fingerprint area shows a probability of a C-C group include a broad peak at 30 wt.%  $\text{Na}_2\text{S}$  salts.

These peaks indicate that all blend compositions produce homogeneous polymer salt electrolytes.

**(ii)** The fixed sulfide ( $\text{Na}_2\text{S}$ ) salt and various (EC) plasticizers to new peaks are observed by Figure 4.5 as follow:

- 1- From the range down to up of 30, 20, to 10 wt.% EC, the band around  $760\text{ cm}^{-1}$  vanished because of less EC. Therefore, extra peaks in EC become visible and transformed from the sample (4) to (5) by 40 to 50 wt.% EC attributed to C-H<sub>2</sub> group.
- 2- In 40 wt.% plasticizer, the C-O group seems to stretch vibration in the sample (4).
- 3- The outstanding peaks are matching to O-H stretching group and the C-H in all samples.
- 4- The greater important broadband chain polymeric attributed to the C-O stretching vibration by 40 wt.% EC in the sample (4).

Observing these peaks illustrates that polymer salt plasticizer has taken place.

## 4.3 ELECTROCHEMICAL IMPEDANCE SPECTROSCOPY (EIS)

### 4.3.1 Conductivity Measurement of (P-Na-S) Electrolyte

To evaluate the conductivity of a polymer electrolyte film, EIS have been conducted. The composition of (P-Na-S) electrolytes characterized with various salt concentrations. The Figures of 4.6 to 4.10 shown the Col-Col plot with bulk resistance of (10, 20, 30, 40, and 50 wt.%) salt additions in the electrolyte.

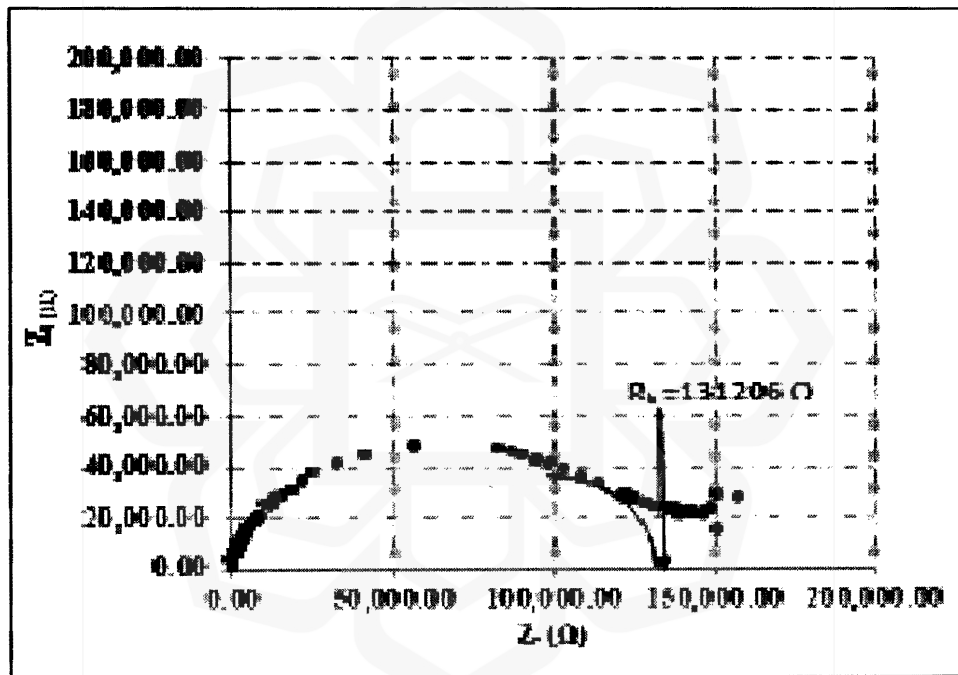


Figure 4.6: The Cole-Cole plot show the bulk resistance  $R_b$  of a 10%  $\text{Na}_2\text{S}$  salt



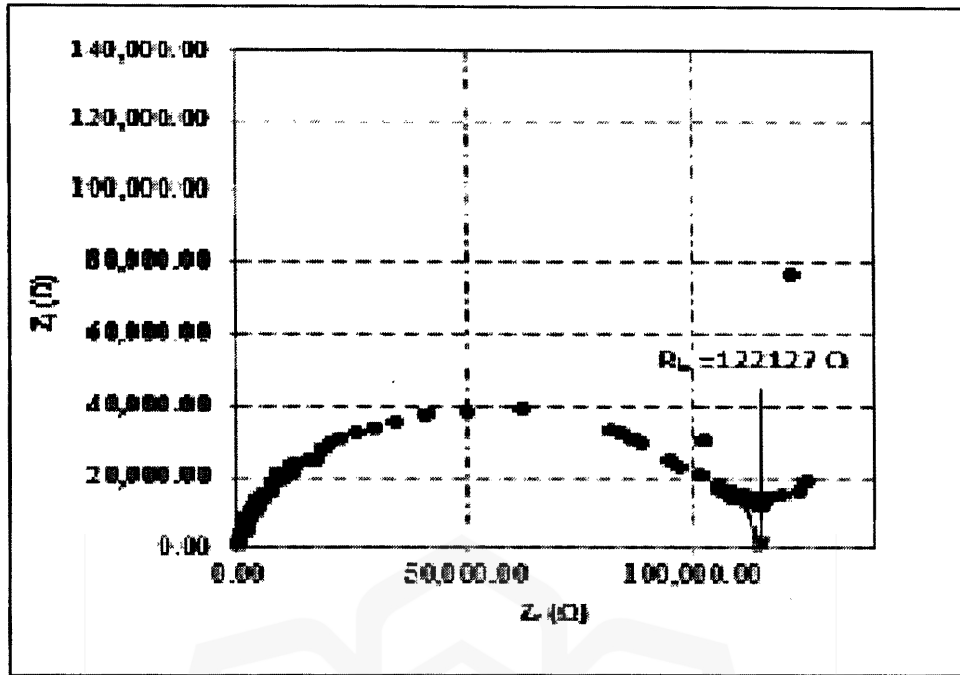


Figure 4.7: The Cole-Cole plot show the bulk resistance  $R_b$  of a 20% Na<sub>2</sub>S salt

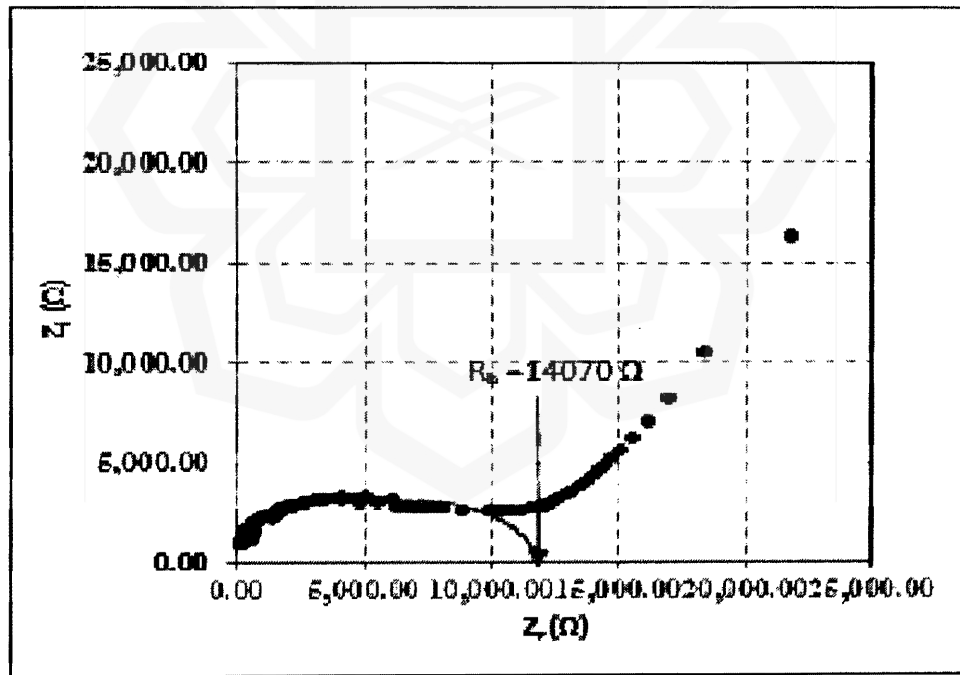


Figure 4.8: The Cole-Cole plot show the bulk resistance  $R_b$  of a 30% Na<sub>2</sub>S salt

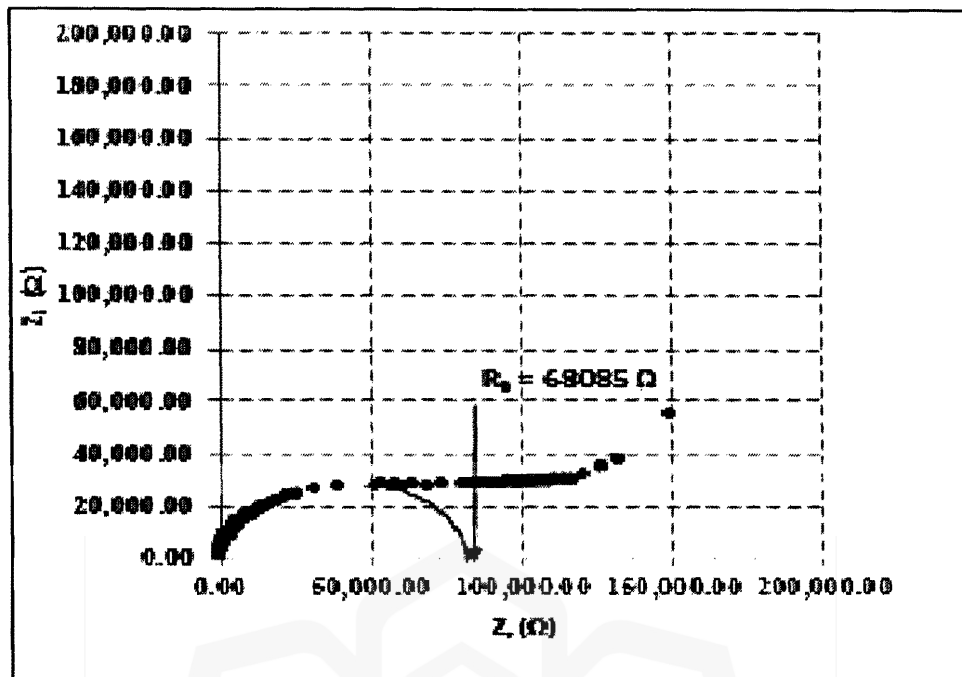


Figure 4.9: The Cole-Cole plot show the bulk resistance  $R_b$  of a 40%  $\text{Na}_2\text{S}$  salt

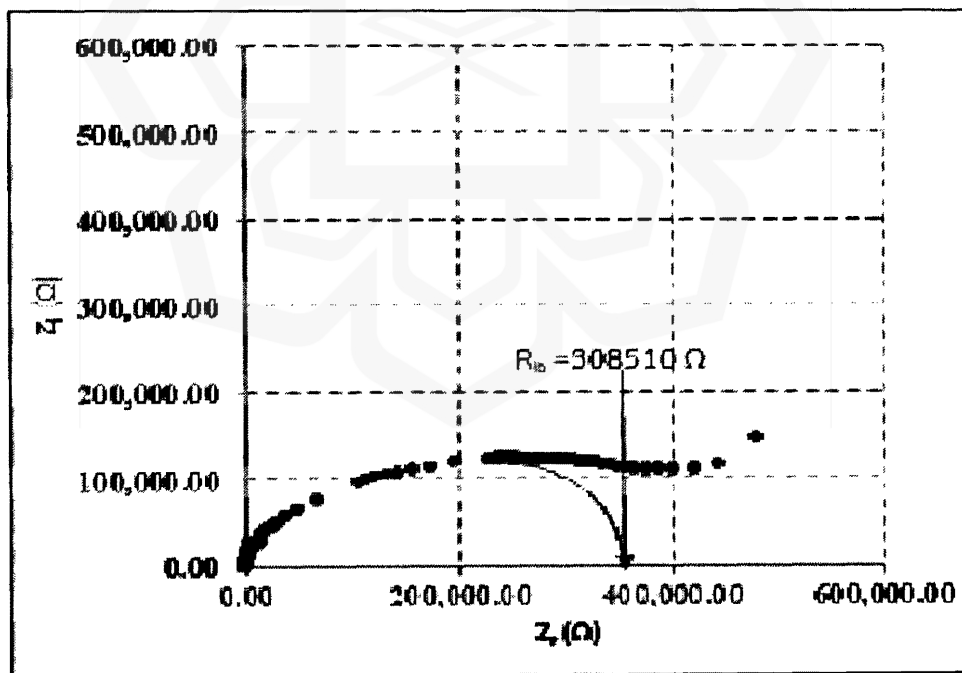


Figure 4.10: The Cole-Cole plot show the bulk resistance  $R_b$  of a 50%  $\text{Na}_2\text{S}$  salt

Figure 4.11 shows the conductivity related to salt concentrations. It illustrates for 10, 20, 30, 40, and 50 wt.% salt content to the (P-Na-S) electrolytes at room temperature.

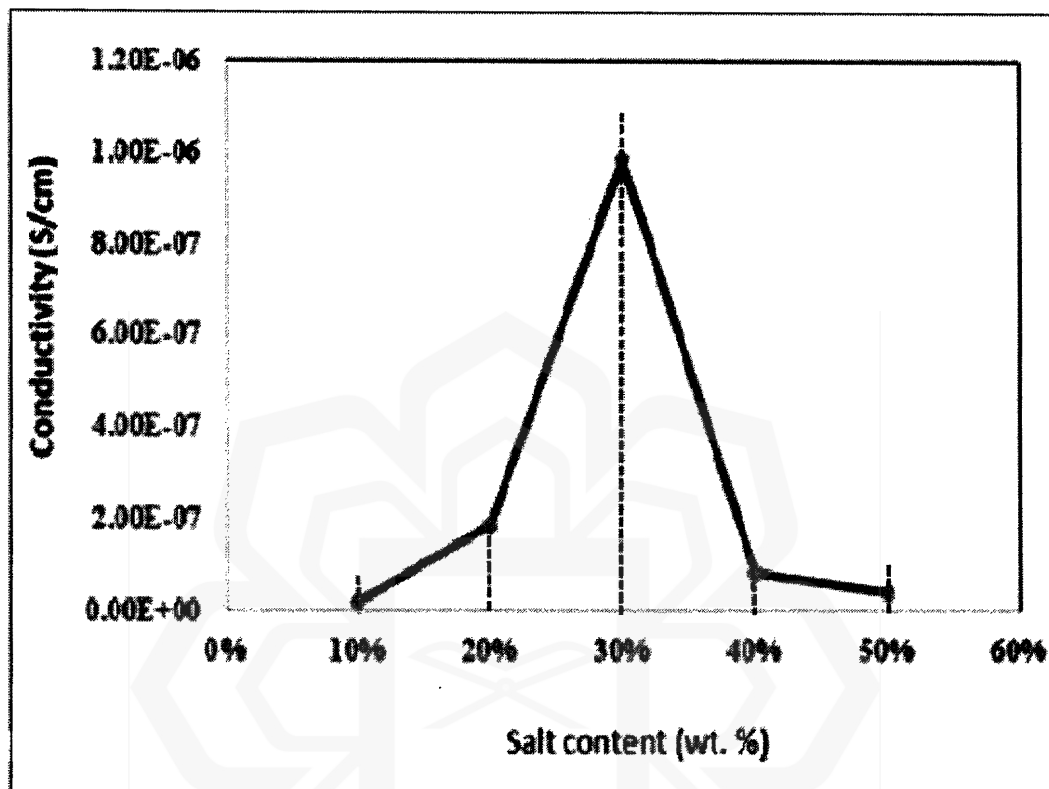


Figure 4.11: The conductivity by various wt.%  $\text{Na}_2\text{S}$  salt shown at room temperature

The conductivity of (P-Na-S) electrolyte film improved when added 30 wt.%  $\text{Na}_2\text{S}$ . Then, the conductivity decreased over 30 wt.% salt. There is a close relationship between the ionic conductivity and the solubility of integrated salt. The solubility around charge-transport ions will decrease with the addition of  $\text{Na}_2\text{S}$ , resulting in increased ion mobility. However, (P-Na-S) electrolyte films augmented because the effect of certain  $\text{Na}_2\text{S}$  salt. When increasing the  $\text{Na}_2\text{S}$  content more than 30 wt.% ion aggregation occurs, which causing lowering the number density of mobile ions. As a result, by rising the salt more than 30 wt.%, the conductivity dropped.

Table 4.5 shows the (P-Na-S) electrolyte conductivity of 5 different sample by various Na<sub>2</sub>S salt concentration at room temperature.

Table 4.6: The conductivity of various salt concentration at room temperature

Na <sub>2</sub> S salt (wt.%)	Conductivity ( $\sigma$ ) Scm <sup>-1</sup>
10	$(1.49 \pm 1.73) \times 10^{-8}$
20	$(1.89 \pm 3.29) \times 10^{-8}$
30	$(9.82 \pm 1.51) \times 10^{-7}$ *
40	$(8.42 \pm 1.01) \times 10^{-8}$
50	$(4.08 \pm 5.54) \times 10^{-8}$

The highest conductivity take place by 30 wt. % salt, which is about  $(9.82 \pm 1.51) \times 10^{-7}$  Scm<sup>-1</sup>. The polymer blend containing 30 wt. % Na<sub>2</sub>S salt shown the highest conductivity (\*) at room temperature. When adding the salt, will increase the conductivity with more ion movement. This process continues till the high level of concentration, then limit the ions free to travel. As a result, the conductivity reduces as the salt concentration increased.

#### 4.3.2 Conductivity Measurement of (P-Na-S)-EC Electrolyte

This part the different amounts of EC were added to the (P-Na-S) electrolytes and then conductivity was measured by EIS. The composition of (P-Na-S)-EC electrolytes characterized with various EC concentrations. The Figures of 4.12 to 4.16 shown the Col-Col plot with bulk resistance of (10, 20, 30, 40, and 50 wt.%) EC additions in the

electrolyte. In addition, the Figures show how the bulk resistance ( $R_b$ ) was evaluated for (10, 20, 30, 40, and 50 wt.%) EC sample plasticizers for solid polymer electrolytes.

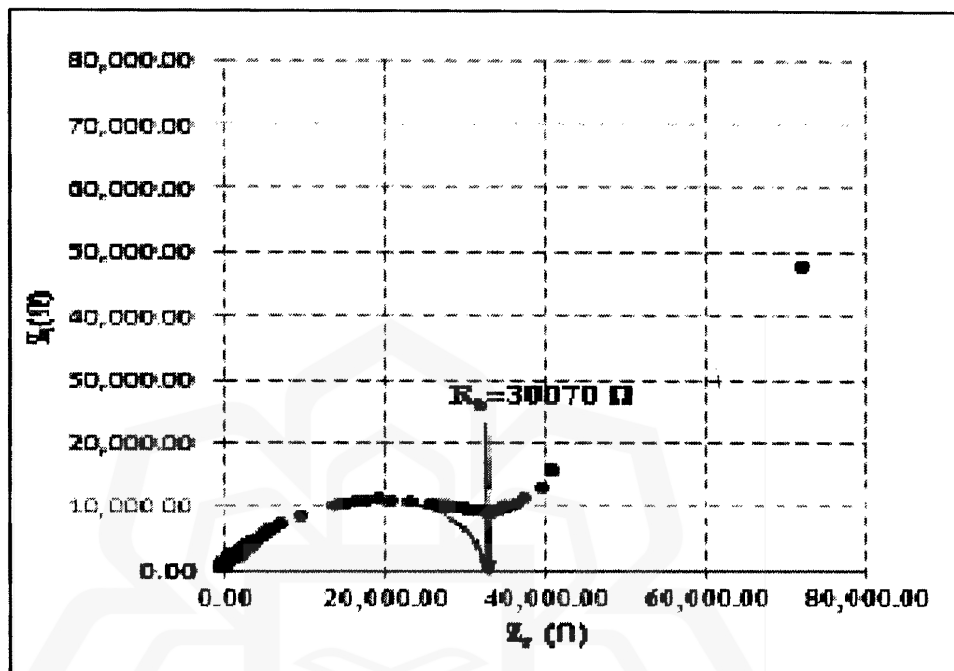


Figure 4.12: The Cole-Cole plot illustrates the bulk resistance  $R_b$  by 10 wt.% EC

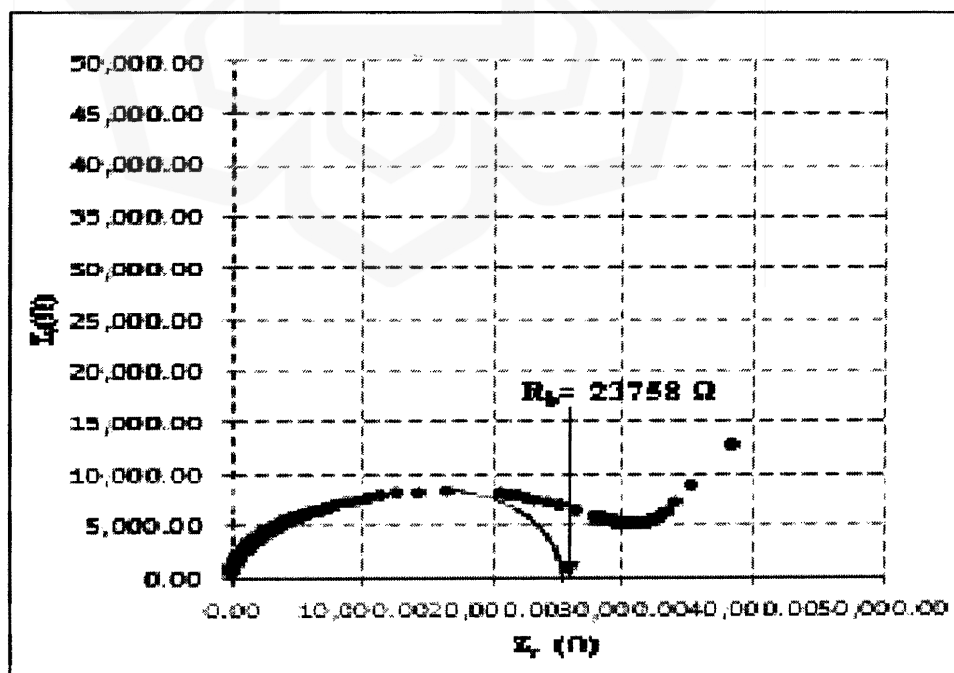


Figure 4.13: The Cole-Cole plot illustrates the bulk resistance  $R_b$  by 20 wt.% EC

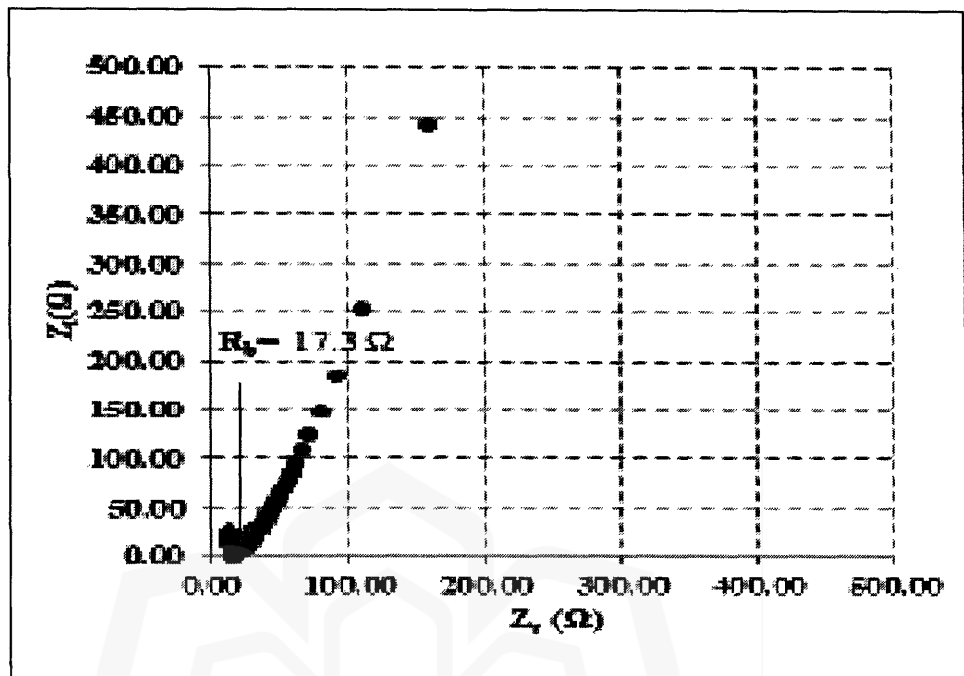


Figure 4.14: The Cole-Cole plot illustrates the bulk resistance  $R_b$  by 30 wt.% EC

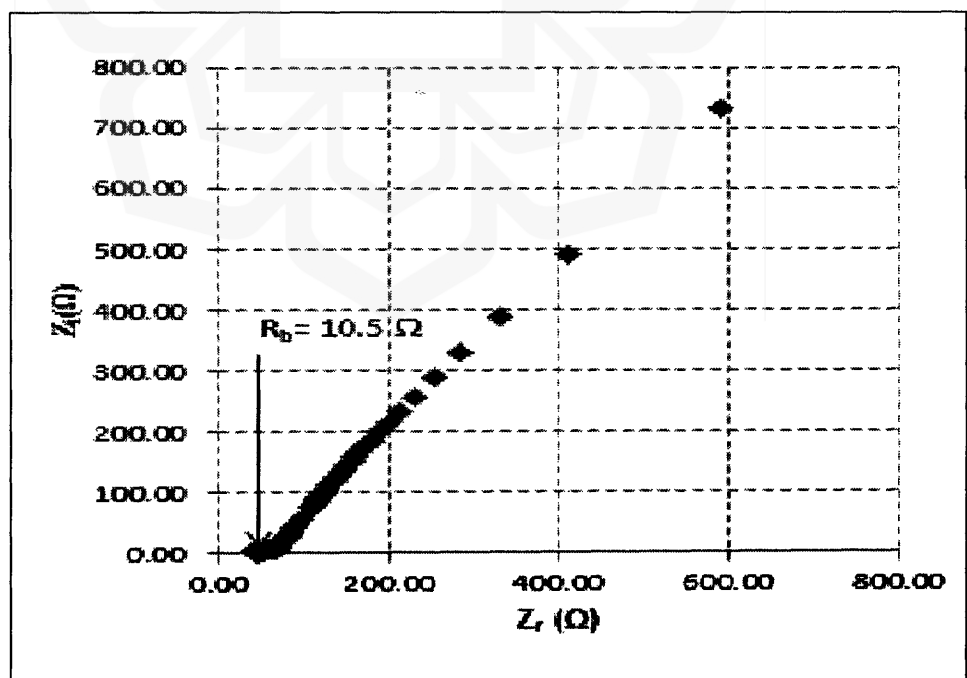


Figure 4.15: The Cole-Cole plot illustrates the bulk resistance  $R_b$  by 40 wt.% EC

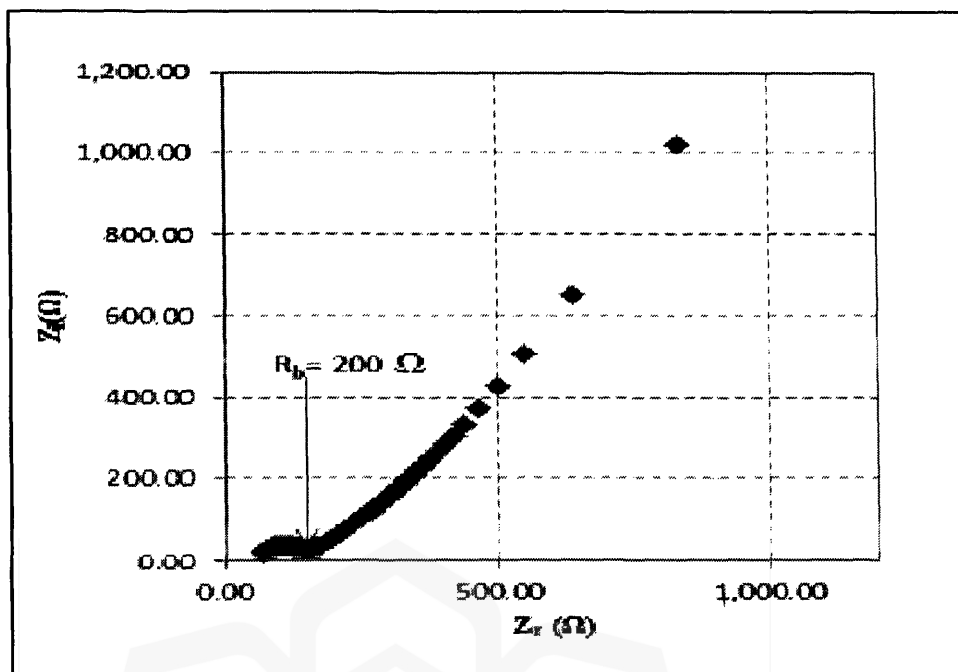


Figure 4.16: The Cole-Cole plot illustrates the bulk resistance  $R_b$  by 50 wt.% EC

Less electrical resistivity of bulk resistance ( $R_b$ ) reflects a highest conductivity ( $\sigma$ ) by 40wt. % EC in the electrolytes based on the Cole-Cole plot in Figure 5.5.

Figure 4.17 shows the various conductivity of ionic (P-Na-S)-EC plasticizer electrolyte at room temperature. The (P-Na-S)-EC film electrolyte has a highest conductivity about  $(2.74 \pm 2.52) \times 10^{-4} \text{ S.cm}^{-1}$  by 40wt.% of EC plasticizer.

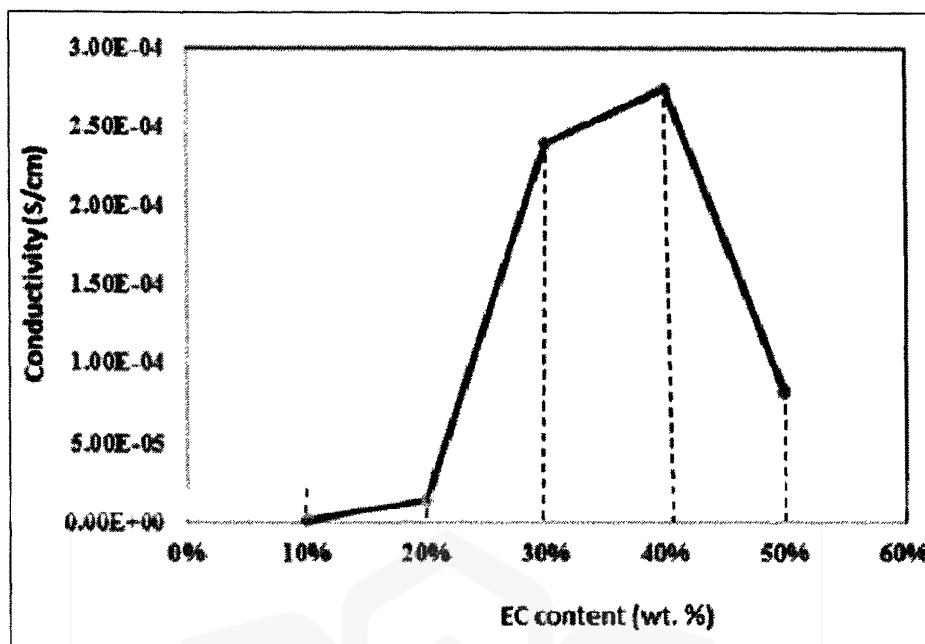


Figure 4.17: The different conductivity by various wt.% EC shown at room temperature

The conductivity improved as the EC content increased from (10, 20, 30, 40, and 50 wt.%) until the maximum conductivity was reached the highest, and then decreased over 40 wt. % EC.

The ionic conductivity is associated to the plasticizer. The EC has a high donor number (16.4), a low molecular weight ( $88.06 \text{ g mol}^{-1}$ ), and the value of dielectric constant was ( $\epsilon = 89.6$ ) (Baharun et al., 2018). When EC added, the charge-transporting ions will be reduced and lead to increased ion mobility.

Furthermore, due to salt dissociation, the EC high dielectric features might decrease between the salt's anion and the cation. The existence of EC in the (P-Na-S) film rise with the increase of salt ions of  $\text{Na}_2\text{S}$  to the complex of the functional group of EC. This leads to an increase in ionic conductivity. However, increasing the EC content caused in ion accumulation which indicates lowering the number density of mobile ions beyond 40%. As a result, as the EC content was increased, the conductivity



decreased. (Kadir, et al., 2010). Tale 5.2 indicates the conductivity of electrolyte (P-Na-S)-EC with various sample of EC at room temperature.

Table 4.7: The conductivity of various EC' concentration at room temperature

EC (wt.%)	Conductivity ( $\sigma$ ) Scm <sup>-1</sup>
10	$(1.06 \pm 0.47) \times 10^{-6}$
20	$(1.43 \pm 0.53) \times 10^{-6}$
30	$(2.39 \pm 2.46) \times 10^{-4}$
40	$(2.74 \pm 2.52) \times 10^{-4*}$
50	$(8.19 \pm 0.54) \times 10^{-5}$

The polymer plasticizer containing 40 wt. % EC shows the highest room temperature conductivity (\*).

Ionic conductivity is found to be an important factor in polymer electrolytes containing Na<sub>2</sub>S salt and EC. The conductivity was increased with the addition of salt due to fast ion mobility. It can be deduced that higher amount of salt increases the number density of mobile ions and the maximum value attained with certain amount. Then, the addition of salt decreased the conductivity due to neutral aggregates which states by re-association of ions (Kadir et al., 2010).

The salt dissociates into ions generates pores between polymer chains and free volume space, preparing ion-transporting channels. This might be assigned to salt aggregation, resulting in crystallinity increase, squeezed ion transport channels, or reduced free volumes Na<sub>2</sub>S salt caused ion diffusion reduction.

Furthermore, the additional of EC can decline thickness of polymer round the charge transport ions, which lead to more mobile of ions. However, more EC caused aggregation of ions that make decreases in conductivity at higher EC content. (Kadir et al., 2010; Deka, & Kumar, 2013). In addition, the polymer chain was unable to effectively transfer extra salt in the EC. This process reduced ion migration and decreased the diffusion (Zhang et al., 2016).

### **4.3.3 Activation Energy Measurement**

#### **4.3.3.1 Activation energy of (P-Na-S)**

The activation energy ( $E_a$ ) is another significant parameter to consider analyzing ion migration. It signified the energy associated with ion migration at the same time. The influence of activation energy states on the desirable condition and ion migration requires smoother ion transformation. Figure 4.18 shows all plots generates for utilizing the Arrhenius equation to calculate the energy activation ( $E_a$ ) using the slope of the linear ratio.

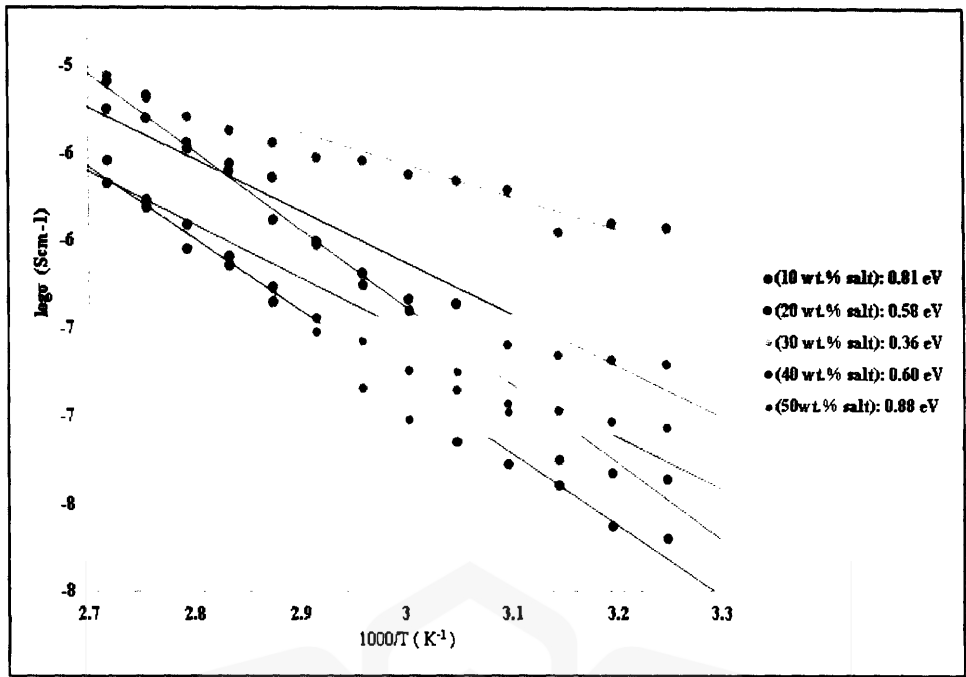


Figure 4.18: Arrhenius plot containing various ( $\text{Na}_2\text{S}$ ) via  $\ln \sigma$  versus  $1000/T$  temperature

In Figure 4.13 shows the temperature range used for various sample between 303 K to 373 K. It is logical to declare that all samples are in perfect harmony with the Arrhenius equation. It is obvious the conductivity of five samples has conducted pathways with the minimum activation energy. Table 4.6. illustrates the evaluation of activation energy based on conductivity results of the electrolyte.

Table 4.8 Activation energy of various salt concentration for the (P-Na-S) electrolyte

$\text{Na}_2\text{S}$ (wt.%) salt	Activation Energy ( $E_a$ ) (eV)
A	0.81
B	0.58
C	0.36
D	0.60
E	0.88

#### 4.3.3.2 Activation energy of (P-Na-S)-EC

The energy activation ( $E_a$ ) for (P-Na-S)-EC is measured by the gradient linear fit via  $\log \sigma$  versus  $1000/T$ . Figure 4.19 shows the value  $E_a$  fitted lines polts.

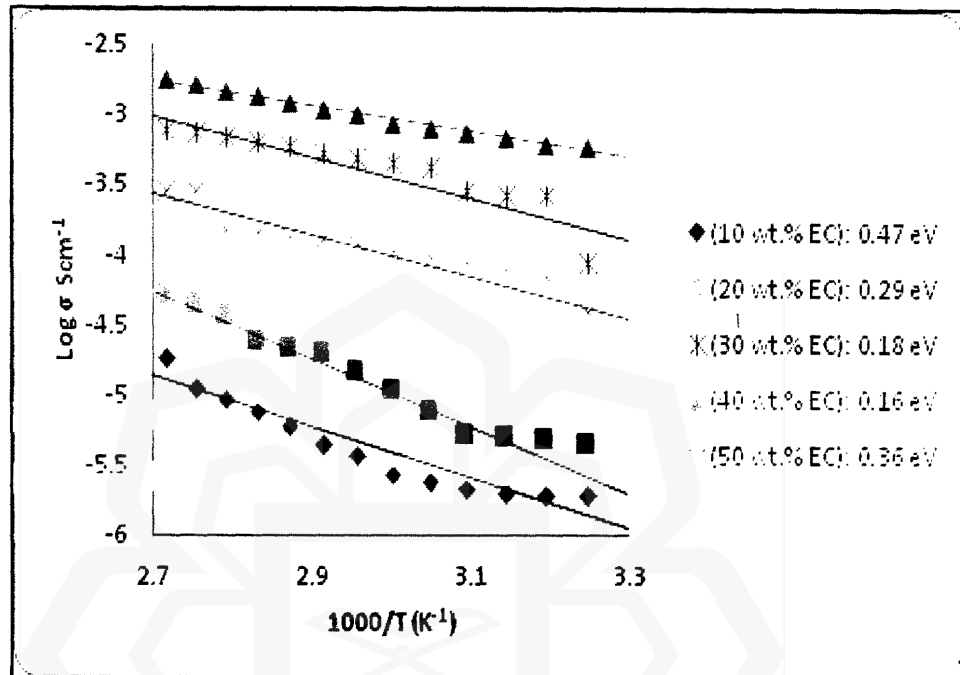


Figure 4.19: Indicates the  $\ln \sigma$  versus  $1000/T$  graphs for various EC plasticizer

The ions needed minimum energy to leap from one vacant region to another, resulting in charge conduction, known as activation energy. As a result, ion hops with a lower barrier, have the highest conductivity which discovered in the (P-Na-S)-EC electrolyte at 40 wt.% EC by activation energy. The polymer electrolytes become more amorphous as plasticizer has been added to the network of polymer. This allows for faster ion movement, leading to the increase the conductivity. The rise in number density of mobile ions is mostly due to the increased conductivity by plasticized EC. Table 419 presents comparison of conductivity and activation energy by various EC contents.

Table 4.9: Shows via various EC comparison the conductivity with activation energy

EC (wt.%)	Activation Energy ( $E_a$ ) (eV)
1	0.47
2	0.29
3	0.18
4	0.16
5	0.36

The highest conductivity of various samples was achieved by 40 wt. % EC plasticizers and lowest activation energy which shown in Table 5.3.

In the electrolyte containing salt and EC, the value of activation energy ( $E_a$ ) is lower. This indicates the longer chain or bulkier groups holding components that essential to greater energy with shorter chain compounds to overcome the energy barrier. Conductivity decreased after extra salt or EC. As seen in Table 6.1, the electrolytes of ionic conductivity (P-Na-S) indicate high value by 30%  $\text{Na}_2\text{S}$  salt. Then the highest conductivity value occurs when additional ( $\text{Na}_2\text{S}$  30 wt.% + EC 40 wt. %) mixed to the electrolyte of (P-Na-S)-EC about  $9.82 \times 10^{-7} \text{ S.cm}^{-1}$  to  $2.74 \times 10^{-4} \text{ S.cm}^{-1}$ , respectively.

Table 4.10: Energy activation and conductivity through of  $\text{Na}_2\text{S}$  salt and EC plasticizer

Factors	30 wt. % $\text{Na}_2\text{S}$	40 wt. % EC
$\sigma$ (S/cm)	$9.82 \times 10^{-7}$	$2.74 \times 10^{-4}$
$E_a$ (eV)	0.36	0.16

The energy activation of ion conduction was calculated based on the Arrhenius relation:  $\sigma = \sigma_0 \exp\left(-\frac{E_a}{RT}\right)$ . The results show that lower the energy of

activation specifies the higher ionic conductivity. The ion could easily overcome the energy barrier to move, provided that the energy activation for ion conduction was relatively lower. This improved ionic mobility and increased ionic conductivity

#### **4.4 DIELECTRIC STUDY OF (P-Na-S) ELECTROLYTE**

To examine the conductivity behavior of polymer electrolytes, we can use dielectric analysis (Aziz, 2018; Kumar & Bhat, 2009). It is considered a favorable method to examine the mechanism of ion transport and polymer segmental relaxation in polymer electrolytes. The impedance spectroscopy technique plays a key role in providing information about the electrical attributes of materials and their convergence area while conducting electrodes. The research measured the films conductivity with poly(AM-co-AA)/Na-CMC/Na<sub>2</sub>S with a frequency range from 50Hz to 1 MHz.

##### **4.4.1 Frequency Dielectric Constant ( $\epsilon_r$ ) at Selected Temperatures**

The conductivity behavior of polymer electrolytes is investigated using dielectric evaluation. The complex permittivity function is a material property that is affected by temperature, polymer electrolyte structural identity, and applied field frequency (Aziz et al., 2019; Okutan & Şentürk, 2008). Besides, depend on the chemical composition and the method of preparation (Rahaman et al., 2015; Chandran & George, 2016).

The dielectric characteristics of the sample (A, B, C, D, and E) with various Na<sub>2</sub>S salts at different temperatures from 303K to 373K are shown in figure 4.20 to 4.24.

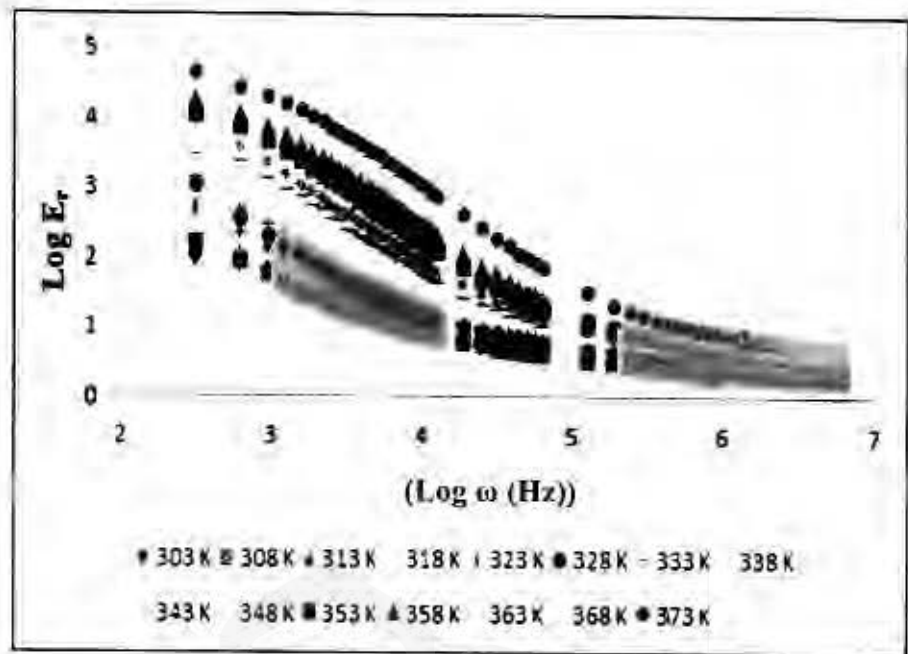


Figure 4.20: Frequency dependence of the dielectric constant ( $E_r$ ) with 10% salt of the electrolyte at different temperatures

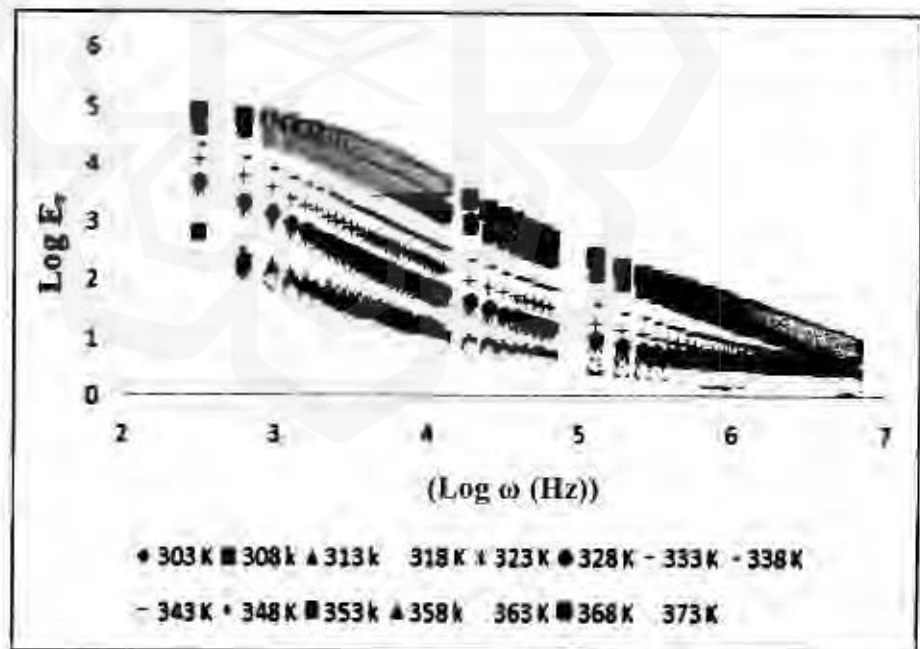


Figure 4.21: Frequency dependence of the dielectric constant ( $E_r$ ) with 20% salt of the electrolyte at different temperatures

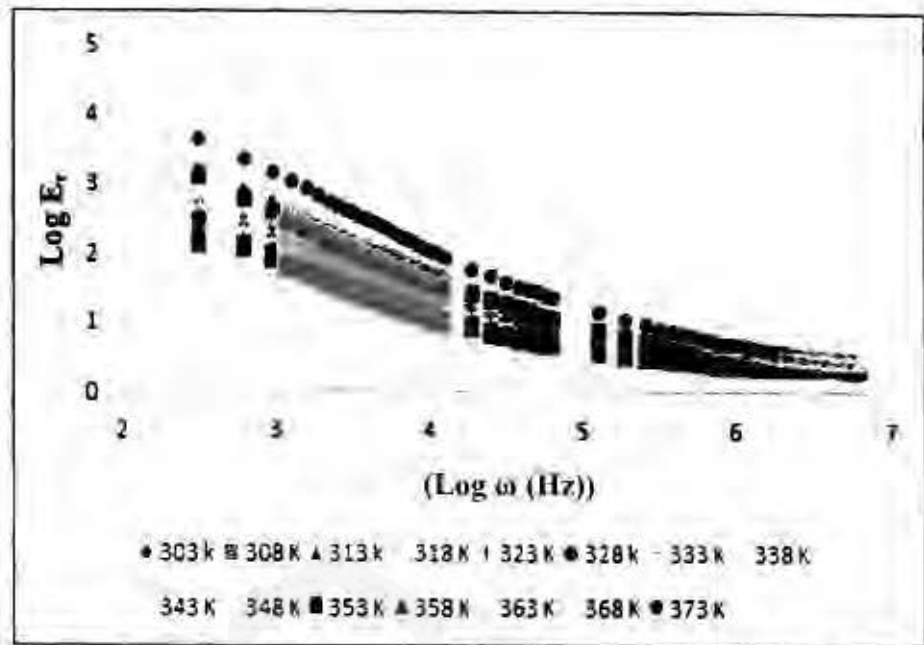


Figure 4.22: Frequency dependence of the dielectric constant ( $E_r$ ) with 30% salt of the electrolyte at different temperatures

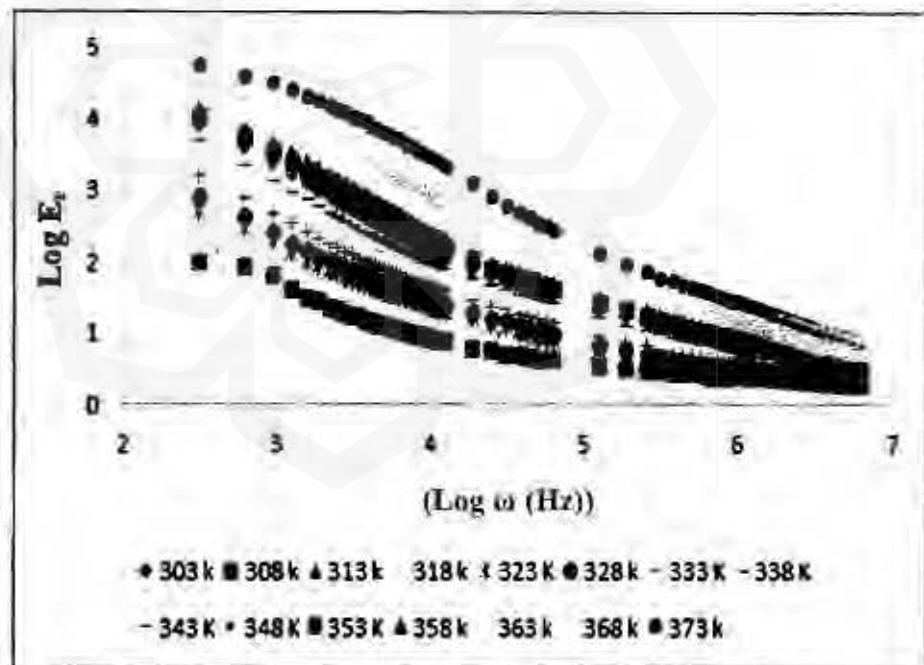


Figure 4.23: Frequency dependence of the dielectric constant ( $E_r$ ) with 40% salt of the electrolyte at different temperatures



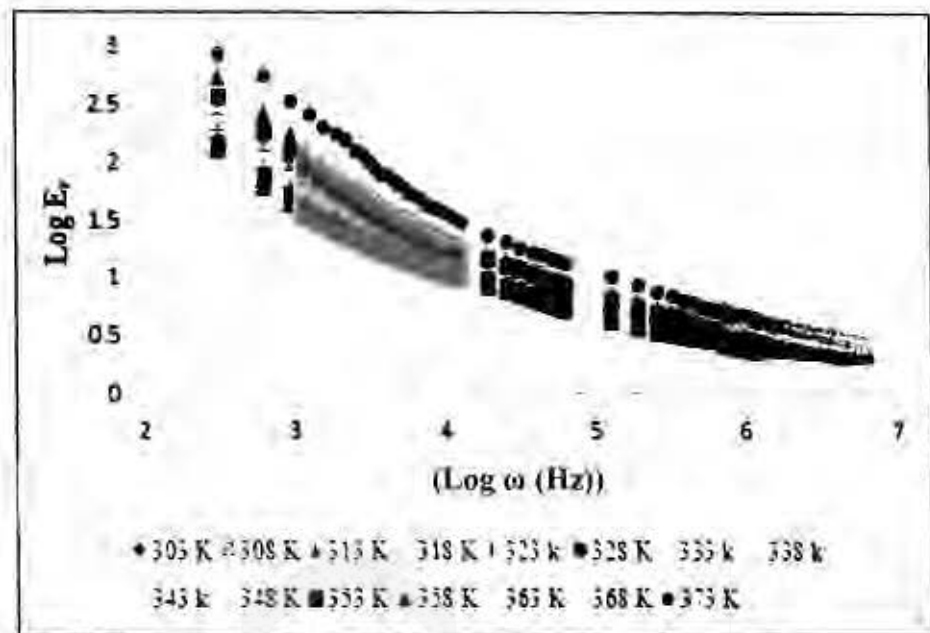


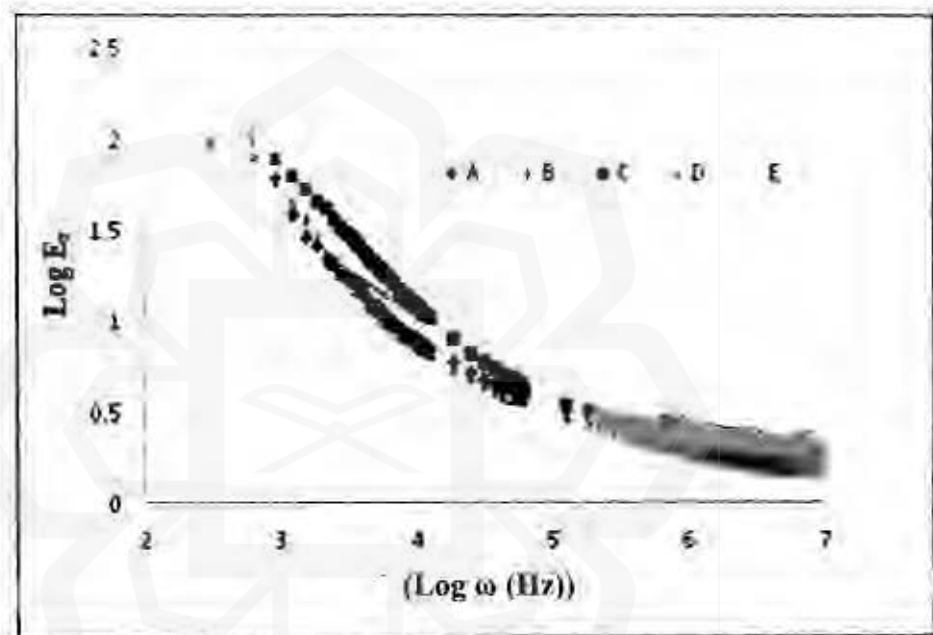
Figure 4.24: Frequency dependence of the dielectric constant ( $E_r$ ) with 50% salt of the electrolyte at different temperatures

Charge carrier density, known as carrier concentration, measured by number of charge carrier per volume. There is a long period in the low frequency region, the mobile ions tend to accumulate at the electrolyte interface, leading in electric field reversal with time. This leads to higher dielectric constant ( $E_r$ ) value. Because of the increasing in carrier density at higher temperatures, it is obvious that the values of ( $E_r$ ) increases (Nithya & Selvan, 2011). Furthermore, at high temperatures, ion aggregates re-dissociate, result in a rise in carrier density or the amount of free ions (Tamilselvi & Hema, 2014).

The dielectric constant ( $E_r$ ) reduced sharply while the frequency increased. This reduction occurs, it is because there was a decrease in space charge polarization influence. In the high-frequency region, it is found that the value of  $E_r$  is almost constant with frequency. This happens because the periodic reversal of the electric field occurred so fast, and the charge carriers did not get sufficient time to orient themselves

in the field direction. Hence, there is no excess ion diffusion in the direction of the field which led to the decrease in the values of dielectric constant (Dcraman et al., 2014). Consequently, the dielectric constant ( $\epsilon_r$ ) remained almost unchanged. However, it raised with the rising temperature at a taken frequency (303K-373K).

The frequency dependence at room temperature, on the other hand, is shown in Figure 4.25.



4.25: Frequency dependence of dielectric constant ( $\epsilon_r$ ) via samples of (P-Na-S) polymer electrolytes at room temperature

Figure 4.25 shows the dielectric constant's ( $\epsilon_r$ ) of the frequency dependence for polymer blend (P-Na-S) electrolyte. It shows there is a variation in dielectric constant with frequency for different salt concentrations. Furthermore, the slight increase in charge carriers within the polymer electrolyte was reflected in the increase in the dielectric constant ( $\epsilon_r$ ). As a result, the dielectric characteristics of the sample (A, B, C, D, and E) at room temperature are shown in Figure 4.25. For all selected samples, the

variance of the real part of the dielectric constant with frequency is around 303K temperature, as measured by  $(\log E_r)$  versus  $(\log \omega)$ .

#### 4.4.2 Frequency Dependence of Loss Tangent ( $\tan \delta$ )

The frequency dependence of permittivity and loss tangent in the presence of interfacial, ionic, and electronic polarization mechanisms. The effect of the experimental frequency range on the relaxation time spectrum is investigated in this work. Figures 4.18 to 4.22, illustrates function of frequency for loss tangent ( $\tan \delta$ ) at various temperature values to obtain a deeper understanding of the relaxation process.

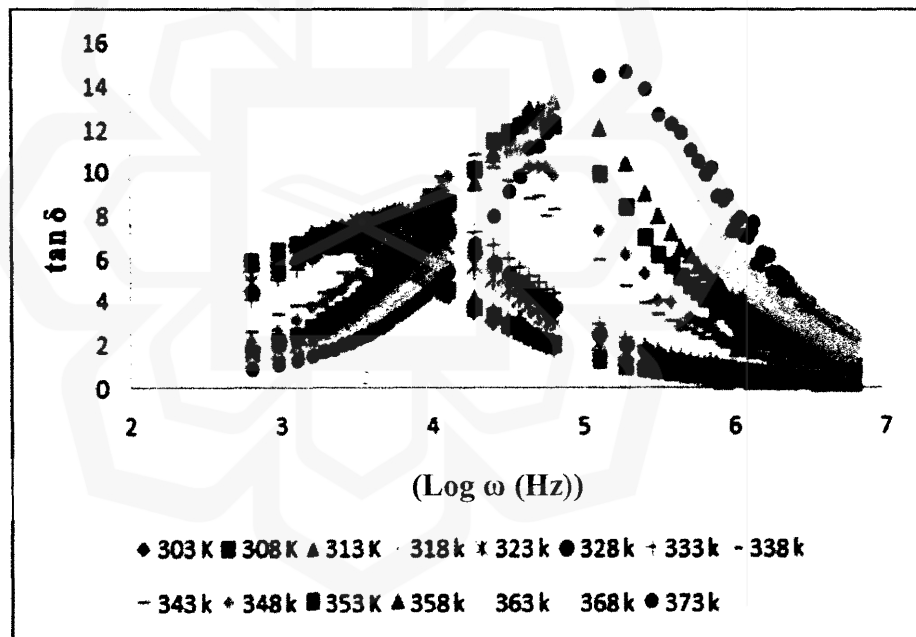


Figure 4.26: The loss tangent ( $\tan \delta$ ) of (P-Na-S) electrolyte at 10 wt.% salt with preferred temperatures

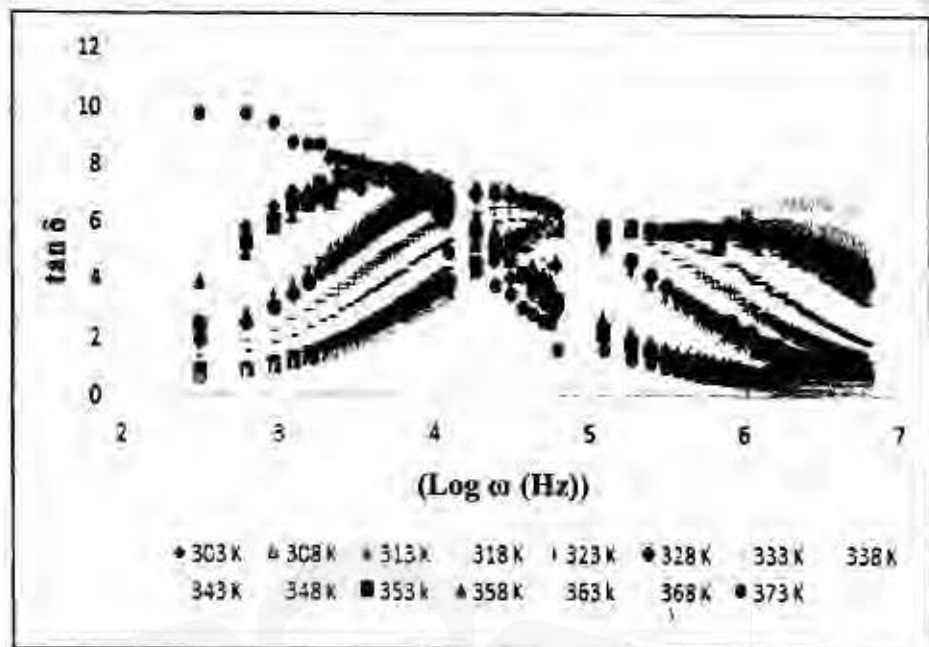


Figure 4.27: The loss tangent ( $\tan \delta$ ) of (P-Na-S) electrolyte at 20 wt.% salt with preferred temperatures

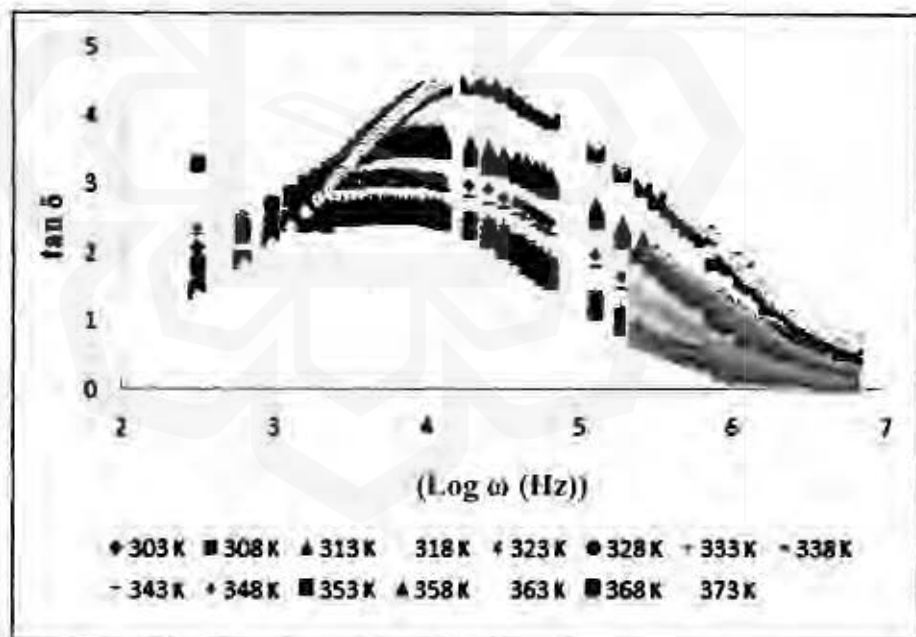


Figure 4.28: The loss tangent ( $\tan \delta$ ) of (P-Na-S) electrolyte at 30 wt.% salt with preferred temperatures

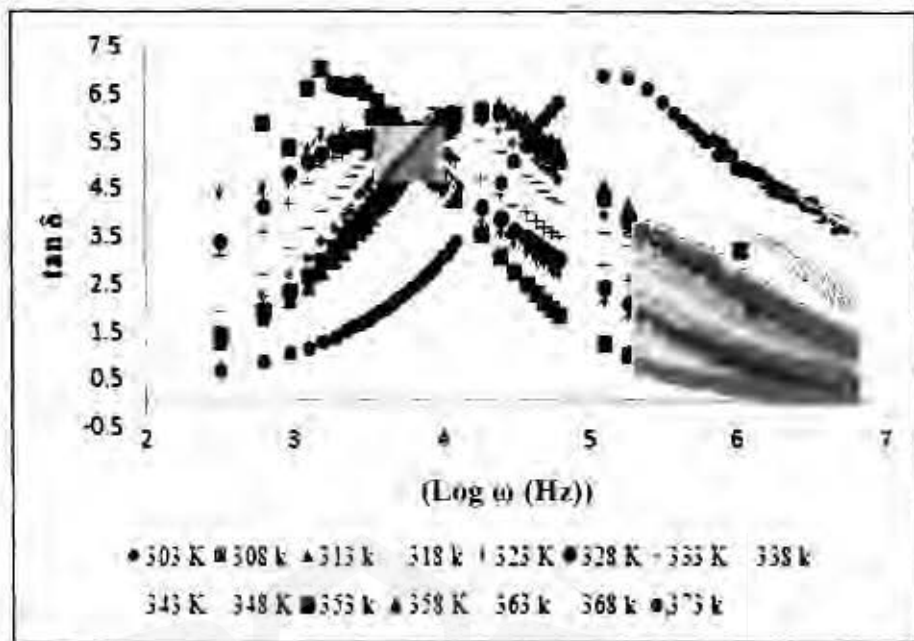


Figure 4.29: The loss tangent ( $\tan \delta$ ) of (P-Na-S) electrolyte at 40 wt.% salt with preferred temperatures

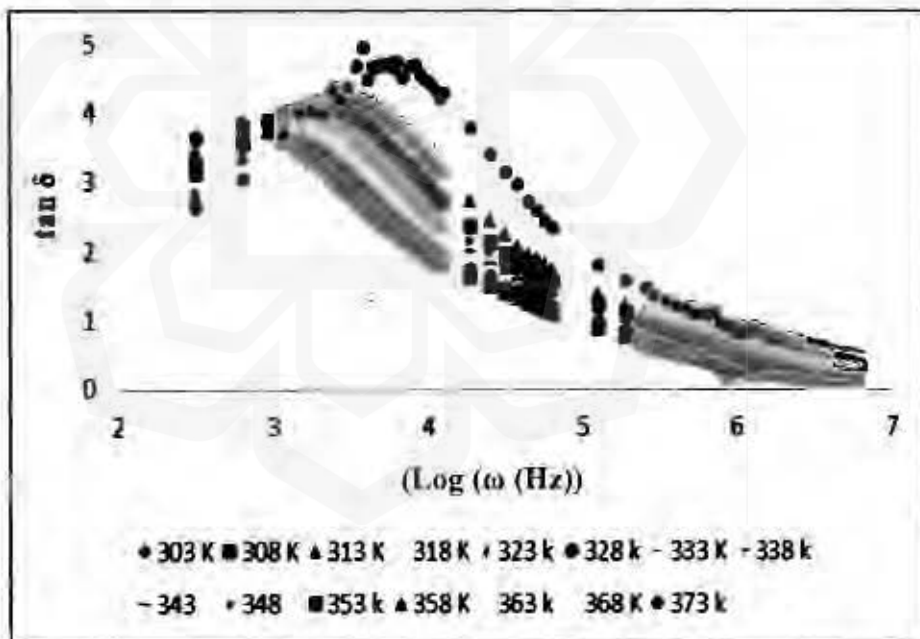


Figure 4.30: The loss tangent ( $\tan \delta$ ) of (P-Na-S) electrolyte at 50 wt.% salt with preferred temperatures

From Figures 4.26 to 4.30 it can be observed that the peaks shifted to higher frequency with temperature. It shows that the relaxation time of mobile ions decreases with the increasing temperature. The phase shift has been estimated to be particularly

small. At higher frequencies, however, the polarization is slow in the electric field. Due to the polarization relaxation time and the field duration, a resonance state is achieved when the loss tangent ( $\tan \delta$ ) is maximum (Yu, et al., 2008).

Figure 4.31 illustrates variations of loss tangent ( $\tan \delta$ ) at room temperature with frequency of the (P-Na-S) polymer electrolyte.

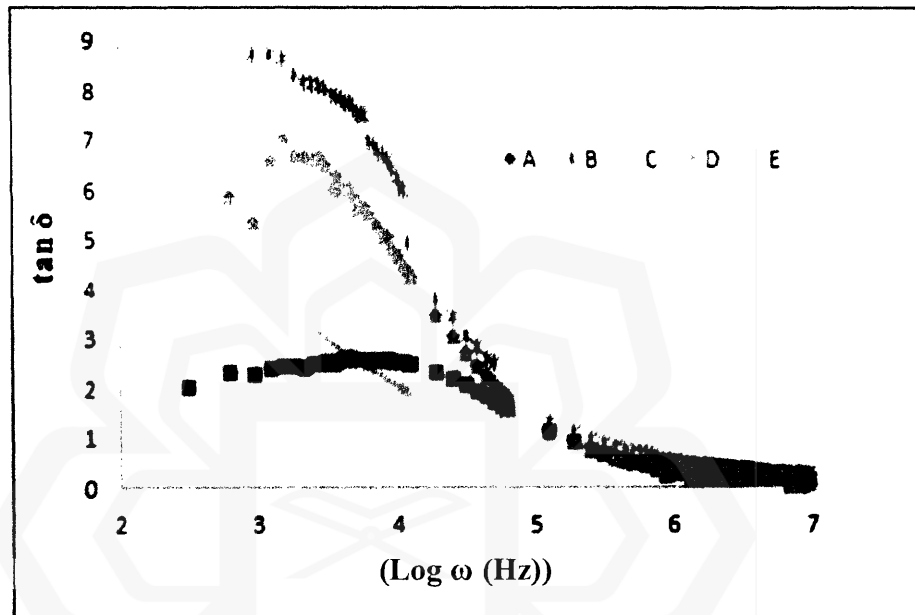


Figure 4.31: The loss tangents ( $\tan \delta$ ) variation with frequency of (P-Na-S) electrolyte at room temperature

Figure 4.31 shows when salt is added to the polymer host, the relaxation peak moves to the high-frequency side. The presence of dielectric relaxation processes and a decrease in relaxation time are evidenced by a shift in the loss peak and a movement in position.

#### 4.4.3 AC Conductivity of Dielectric Properties

The alternating-current (AC) electrical properties in the electrolyte depends not only the mobile ions which cause the direct-current (DC) conductivity but also relatively ions, or dipoles. With the calculated frequency range, the spectrum is divided into two distinct areas. The low-frequency spike is caused by space charge polarization at the blocking

electrodes and notices electrode-electrolyte interfacial phenomena (Hasegawa & Yamamoto, 1994). The conductivities frequency dependence of  $\log(\sigma_{ac})$  is shown in Figures 4.32 to 4.36.

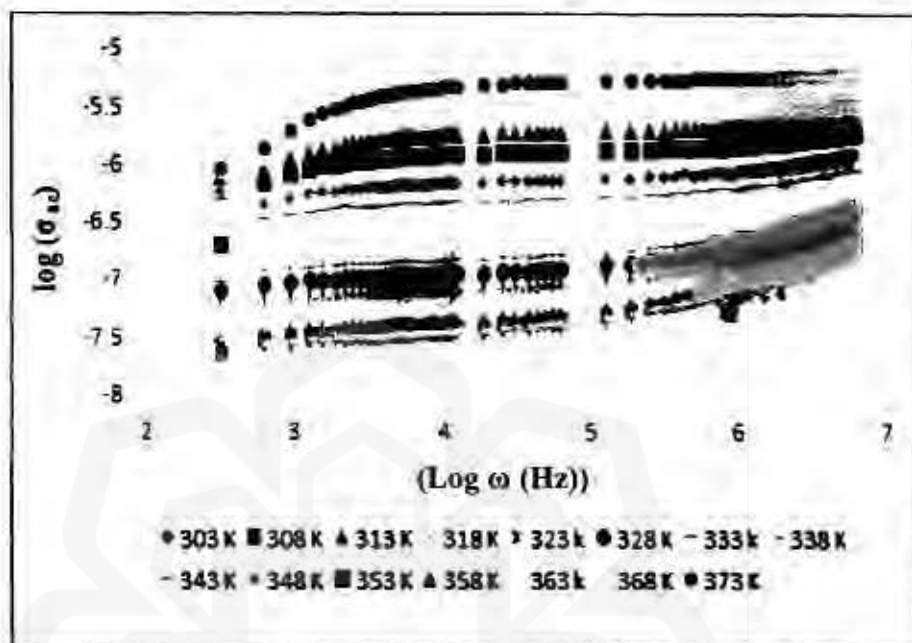


Figure 4.32. Measurement of  $\log \sigma_{ac}$  by 10 wt.% salt of (P-Na-S) at selected temperature

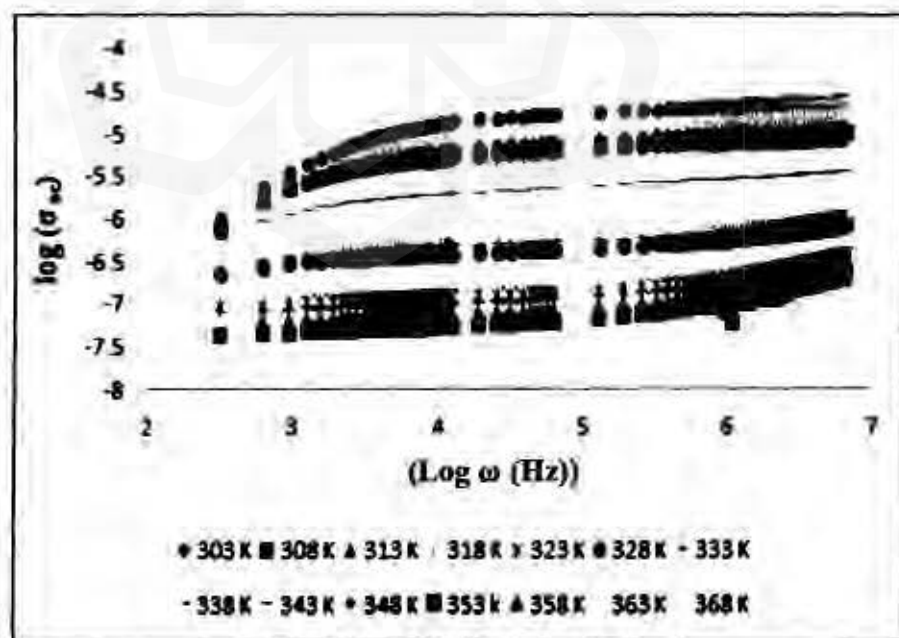


Figure 4.33. Measurement of  $\log \sigma_{ac}$  by 20 wt.% salt of (P-Na-S) at selected temperature

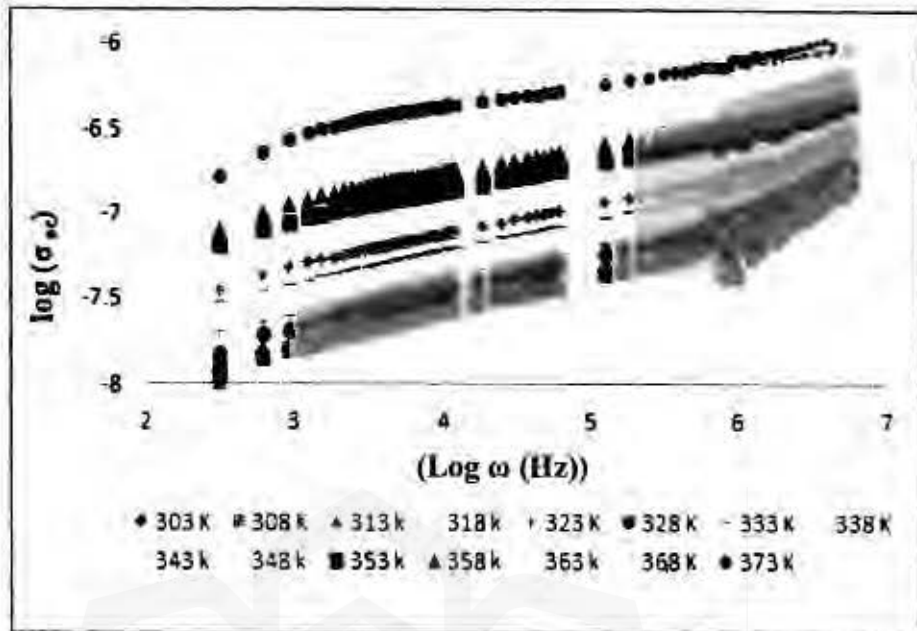


Figure 4.34: Measurement of  $\log \sigma_{ac}$  by 30 wt.% salt of (P-Na-S) at selected temperature

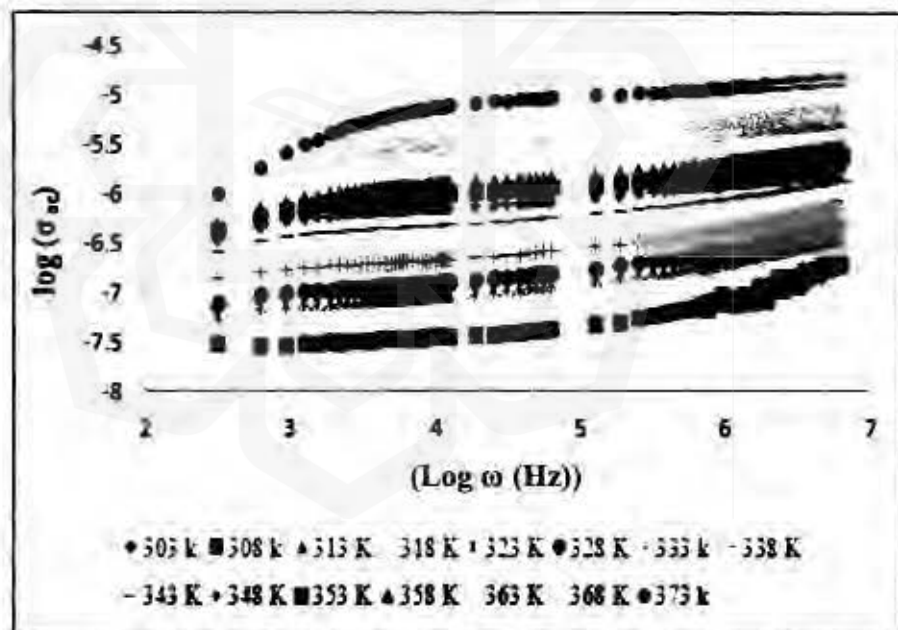


Figure 4.35: Measurement of  $\log \sigma_{ac}$  by 40 wt.% salt of (P-Na-S) at selected temperature



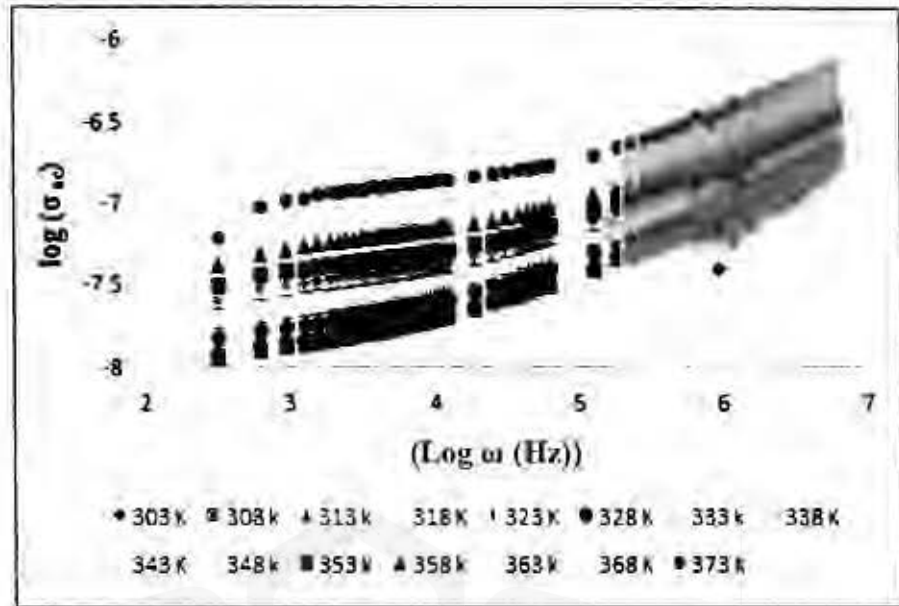


Figure 4.36: Measurement of  $\text{Log } \sigma_{ac}$  by 10 wt.% salt of (P-Na-S) at selected temperature

The complexed polymer electrolyte of DC conductivity ( $\sigma_{dc}$ ) comes next after the frequency-independent plateau area. The value of dc conductivity at all temperatures is obtained to the zero-frequency region.  $\log(\sigma_{ac})$  versus  $\text{Log}(\omega)$  seems to be linear at higher temperatures leading to dc conduction (Ramesh & Arof, 2001). The other compositions appear to have a similar pattern of dependence.

As shown in Figure 4.29, the  $\log \sigma_{ac}$  was used at room temperature for different concentrations of salt.

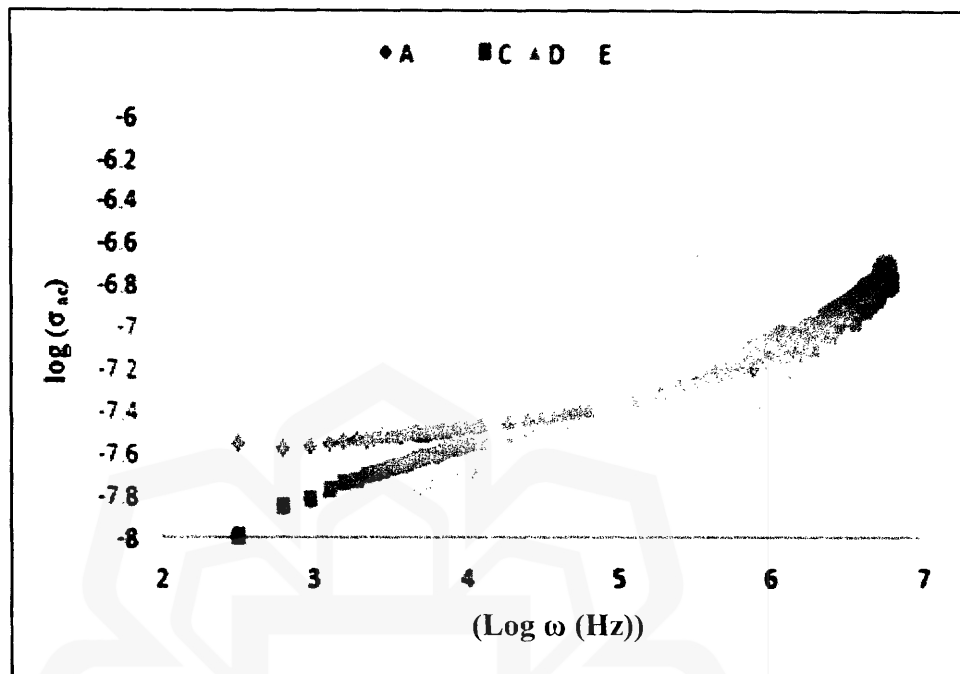


Figure 4.37: Log ( $\omega$ ) conductivity with frequency spectra vs. Variation  $\log (\sigma_{ac})$  of (P-Na-S) electrolyte at room temperature

The mobility of charge carriers tends to be high in the high-frequency areas. Therefore, the conductivity rises with the frequency. The change of conductivity tends to stabilize at high frequencies. The conductivity behavior can be divided according to the frequency in Figure 4.37. In the low-frequency field, the conductivity tends to be constant and is referred to dc conductivity.

#### 4.5 DIELECTRIC STUDY OF (P-Na-S)-EC ELECTROLYTE

It is a method for understanding the carrier transport properties of polymer electrolytes by studying the ion transportation mechanism in conjunction with the polymer phase. The complex electrolyte feature is the material properties affected by temperature, the polymer electrolyte character, and the frequency of the applied region (Aziz et al.,

2019). The films' conductivity with (P-Na-S)-EC plasticizer were used to measure the frequency ranging from 50Hz to 1 MHz.

#### **4.5.1 Frequency Dielectric Constant ( $\epsilon_r$ ) at Selected Temperatures**

**The effect of temperature on the dielectric constant is such as frequency. Suppose** temperature rises, polar molecules' mobility increases, which led to an increase in the dielectric constant. In low temperature, the molecules' alignment in the dielectric material seems difficult. If temperature rises, the dipoles moment become dominant in the dielectric materials leading to a rise in the dielectric constant:

Generally, when the frequency rises, the net polarization materials fall because each polarization performance stops contributing, and its dielectric constant falls. The reason is that the changes in structure in a phase change and the dielectric constant relies heavily on the structure.

It can be seen in Figures 4.38 to 4.42, The dielectric constant ( $\epsilon_r$ ) values rise at higher temperatures because there is a rise in carrier density, resulting in the rise of free ions number or carrier density. The measurement of dielectric properties with various EC contains (10, 20, 30, 40, and 50wt. %) in the range of 303K to 373K temperatures.

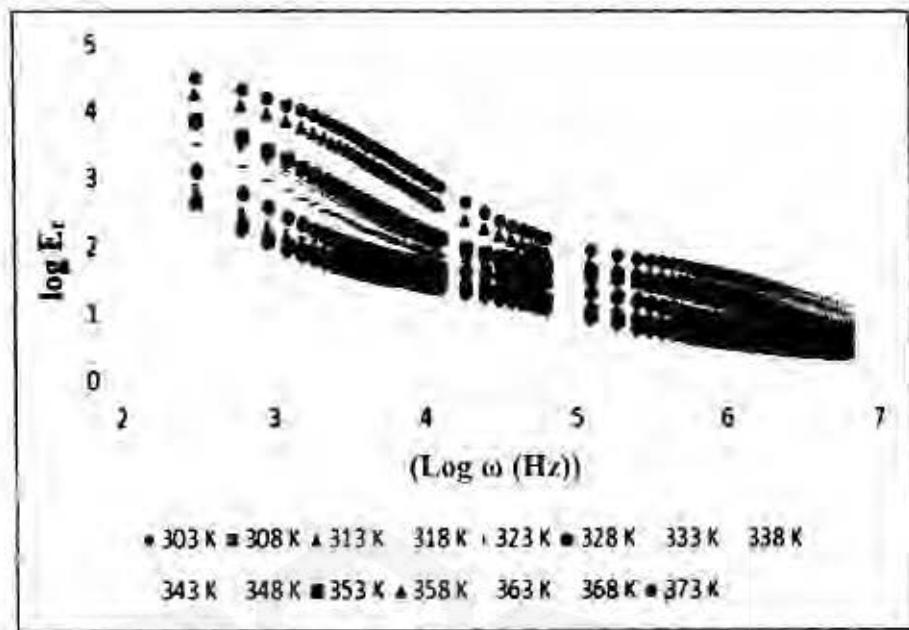


Figure 4.38: Dielectric constant's frequency ( $\log E_r$ ) by 10 wt. % EC plasticizers at preferred temperatures

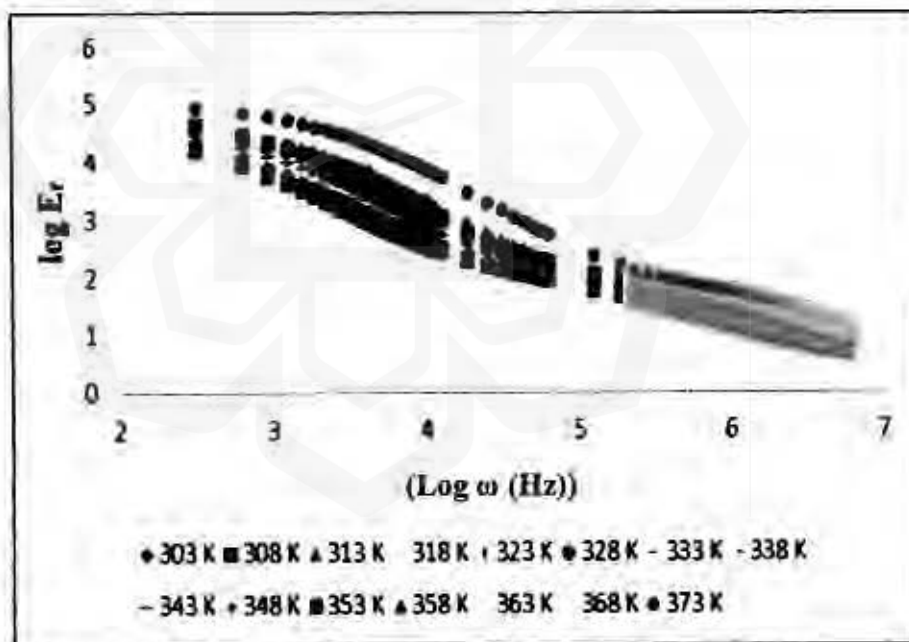


Figure 4.39: Dielectric constant's frequency ( $\log E_r$ ) by 20 wt. % EC plasticizers at preferred temperatures

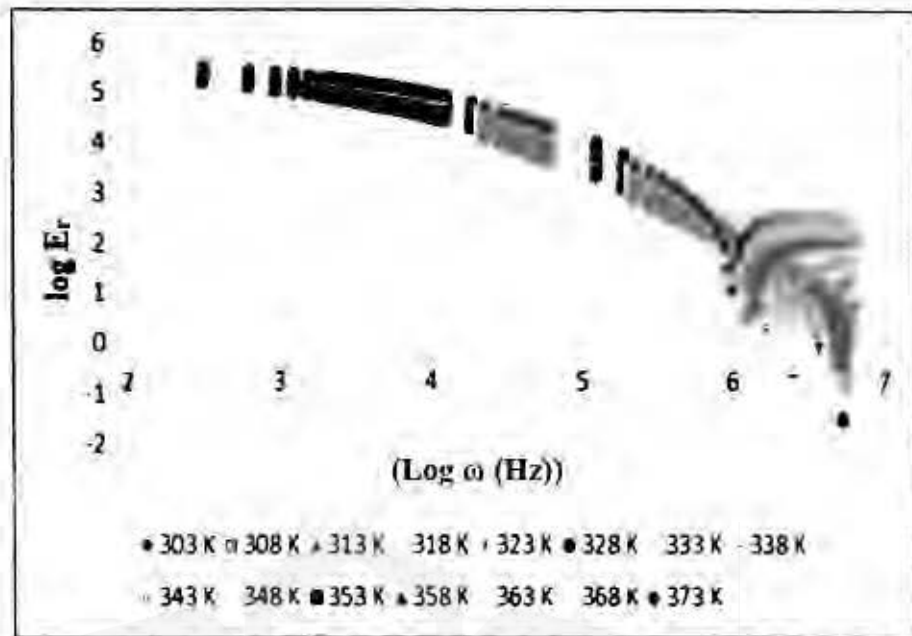


Figure 4.40: Dielectric constant's frequency ( $\log E_r$ ) by 30 wt. % EC plasticizers at preferred temperatures

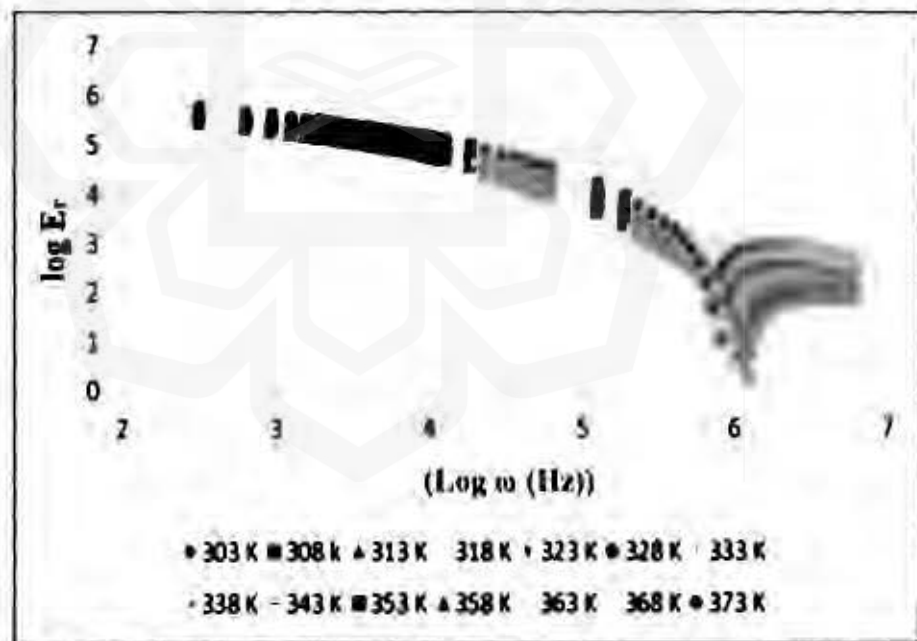


Figure 4.41: Dielectric constant's frequency ( $\log E_r$ ) by 40 wt. % EC plasticizers at preferred temperatures

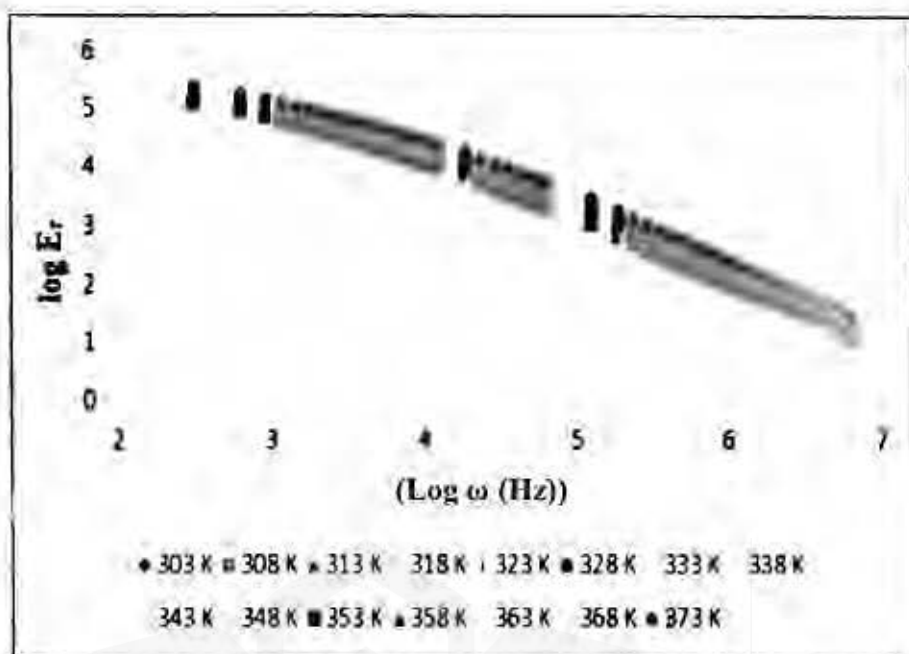


Figure 4.42: Dielectric constant's frequency ( $\log E_r$ ) by 50 wt. % EC plasticizers at preferred temperatures

As a result, resources have increased carrier concentration and mobility, which led to increased conductivity. Based on the findings, it can be expected that dielectric analysis as a useful tool for studying the conductivity measurements of the polymer electrolytes.

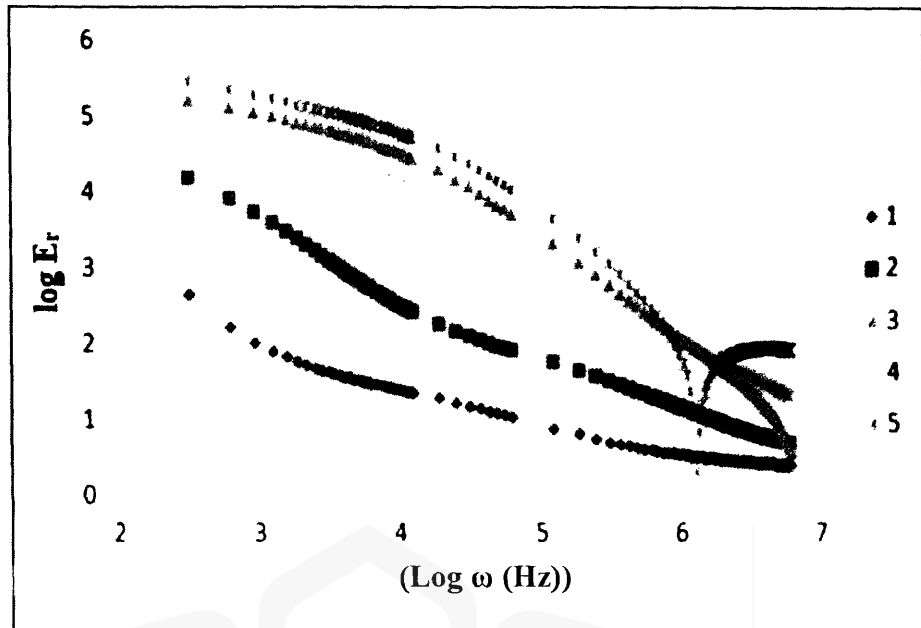


Figure 4.43: Dielectric constants of frequency ( $\log E_r$ ) dependence using different wt. % EC plasticizers

The dielectric frequency versus constant frequency at room temperature is shown in Figure 4.43. The continuous frequency ( $\log E_r$ ) was conducted for five experimentations of electrolytes (P-Na-S) with different EC plasticizers. As you can see in the graph, the solid lines represent the relevant result. There is a direct link between dielectric constant and free charge carrier numbers, and it is enhanced once the salt has been added to the polymer matrix. Electrolyte polarization persistence causes a higher value related to the dielectric constant at lower frequency, which is related to the increase of the total dissociation of the salt ions.

#### 4.5.2 Dielectric Loss Tangent ( $\tan\delta$ )

Figures 4.44 to 4.48, shows the loss tangent versus frequency via electrolyte (P-Na-S) by different EC, known as the loss tangent.

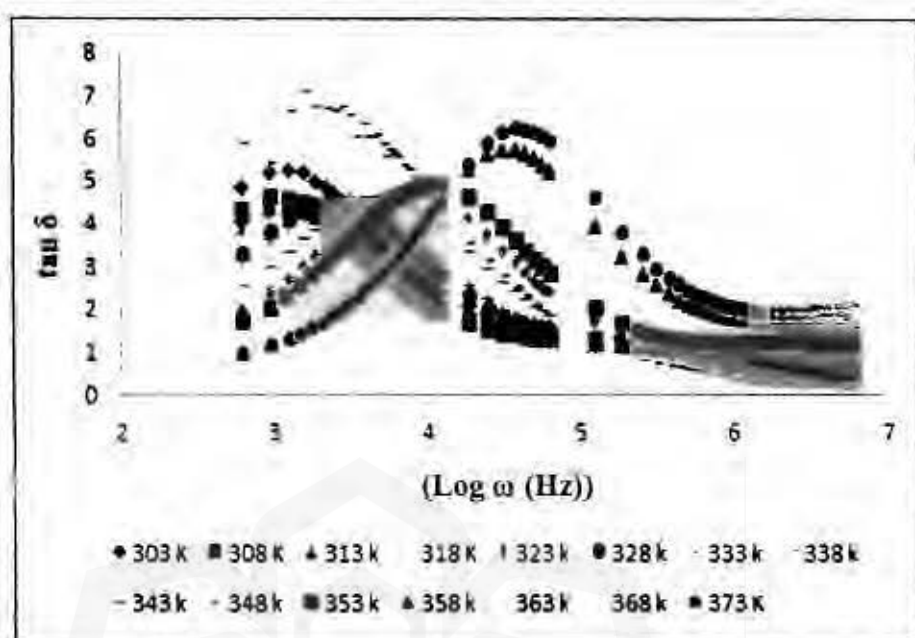


Figure 4.44: The tangent loss's ( $\tan \delta$ ) frequency for polymer blend by 10 wt. % EC plasticizers



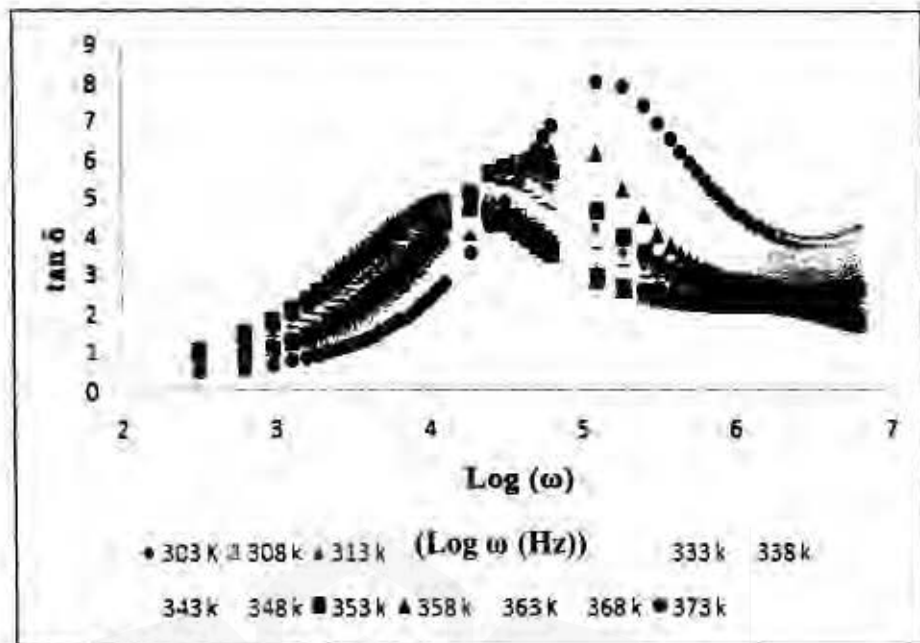


Figure 4.45: The tangent loss's ( $\tan \delta$ ) frequency for polymer blend by 20 wt. % EC plasticizers

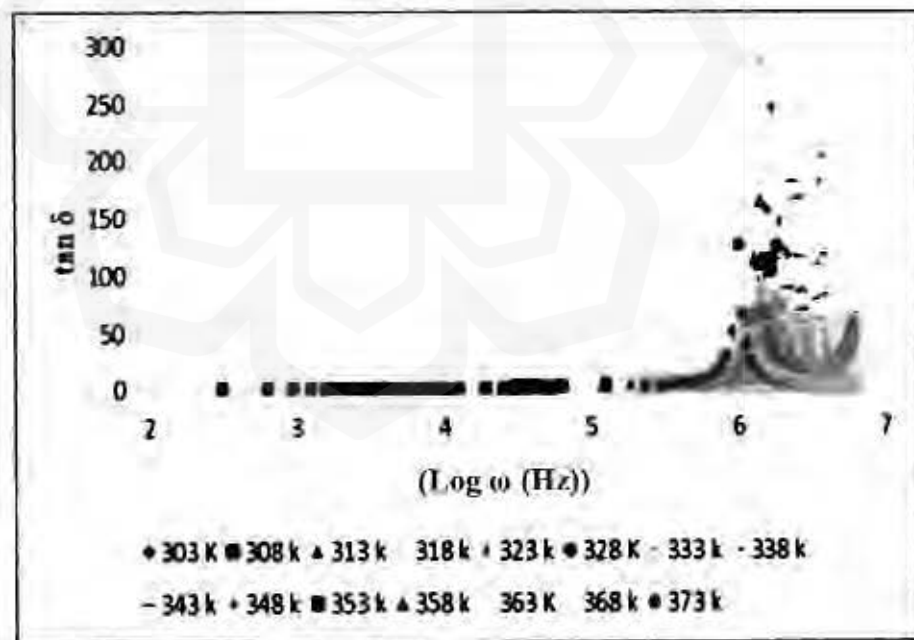


Figure 4.46: The tangent loss's ( $\tan \delta$ ) frequency for polymer blend by 30 wt. % EC plasticizers

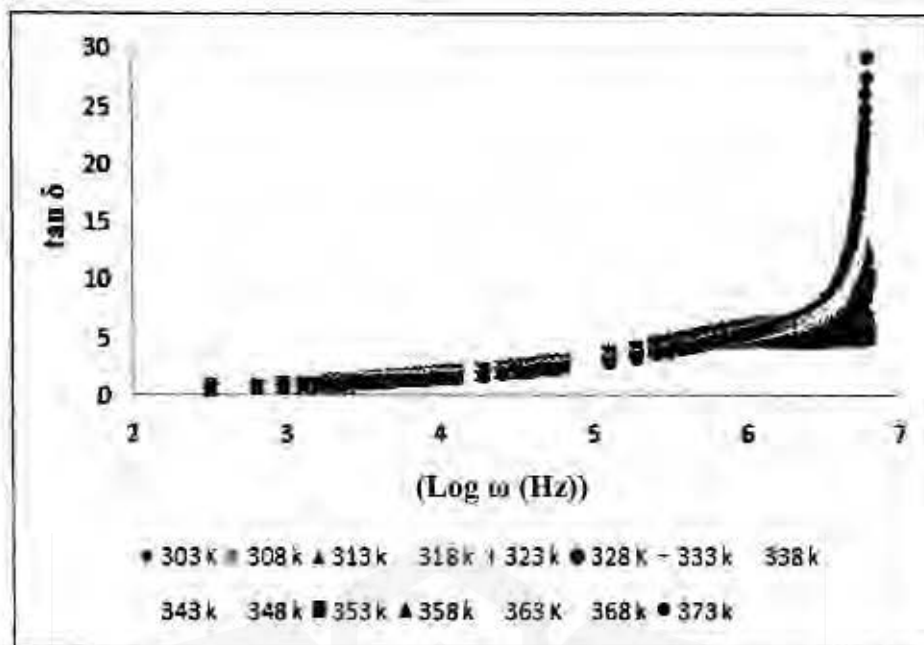


Figure 4.47: The tangent loss's ( $\tan \delta$ ) frequency for polymer blend by 40 wt. % EC plasticizers

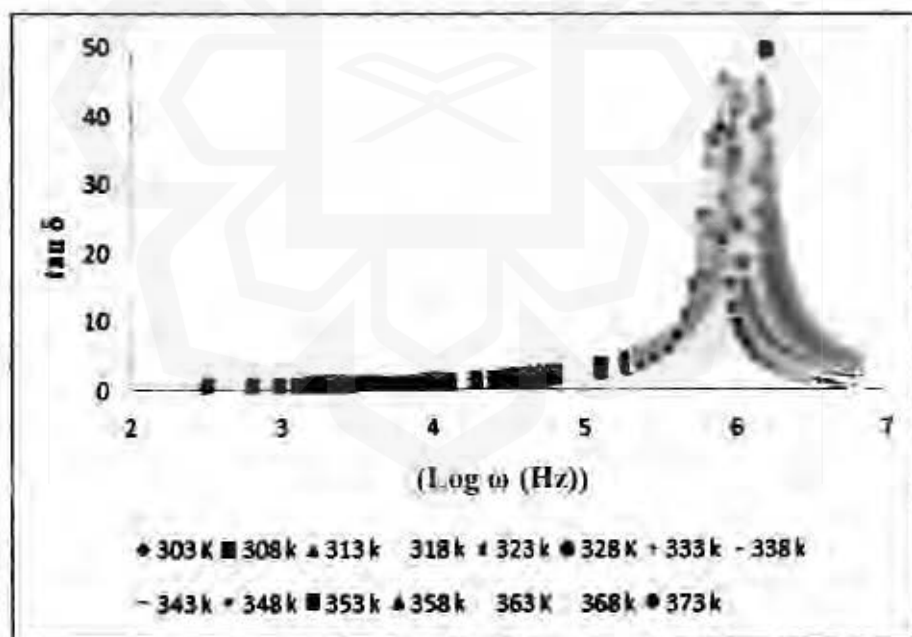


Figure 4.48: The tangent loss's ( $\tan \delta$ ) frequency for polymer blend by 50 wt. % EC plasticizers

To understand the variation of ac conductivity with the frequency, the regions plot of figures divided into three different regions: the first region is low-frequency: the

second region is moderate-frequency, and the third region is high-frequency. In the current configuration, all graphs indicate a singular relaxation peak, showing ionic conductivity. The temperature affects the molecules, which leads to the migration of thermally excited carriers from energy levels, which improves AC conductivity.

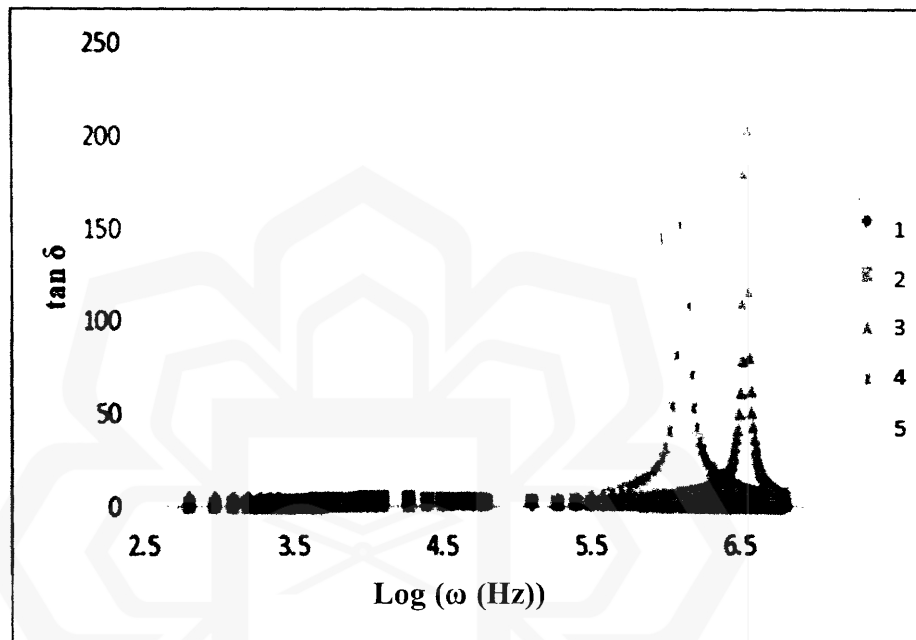


Figure 4.49: Frequency dependence of loss tangent ( $\tan\delta$ ) electrolytes membrane at room temperature with various EC

In Figure 4.49 The relaxation peak moves to the high-frequency side, showing quicker ion dynamics movement from one coordinate region to the next at the room temperature. It is because a reduction in relaxation time with equilibrium concentration.

### 4.5.3 Measurement of AC Conductivity of Dielectric Properties

Figures 4.50 to 4.54, shows the dielectric conductivity measured for polymer electrolytes (P-Na-S)-EC at (303 to 373 K) temperatures.

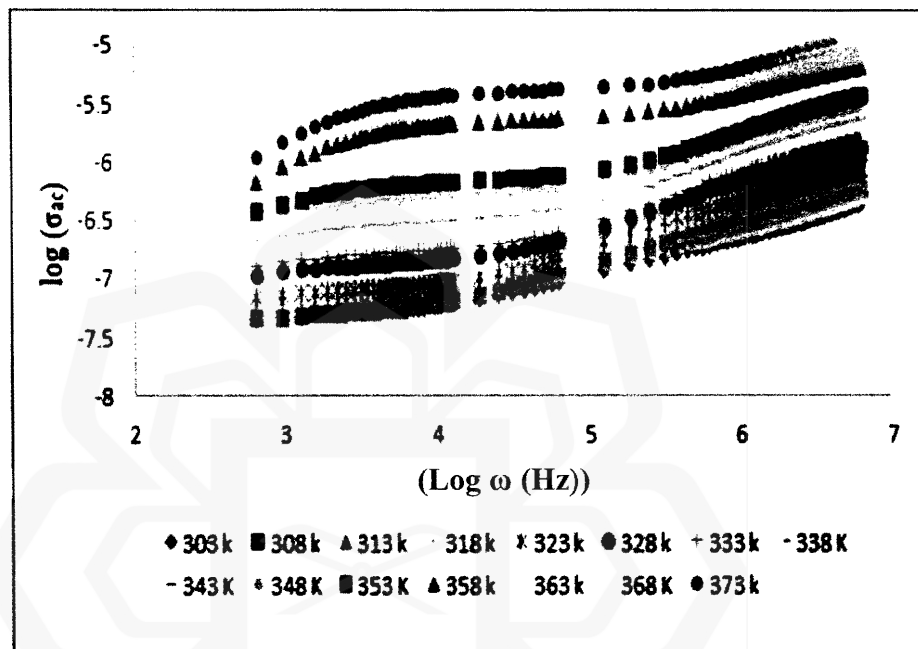


Figure 4.50: Spectra conductivity of polymer electrolyte (P-Na-S) by 10 wt. % EC at preferred temperatures

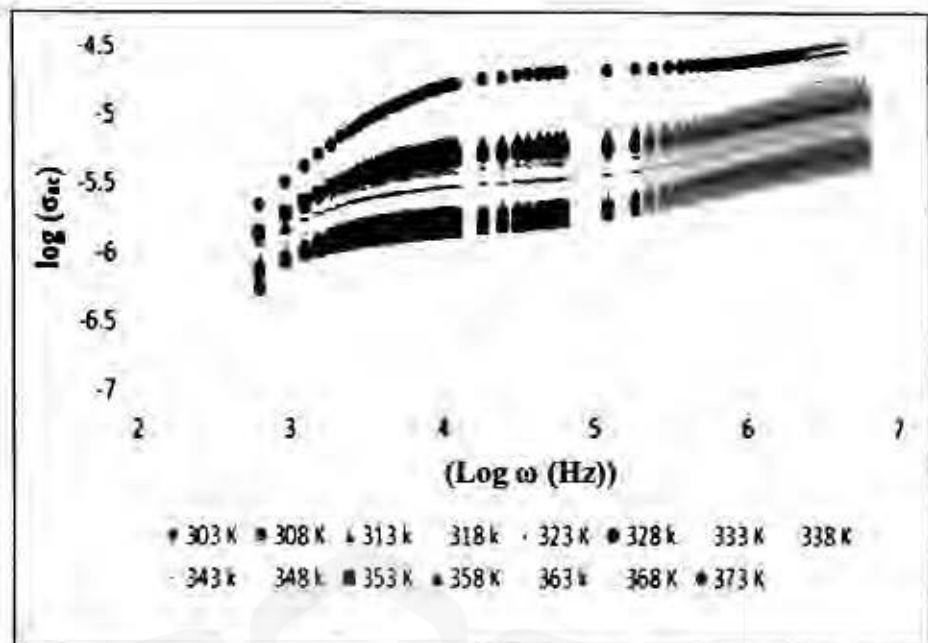


Figure 4.51: Spectra conductivity of polymer electrolyte (P-Na-S) by 20 wt. % EC at preferred temperatures

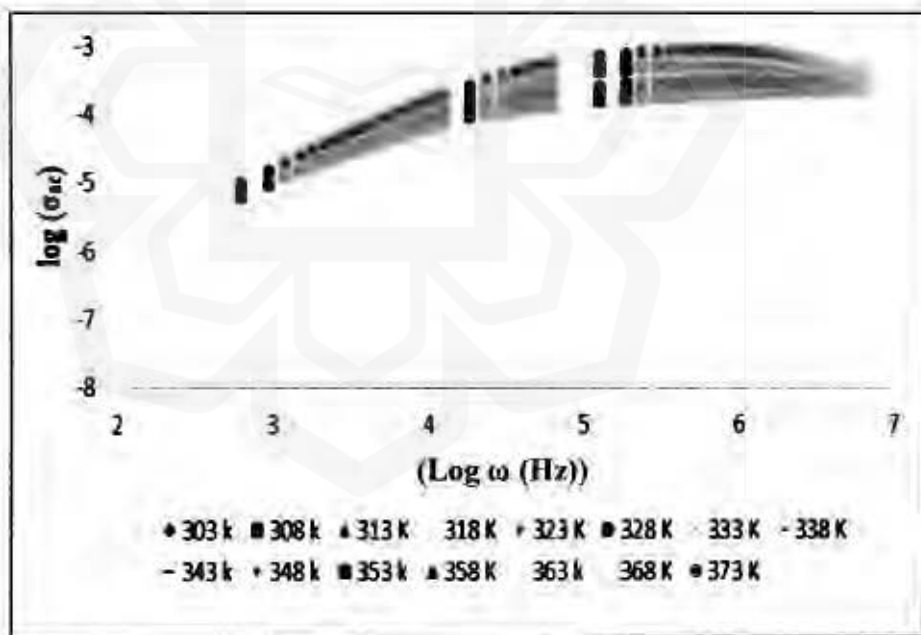


Figure 4.52: Spectra conductivity of polymer electrolyte (P-Na-S) by 30 wt. % EC at preferred temperatures

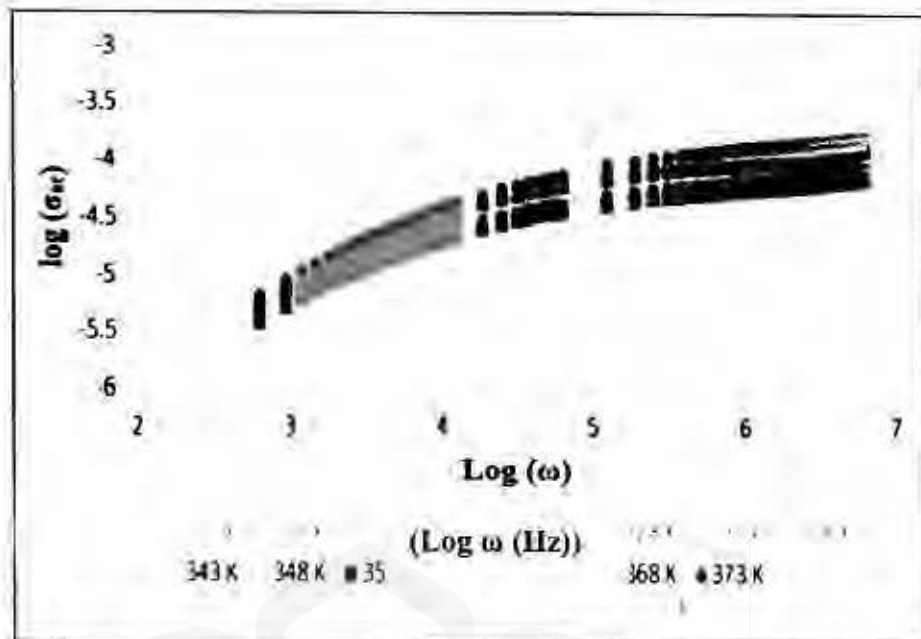


Figure 4.53: Spectra conductivity of polymer electrolyte (P-Na-S) by 40 wt. % EC at preferred temperatures

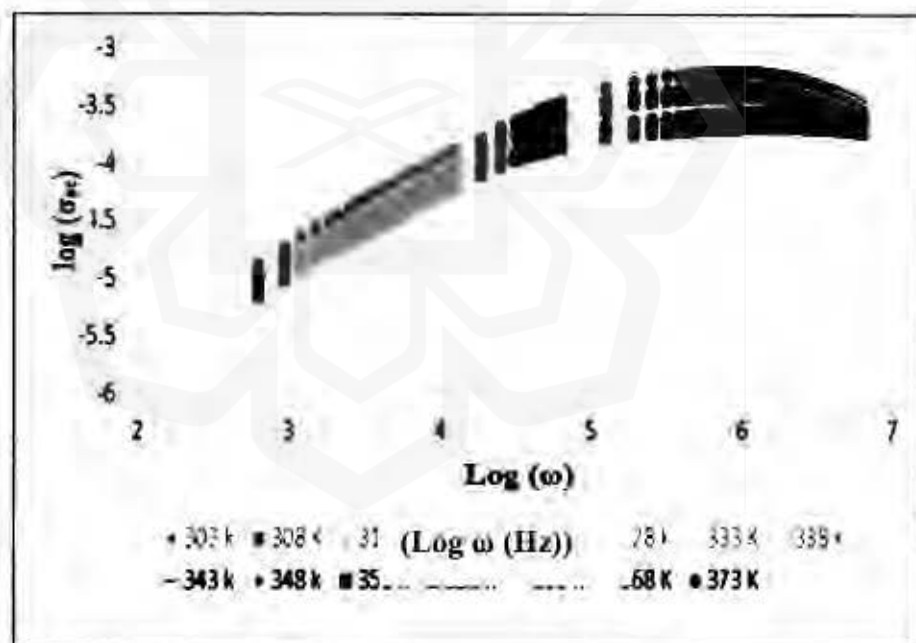


Figure 4.54: Spectra conductivity of polymer electrolyte (P-Na-S) by 50 wt. % EC at preferred temperatures

Within the calculated frequency range, the spectrum is divided into two distinct areas. The low-frequency spike is characterized to charge polarization space at the

blocking electrodes and explains electrode-electrolyte interfacial phenomena (Yamamoto et al. 1994). This might be backed up by the frequency plateau area related to  $\sigma_{dc}$  of the polymer electrolyte complex. The conductivity value of  $\sigma_{dc}$  at all temperatures is obtained by the plateau area to frequency of zero. The mobility of charge carriers tends to be high in the high-frequency region; therefore, the frequency of conductivity enhances (Ramesh & Arof, 2001).

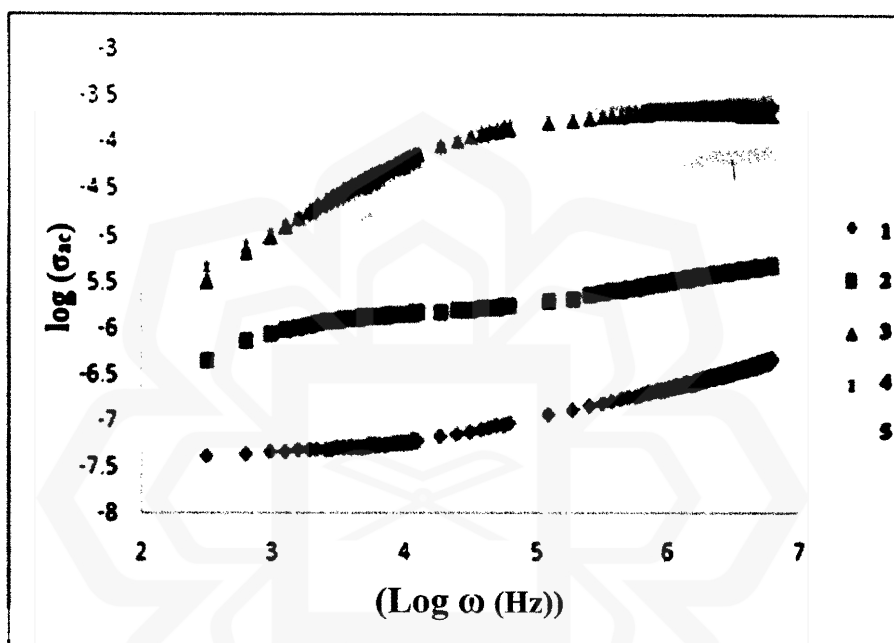


Figure 4.55:  $\log(\sigma_{ac})$  conductivity versus  $\text{Log}(\omega)$  with different (P-Na-S)-EC electrolyte at room temperature

In Figure 4.55 at room temperature with the addition of plasticizer, the overall effect shows various in conductivity range. When the frequency region is low, the ac conductivity dispersion shows at higher frequencies. Apart from dispersion in the region of low frequency, the deviation from  $\sigma_{dc}$  is more notable on the plasticizer. Plasticization causes a divergence from the dc value, which shows in the conductivity range, appear in the low-frequency region. It is because of increased ionic conduction.

#### 4.6 XRD PATTERN WITHOUT SALT, BY Na<sub>2</sub>S AND EC PLASTICIZER

The crystallinity and amorphousness of the samples were determined using X-ray diffractometer. X-rays with 1.5406 Å wavelengths were produced by Cu K $\alpha$  source between 10 to 80 degrees with  $2\theta$  angle.

Figure 4.56 shows the XRD diffraction pattern for poly (acrylamide-co-acrylic acid) and sodium cellulose carboxylic (Na-CMC).

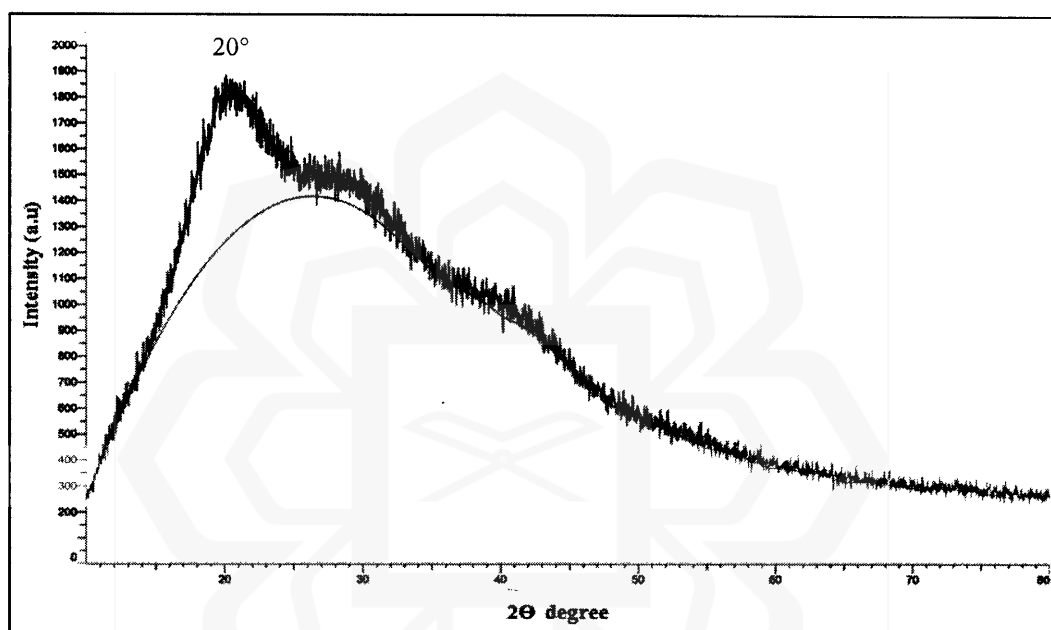


Figure 4:56 Shows polymer with Poly (AM-co-AA) and Na-CMC without Na<sub>2</sub>S salt

The sample did not have any sharp peaks in XRD patterns, with only a large peak at  $2\theta = 20^\circ$  of polymer networks (Varaprasad & Sadiku, 2017) as shown in Figure 4.56. The XRD peaks are low and broad due to the small size effect and incomplete inner structure of the particle.

The higher conductivity with 30% salt was used for the XRD pattern. Figure 4.57 shows the XRD patterns of (P-Na-S) polymers and their complexes with 30 wt.% salt. Visual inspection reveals that the solid polymer electrolyte is partially amorphous.



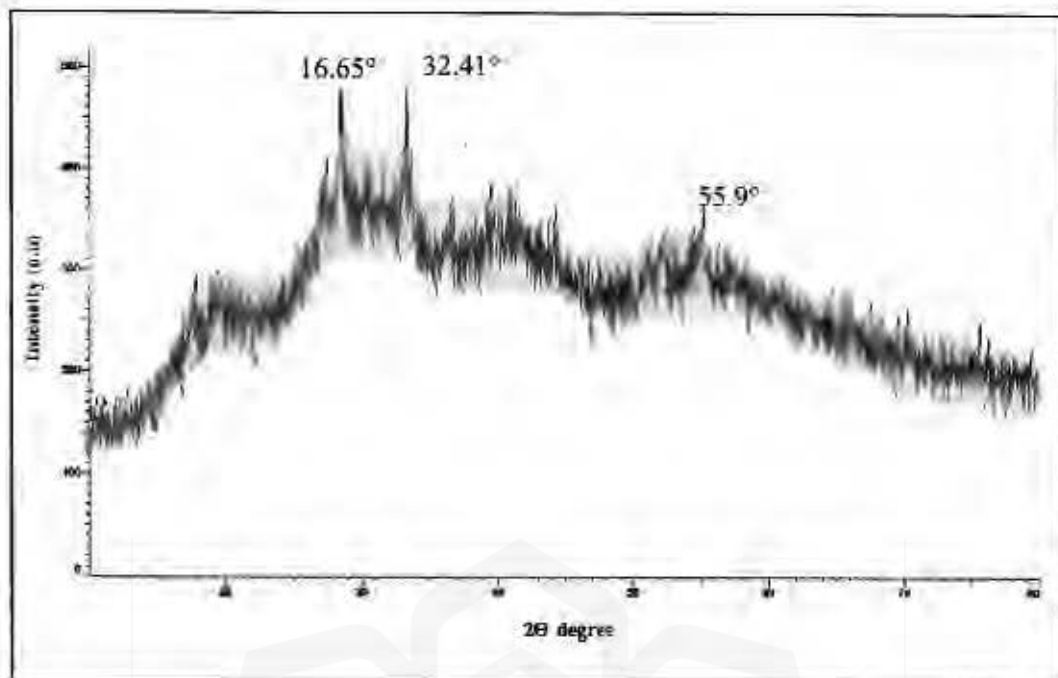


Figure 4.57: Shows polymer with Poly (AM-co-AA) and Na-CMC by 30 wt.%  $\text{Na}_2\text{S}$  salt

In Figure 4.57 can be seen the recrystallization of salt at  $2\theta = 16.65^\circ$  and  $32.41^\circ$  (Baharun et al., 2018). The crystalline peak is also visible at  $2\theta = 55.9^\circ$ , when the sodium sulfide salt is added, the sample becomes more amorphous, which should improve ion migration in the electrolyte (Li et al., 2005). Upon further salt, specifies that the polymer is unable to accommodate all the salt added during film formation. An changes in the polymer matrix which causes an up-shifting of the XRD peak, indicating polymer-salt interaction due to cation ( $\text{Na}^+$  ion) complexation (Arya & Sharma, 2018). There is evidence that salt can influences the composition of the blend polymer matrix. Ions can disrupt the regular arrangement of the salt polymer backbone and aggregate through non-polar hydrophobic chains, disrupting the crystalline phase of the polymer and causing the (P-Na-S) film to become amorphous.

In Figure 4.58 shows the specific XRD diffraction peaks ( $2\theta$ ) with 40 wt.% EC plasticizers for the polymeric electrolyte in the range of 10 to 80 degree.

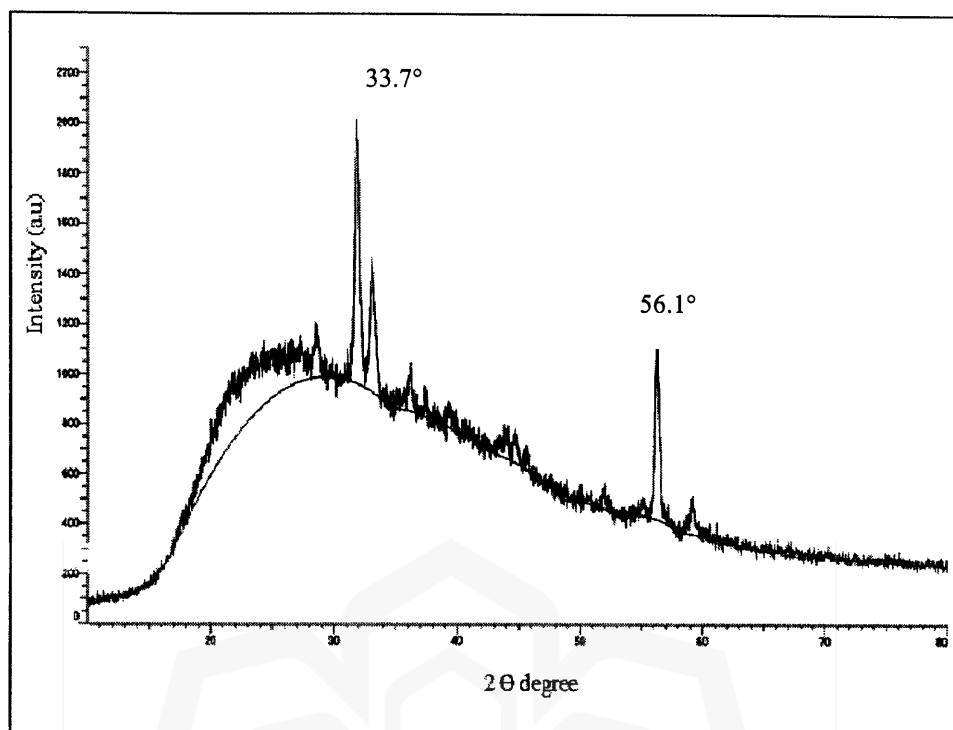


Figure 4.58: Indicates XRD diffraction for 40 wt. % EC

The characteristic peaks ( $2\theta$ ) of semi-crystalline (P-Na-S)-EC electrolyte film, appear in the range between 20 and 60 theta degrees. It shows recrystallization at maximum peak about 33.7 and 56.1 ° which are attributed to the salt and EC. The excess salt recrystallized on the surface of the film in two regions. In fact the sample should become more amorphous for enhance ion migration in the electrolyte (Li et al., 2005). On the other hand, the pattern shows recrystallized texture by additional EC. As a result, the polymer complex is unable to accommodate all the salt added during film formation by additional EC.

#### 4.7 ANALYSIS OF MOBILE ION CONDUCTIVITY

As discussed in earlier sections, the electrolytes in QDSSCs are responsible, not only for the regeneration electron but also for charge transport between anode and cathode in the solar cell. Numerous efforts have been made to design novel and efficient

electrolyte formulations to achieve optimal performance for QDSSC. This electrolyte has been developed by solution casting technique. The current work, two-step method was used to prepare electrolyte based on Na<sub>2</sub>S salt and EC in solid polymer electrolyte (SPEs). The use of water as the only solvent for the S<sup>2-</sup>/Sx<sup>2-</sup> redox mediator would assure the realization of safe, cheap, and eco-friendly materials for electrolyte. Activation energy (E<sub>A</sub>) and ionic conductivity at room temperature for each sample are listed in Table 4.8. According to the Table, at room temperature ionic conductivity (RTIC), initially increases with Na<sub>2</sub>S concentration until a maximum conductivity is obtained at  $(9.82 \pm 1.51) \times 10^{-7} \text{ Scm}^{-1}$  for the electrolyte containing 30% Na<sub>2</sub>S salt. Further increase of Na<sub>2</sub>S concentration above 30% shows a decline in RTIC. At more than 30% Na<sub>2</sub>S salt, mobile ions are getting too close to one another, and thus lead to neutral ion pairs and/or aggregates formation. This reduces the concentration of free or mobile charges. The bulky ion aggregates also have lower mobility as compared to free ions. The variation of (E<sub>A</sub>) with Na<sub>2</sub>S content is in opposite trend to that of conductivity. This phenomenon suggests that the low activation energy promotes an easier migration from one donor site to another and consequently results in higher ionic conductivity (Buraidah et al., 2009). On the other hand, EC added to increase the conductivity and set between 10 to 50 % which reaches 40% maximum conductivity at  $(2.74 \pm 2.52) \times 10^{-4} \text{ Scm}^{-1}$ . Adding of plasticizers in polymer electrolyte is one of the most effective approaches to improve the mobility of ionic or/and the interfacial interaction among ionic and polar groups in polymer chains. The choice of plasticizer and its concentration can affect film permeability and mechanical properties (Sheldon et al. 1989 & Roy et al., 2009). The other advantage of plasticization is to modify the polymeric matrix and provide the enhanced conductivity. In general, low molecular weight and high dielectric constant additive, such as, ethylene

carbonate (EC), is used to modify the permeability of the polymer film (Bhide et al., 2007). The addition of plasticizer in polymer matrix tends to decrease the glass transition temperature and increase deformability, elasticity, abrasion resistance, and elastic recovery in the electrolyte system. Use of plasticizers also increases the salt-solvating power which leads to an increase in amorphous content of the polymer matrix and tends to dissociate ion-pairs into free cations and anions thereby leading to an overall enhancement in conductivity. As a result, this change indicates the polymer-salt-plasticizer interaction as well as the decrease in crystalline behavior of the composite electrolyte.

#### **4.8 SUMMARY**

This chapter presents the result and discussion of the FTIR with the functional groups of poly(acrylamide-*co*-acrylic acid) powder and film formation and Na-CMC individually . Then, explains the FTIR spectra with poly(acrylamide-*co*-acrylic acid) and Na-CMC film formation with and without salt. Also, describes the findings and discusses the functional group of polymer chains with different Na<sub>2</sub>S salts and ethylene carbonate (EC) by FTIR technique. In addition, Impedance spectroscopy (EIS) measures the conductivity from 10, 20 ,30 ,40, and 50 wt.% of salt and EC addition separately. Following, measure the activation energy of both electrolyte for ionic conductivity of electrolytes and activation energy with optimum achievement by salt and EC. Consequently, discussed the dielectric study through dielectric constant ( $\epsilon_r$ ), frequency dependence of loss tangent ( $\tan \delta$ ), and AC conductivity of all samples with the fixed temperature from 303 to 373 K. Lastly, the XRD patterns shown studied

without salt and the enhanced 30% Na<sub>2</sub>S salt and 40% EC to differentiate crystallinity and amorphous concept through the highest electrical conductivity.



## CHAPTER FIVE

### CONCLUSION

#### 5.1 CONCLUSION

Two distinct sets of polymer electrolytes were prepared based on Na<sub>2</sub>S with and without ethylene carbonate (EC) and characterized by FTIR, XRD and EIS techniques to achieve the objectives related to the preparation and characterization of (P-Na-S) electrolytes. To begin, five polymer electrolytes based on Na<sub>2</sub>S were prepared and characterized using FTIR, XRD, and EIS techniques. Higher conductivity at  $9.82 \times 10^{-7}$  S.cm<sup>-1</sup> was attained by the (P-Na-S) with 30 wt.% Na<sub>2</sub>S salt. To increase electrolyte enhancement, which was another goal of this research, different percentages of EC based (P-Na-S) were selected as an additive to improve the conductivity that obtained by 40 wt.% EC at  $2.74 \times 10^{-4}$  S.cm<sup>-1</sup>.

Consequently, the minimum activation energy was verified by the Arrhenius equation with approximately 0.36 eV and 0.16 eV for additional salt (30 wt.%) and EC (40 wt.%) respectively. Effect of salt and plasticizer on dielectric behavior, electrical conductivity, and other physical property was clearly visible on the pristine electrolytes. The better electrical conductivity depends on the combination of plasticizers. The maximum conductivity was obtained with (Na<sub>2</sub>S salt 30 wt.% + EC wt. 40%).

FTIR spectra, shown the characteristic bands are shifted, and no new peaks observed after the mixing of components with additional salt and EC. The XRD shows extra salt for the polymer electrolytes and additional EC grow into more amorphous and reduces crystallinity.

Developing new knowledge based on previously existing survey by doing thorough and innovative research for the reason that of achieve new outcomes based on unique materials and a new strategy to specifying the contribution to the knowledge by analysis and data collection of acceptable results.

## **7.2 RECOMMENDATIONS**

- 1- The conductivity of solid polymer electrolyte has been optimized. Nevertheless, still there are rooms need to be improved for higher conductivity of the electrolyte.
- 2- Further study needs to be carried out to expand this research in the future. The findings provide the following understandings for the future research.
- 3- More research on ion activities and movement of these electrolyte systems, transmission numbers would provide more insight into the literature.
- 4- If proper materials are added, they might modify the (P-Na-S) electrolyte.
- 5- Another study may add more knowledge to the research by modelling of (P-Na-S) and (P-Na-S)-EC plasticizers.

## REFERENCES

- Ahmed, H. M. (2016). Shujahadeen B. Aziz, Rebar T. Abdulwahid, Hazhar A. Rsaul &. *J Mater Sci: Mater Electron*, 27, 4163-4171.
- Arica, B., Çaliş, S., Atilla, P., Durlu, N. T., Cakar, N., Kaş, H. S., & Hincal, A. A. (2005). In vitro and in vivo studies of ibuprofen-loaded biodegradable alginate beads. *Journal of microencapsulation*, 22(2), 153-165.
- Archana, T., Subashini, G., Grace, A. N., Arivanandhan, M., & Jayavel, R. (2021). The effect of TEOS concentration in polysulphide electrolyte and CuS counter electrode on enhancing the performance of CdS quantum dot sensitized solar cells. *Journal of Applied Electrochemistry*, 1-12.
- Arya, A., & Sharma, A. (2018). Structural, electrical properties and dielectric relaxations in Na<sup>+</sup>-ion-conducting solid polymer electrolyte. *Journal of Physics: Condensed Matter*, 30(16), 165402.
- Ates, M., Karazehir, T., & Sarac, A. S. (2012). Conducting polymers and their applications. *development*, 51, 52.
- Aziz, S. B. (2018). The mixed contribution of ionic and electronic carriers to conductivity in chitosan based solid electrolytes mediated by CuNt salt. *Journal of Inorganic and Organometallic Polymers and Materials*, 28(5), 1942-1952.
- Aziz, S. B., Brza, M., Kadir, M., Hamsan, M., Abidin, Z., Tahir, D. A., & Abdullah, O. G. (2019). Investigation on Degradation and Viscoelastic Relaxation of Li Ion in Chitosan Based Solid Electrolyte. *Int. J. Electrochem. Sci*, 14, 5521-5534.
- Balan, V., Mihai, C. T., Cojocaru, F. D., Uritu, C. M., Dodi, G., Botezat, D., & Gardikiotis, I. (2019). Vibrational spectroscopy fingerprinting in medicine: from molecular to clinical practice. *Materials*, 12(18), 2884.
- Baharun, N., Mingsukang, M., Buraidah, M., Woo, H., & Arof, A. (2018). *Electrical Properties of Plasticized Sodium-Carboxymethylcellulose (Na-CMC) Based Polysulfide Solid Polymer Electrolyte*. Paper presented at the 2018 20th International Conference on Transparent Optical Networks (ICTON).
- Baharun, N. N. S., Mingsukang, M. A., Buraidah, M. H., Woo, H. J., Teo, L. P., & Arof, A. K. (2020). Development of solid polymer electrolytes based on sodium-carboxymethylcellulose (NaCMC)-polysulphide for quantum dot-sensitized solar cells (QDSSCs). *Ionics*, 26(3), 1365-1378.
- Bao, Y., Ma, J., & Li, N. (2011). Synthesis and swelling behaviors of sodium carboxymethyl cellulose-g-poly(AA-co-AM-co-AMPS)/MMT superabsorbent hydrogel. *Carbohydrate Polymers*, 84(1), 76-82.



- Baskaran, R., Selvasekarapandian, S., Hirankumar, G., & Bhuvaneswari, M. (2004). Dielectric and conductivity relaxations in PVAc based polymer electrolytes. *Ionics*, 10(1-2), 129-134.
- Bella, F., Sacco, A., Pugliese, D., Laurenti, M., & Bianco, S. (2014). Additives and salts for dye-sensitized solar cells electrolytes: what is the best choice? *Journal of Power Sources*, 264, 333-343.
- Bencsik, G., Lukács, Z., & Visy, C. (2010). Photo-electrochemical sensor for dissolved oxygen, based on a poly (3, 4-ethylenedioxythiophene)/iron oxalate hybrid electrode. *Analyst*, 135(2), 375-380.
- Bhambhani, P. (2018). Quantum dot-sensitized solar cells: a review. *Bulletin of Electrical Engineering and Informatics*, 7(1), 42-54
- Bhide, A., & Hariharan, K. (2007). Ionic transport studies on (PEO) 6: NaPO<sub>3</sub> polymer electrolyte plasticized with PEG400. *European Polymer Journal*, 43(10), 4253-4270.
- Bidikoudi, M., Zubeir, L. F., & Falaras, P. (2014). Low viscosity highly conductive ionic liquid blends for redox active electrolytes in efficient dye-sensitized solar cells. *Journal of Materials Chemistry A*, 2(37), 15326-15336.
- Bosi, M., & Pelosi, C. (2007). The potential of III-V semiconductors as terrestrial photovoltaic devices. *Progress in Photovoltaics: Research and Applications*, 15(1), 51-68.
- Buraidah, M. H., Teo, L. P., Majid, S. R., & Arof, A. K. (2009). Ionic conductivity by correlated barrier hopping in NH<sub>4</sub>I doped chitosan solid electrolyte. *Physica B: Condensed Matter*, 404(8-11), 1373-1379.
- Burke, A. (2000). Ultracapacitors: why, how, and where is the technology. *Journal of power sources*, 91(1), 37-50.
- Bykov, I. (2008). Characterization of natural and technical lignin using FTIR spectroscopy.
- Cao, M.-S., Song, W.-L., Hou, Z.-L., Wen, B., & Yuan, J. (2010). The effects of temperature and frequency on the dielectric properties, electromagnetic interference shielding and microwave-absorption of short carbon fiber/silica composites. *Carbon*, 48(3), 788-796.
- Cass, P., Knower, W., Preece, E., Holmes, N. P., & Hughes, T. (2010). Preparation of hydrogels via ultrasonic polymerization. *Ultrasonics sonochemistry*, 17(2), 326-332.
- Chandran, A., & George, K. C. (2014). Defect induced modifications in the optical, dielectric, and transport properties of hydrothermally prepared ZnS nanoparticles and nanorods. *Journal of nanoparticle research*, 16(3), 1-17.

- Chauhan, L., Shukla, A. K., & Sreenivas, K. (2015). Dielectric and magnetic properties of Nickel ferrite ceramics using crystalline powders derived from DL alanine fuel in sol-gel auto-combustion. *Ceramics International*, 41(7), 8341-8351.
- Chen, H., & Yang, S. (2016). Hierarchical nanostructures of metal oxides for enhancing charge separation and transport in photoelectrochemical solar energy conversion systems. *Nanoscale Horizons*, 1(2), 96-108.
- Chen, Y.-S., Choi, H., & Kamat, P. V. (2013). Metal-cluster-sensitized solar cells. A new class of thiolated gold sensitizers delivering efficiency greater than 2%. *Journal of the American Chemical Society*, 135(24), 8822-8825.
- Chien, D. T., Long, P. D., Van Hoi, P., & Chi, L. H. (2011). Nanocomposite Thin Film TiO<sub>2</sub>/CdS Electrodes Prepared by Thermal Evaporation Process for Photovoltaic Applications. *Communications in Physics*, 21(1), 57.
- Chou, C.-Y., Lee, C.-P., Vittal, R., & Ho, K.-C. (2011). Efficient quantum dot-sensitized solar cell with polystyrene-modified TiO<sub>2</sub> photoanode and with guanidine thiocyanate in its polysulfide electrolyte. *Journal of Power Sources*, 196(15), 6595-6602.
- Cho, W., Kim, Y. R., Song, D., Choi, H. W., & Kang, Y. S. (2014). High-efficiency solid-state polymer electrolyte dye-sensitized solar cells with a bi-functional porous layer. *Journal of Materials Chemistry A*, 2(42), 17746-17750.
- Chow, T., He, W., & Ji, J. (2006). Hybrid photovoltaic-thermosyphon water heating system for residential application. *Solar energy*, 80(3), 298-306.
- Dahbi, M., Nakano, T., Yabuuchi, N., Ishikawa, T., Kubota, K., Fukunishi, M., Oji, H. (2014). Sodium carboxymethyl cellulose as a potential binder for hard-carbon negative electrodes in sodium-ion batteries. *Electrochemistry Communications*, 44, 66-69.
- Dang, R., Wang, Y., Zeng, J., Huang, Z., Fei, Z., & Dyson, P. J. (2017). Benzimidazolium salt-based solid-state electrolytes afford efficient quantum-dot sensitized solar cells. *Journal of Materials Chemistry A*, 5(26), 13526-13534
- Dar, M. A., Majid, K., Batoor, K. M., & Kotnala, R. K. (2015). Dielectric and impedance study of polycrystalline Li<sub>0.35-0.5</sub>XCd<sub>0.35-0.5</sub>XO<sub>4</sub> ferrites synthesized via a citrate-gel auto combustion method. *Journal of Alloys and Compounds*, 632, 307-320.
- Deka, M., & Kumar, A. (2013). Dielectric and conductivity studies of 90 MeVO<sub>7+</sub> ion irradiated poly (ethylene oxide)/montmorillonite based ion conductor. *Journal of Solid State Electrochemistry*, 17(4), 977-986.

- Deraman, S. K., Mohamed, N. S., & Subban, R. H. Y. (2014). Ionic liquid incorporated PVC based polymer electrolytes: electrical and dielectric properties. *Sains Malaysiana*, 43(6), 877-883.
- Diguna, L. J., Shen, Q., Kobayashi, J., & Toyoda, T. (2007). High efficiency of CdSe quantum-dot-sensitized TiO<sub>2</sub> inverse opal solar cells. *Applied Physics Letters*, 91(2), 023116.
- Dissanayake, M. A. K. L., Jaseetharan, T., Senadeera, G. K. R., & Kumari, J. M. K. W. (2020). Efficiency enhancement in PbS/CdS quantum dot-sensitized solar cells by plasmonic Ag nanoparticles. *Journal of Solid State Electrochemistry*, 24(2), 283-292.
- Du, J., Du, Z., Hu, J.-S., Pan, Z., Shen, Q., Sun, J., Zhong, X. (2016). Zn–Cu–In–Se quantum dot solar cells with a certified power conversion efficiency of 11.6%. *Journal of the American Chemical Society*, 138(12), 4201-4209.
- Duan, J., Tang, Q., He, B., & Chen, H. (2015). All-solid-state quantum dot-sensitized solar cell from plastic crystal electrolyte. *RSC Advances*, 5(42), 33463-33467.
- Duan, J., Tang, Q., Sun, Y., He, B., & Chen, H. (2014). Solid-state electrolytes from polysulfide integrated polyvinylpyrrolidone for quantum dot-sensitized solar cells. *RSC advances*, 4(105), 60478-60483.
- Duan, J., Zhang, H., Tang, Q., He, B., & Yu, L. (2015). Recent advances in critical materials for quantum dot-sensitized solar cells: a review. *Journal of Materials Chemistry A*, 3(34), 17497-17510.
- Du, X., He, X., Zhao, L., Chen, H., Li, W., Fang, W., ... & Chen, H. (2016). TiO<sub>2</sub> hierarchical porous film constructed by ultrastable foams as photoanode for quantum dot-sensitized solar cells. *Journal of Power Sources*, 332, 1-7.
- Dyre, J. C. (1988). The random free-energy barrier model for ac conduction in disordered solids. *Journal of Applied Physics*, 64(5), 2456-2468.
- Eftekhari, A. (2011). *Nanostructured conductive polymers: John Wiley & Sons*.
- Erizal, E. (2012). Synthesis of poly (acrylamide-co-acrylic acid)-starch based superabsorbent hydrogels by gamma radiation: study its swelling behavior. *Indonesian Journal of Chemistry*, 12(2), 113-118.
- Evangelista, R. M., Makuta, S., Yonezu, S., Andrews, J., & Tachibana, Y. (2016). Semiconductor quantum dot sensitized solar cells based on ferricyanide/ferrocyanide redox electrolyte reaching an open circuit photovoltage of 0.8 V. *ACS applied materials & interfaces*, 8(22), 13957-13965.
- Fan, L. Z., & Maier, J. (2006). Composite effects in poly (ethylene oxide)–succinonitrile based all-solid electrolytes. *Electrochemistry communications*, 8(11), 1753-1756.

- Fang, B., Kim, M., Fan, S.Q., Kim, J. H., Wilkinson, D. P., Ko, J., & Yu, J.-S. (2011). Facile synthesis of open mesoporous carbon nanofibers with tailored nanostructure as a highly efficient counter electrode in CdSe quantum-dot-sensitized solar cells. *Journal of Materials Chemistry*, 21(24), 8742-8748.
- Feng, W., Zhao, L., Du, J., Li, Y., & Zhong, X. (2016). Quasi-solid-state quantum dot sensitized solar cells with power conversion efficiency over 9% and high stability. *Journal of Materials Chemistry A*, 4(38), 14849-14856.
- Fuke, N., Hoch, L. B., Kuposov, A. Y., Manner, V. W., Werder, D. J., Fukui, A., Sykora, M. (2010). CdSe quantum-dot-sensitized solar cell with ~ 100% internal quantum efficiency. *Acs Nano*, 4(11), 6377-6386.
- Fukui, A., Fuke, N., Komiya, R., Koide, N., Yamanaka, R., Katayama, H., & Han, L. (2009). Dye-sensitized photovoltaic module with conversion efficiency of 8.4%. *Applied physics express*, 2(8), 082202.
- Grätzel, M. (2001). Photoelectrochemical cells. *Nature*, 414(6861), 338-344.
- Grätzel, M. (2005). Solar energy conversion by dye-sensitized photovoltaic cells. *Inorganic Chemistry*, 44(20), 6841-6851.
- Grinis, L., Kotlyar, S., Rühle, S., Grinblat, J., & Zaban, A. (2010). Conformal nano-sized inorganic coatings on mesoporous TiO<sub>2</sub> films for low-temperature dye-sensitized solar cell fabrication. *Advanced functional materials*, 20(2), 282-288.
- Halls, J., Walsh, C., Greenham, N., Marseglia, E., Friend, R., Moratti, S., & Holmes, A. (1995). *Efficient photodiodes from interpenetrating polymer networks*.
- Hao, F., & Lin, H. (2013). Recent molecular engineering of room temperature ionic liquid electrolytes for mesoscopic dye-sensitized solar cells. *RSC Advances*, 3(45), 23521-23532.
- Hasegawa, A., & Yamamoto, A. (1994). Deep, low-frequency microearthquakes in or around seismic low-velocity zones beneath active volcanoes in northeastern Japan. *Tectonophysics*, 233(3-4), 233-252.
- Heeger, A. J., & Braun, D. (2003). Visible light emitting diodes fabricated from soluble semiconducting polymers: *Google Patents*.
- Hafiza, M. N., & Isa, M. I. N. (2018). Conduction mechanism via correlated barrier hopping in EC-plasticized 2-hydroxyethyl cellulose-ammonium nitrate solid polymer electrolyte. In IOP Conference Series: *Materials Science and Engineering* (Vol. 440, No. 1, p. 012039). IOP Publishing.
- Hishikawa, Y. (2005). Characterization of the silicon-based thin film multi-junction solar cells. *MRS Online Proceedings Library Archive*, 862.

- Hod, I., & Zaban, A. (2013). Materials and interfaces in quantum dot sensitized solar cells: challenges, advances and prospects. *Langmuir*, 30(25), 7264-7273.
- Ingle, R. V., Supekar, A. T., Bhalekar, V. P., Prasad, B., & Pathan, H. M. (2020). The Influence of Polysulfide Solvent on the Performance of Cadmium Sulfide Sensitized Zirconium Dioxide-Based Quantum Dots. *ES Materials & Manufacturing*, 9, 12-20.
- Jiang, G., Pan, Z., Ren, Z., Du, J., Yang, C., Wang, W., & Zhong, X. (2016). Poly (vinyl pyrrolidone): a superior and general additive in polysulfide electrolytes for high efficiency quantum dot sensitized solar cells. *Journal of Materials Chemistry A*, 4(29), 11416-11421.
- Jiang, H., Hong, L., Venkatasubramanian, N., Grant, J. T., Eyink, K., Wiacek, K., Bunning, T. J. (2007). The relationship between chemical structure and dielectric properties of plasma-enhanced chemical vapor deposited polymer thin films. *Thin solid films*, 515(7-8), 3513-3520.
- Jiao, S., Du, J., Du, Z., Long, D., Jiang, W., Pan, Z., Zhong, X. (2017). Nitrogen-doped mesoporous carbons as counter electrodes in quantum dot sensitized solar cells with a conversion efficiency exceeding 12%. *The journal of physical chemistry letters*, 8(3), 559-564.
- Jing, Z., Xu, A., Liang, Y. Q., Zhang, Z., Yu, C., Hong, P., & Li, Y. (2019). Biodegradable poly (acrylic acid-co-acrylamide)/poly (vinyl alcohol) double network hydrogels with tunable mechanics and high self-healing performance. *Polymers*, 11(6), 952.
- Johnson, L., Billigmeier, J., & Lieb, J. (2005). Power system for a telecommunication facility. *Google Patents*.
- Jovanovski, V., González-Pedro, V., Giménez, S., Azaceta, E., Cabañero, G., Grande, H., & Bisquert, J. (2011). A sulfide/polysulfide-based ionic liquid electrolyte for quantum dot-sensitized solar cells. *Journal of the American Chemical Society*, 133(50), 20156-20159.
- Jun, H., Careem, M., & Arof, A. (2013). Quantum dot-sensitized solar cells-perspective and recent developments: a review of Cd chalcogenide quantum dots as sensitizers. *Renewable and sustainable energy reviews*, 22, 148-167.
- Kadir, M., Majid, S., & Arof, A. (2010). Plasticized chitosan–PVA blend polymer electrolyte based proton battery. *Electrochimica Acta*, 55(4), 1475-1482.
- Kamat, P. V. (2008). Quantum dot solar cells. Semiconductor nanocrystals as light harvesters. *The Journal of Physical Chemistry C*, 112(48), 18737-18753.
- Kharzi, S., Haddadi, M., & Malek, A. (2006). Development of a voltage regulator for solar photovoltaic cathodic protection system. *Revue des énergies renouvelables*, 9(4), 259-266.

- Koops, C. G. (1951). On the dispersion of resistivity and dielectric constant of some semiconductors at audiofrequencies. *Physical Review*, 83(1), 121.
- Korri Youssoufi, H., Yassar, A., Baiteche, S., Hmyene, M., & Garnier, F. (1994). Designing polypyrrole-based sensors: selective electrochemical cation in aza crown ethers. *Synthetic Metals*, 67(1), 251-254.
- Kouhnavard, M., Ikeda, S., Ludin, N. A., Khairudin, N. A., Ghaffari, B., Mat-Teridi, M., Sopian, K. (2014). A review of semiconductor materials as sensitizers for quantum dot-sensitized solar cells. *Renewable and sustainable energy reviews*, 37, 397-407.
- Kumaran, V. S., Ng, H., Ramesh, S., Ramesh, K., Vengadaesvaran, B., & Numan, A. (2018). The conductivity and dielectric studies of solid polymer electrolytes based on poly (acrylamide-co-acrylic acid) doped with sodium iodide. *Ionic*, 24(7), 1947-1953.
- Kumar, M. S., & Bhat, D. K. (2009). Polyvinyl alcohol-polystyrene sulphonic acid blend electrolyte for supercapacitor application. *Physica B: Condensed Matter*, 404(8-11), 1143-1147.
- Kumar, M., Tiwari, T., & Srivastava, N. (2012). Electrical transport behaviour of bio-polymer electrolyte system: Potato starch + ammonium iodide. *Carbohydrate polymers*, 88(1), 54-60.
- Kumar, D. K., Loskot, J., Kříž, J., Bennett, N., Upadhyaya, H. M., Sadhu, V., & Reddy, K. R. (2020). Synthesis of SnSe quantum dots by successive ionic layer adsorption and reaction (SILAR) method for efficient solar cells applications. *Solar Energy*, 199, 570-574.
- Kusuma, J., & Balakrishna, R. G. (2020). Ceramic grains: Highly promising hole transport material for solid state QDSSC. *Solar Energy Materials and Solar Cells*, 209, 110445.
- Laban, W. A., & Etgar, L. (2013). Depleted hole conductor-free lead halide iodide heterojunction solar cells. *Energy & Environmental Science*, 6(11), 3249-3253.
- Lafsah, M. D. (2012). THD and efficiency study for PV grid-connected. *Universiti Malaysia Pahang*.
- Lang, K. R. (2007). *Sun, Earth and Sky: Springer Science & Business Media*.
- Lee, H., Wang, M., Chen, P., Gamelin, D. R., Zakeeruddin, S. M., Gratzel, M., & Nazeeruddin, M. K. (2009). Efficient CdSe quantum dot-sensitized solar cells prepared by an improved successive ionic layer adsorption and reaction process. *Nano letters*, 9(12), 4221-4227.

- Lee, K. H., Park, J. K., & Kim, W. J. (1999). Preparation and ion conductivities of the plasticized polymer electrolytes based on the poly (acrylonitrile-co-lithium methacrylate). *Journal of Polymer Science Part B: Polymer Physics*, 37(3), 247-252.
- Lee, Y.-L., & Chang, C.-H. (2008). Efficient polysulfide electrolyte for CdS quantum dot-sensitized solar cells. *Journal of Power Sources*, 185(1), 584-588.
- Lee, Y.-L., Huang, B.-M., & Chien, H.-T. (2008). Highly efficient CdSe-sensitized TiO<sub>2</sub> photoelectrode for quantum-dot-sensitized solar cell applications. *Chemistry of Materials*, 20(22), 6903-6905.
- Lee, Y. L., & Lo, Y. S. (2009). Highly efficient quantum-dot-sensitized solar cell based on co-sensitization of CdS/CdSe. *Advanced functional materials*, 19(4), 604-609.
- Lestriez, B., Bahri, S., Sandu, I., Roué, L., & Guyomard, D. (2007). On the binding mechanism of CMC in Si negative electrodes for Li-ion batteries. *Electrochemistry Communications*, 9(12), 2801-2806.
- Li, B., Wang, L., Kang, B., Wang, P., & Qiu, Y. (2006). Review of recent progress in solid-state dye-sensitized solar cells. *Solar Energy Materials and Solar Cells*, 90(5), 549-573.
- Li, L., Yang, X., Gao, J., Tian, H., Zhao, J., Hagfeldt, A., & Sun, L. (2011). Highly efficient CdS quantum dot-sensitized solar cells based on a modified polysulfide electrolyte. *Journal of the American Chemical Society*, 133(22), 8458-8460.
- Li, X.-C. C., & Ueno, K. (2004). Deuterated semi-conducting organic compounds used for opto-electronic devices: *Google Patents*.
- Li, Z., Su, G., Wang, X., & Gao, D. (2005). Micro-porous P (VDF-HFP)-based polymer electrolyte filled with Al<sub>2</sub>O<sub>3</sub> nanoparticles. *Solid State Ionics*, 176(23-24), 1903-1908.
- Liao, Y., Zhang, J., Liu, W., Que, W., Yin, X., Zhang, D., Zhang, H. (2015). Enhancing the efficiency of CdS quantum dot-sensitized solar cells via electrolyte engineering. *Nano Energy*, 11, 88-95.
- Lin, O. H., Kumar, R. N., Rozman, H. D., & Noor, M. A. M. (2005). Grafting of sodium carboxymethylcellulose (CMC) with glycidyl methacrylate and development of UV curable coatings from CMC-g-GMA induced by cationic photoinitiators. *Carbohydrate polymers*, 59(1), 57-69.
- Loiudice, A., Rizzo, A., Corricelli, M., Curri, M. L., Belviso, M. R., Cozzoli, P. D., Gigli, G. (2014). Room-temperature treatments for all-inorganic nanocrystal solar cell devices. *Thin Solid Films*, 560, 44-48.

- Lopez, C. G., Rogers, S. E., Colby, R. H., Graham, P., & Cabral, J. T. (2015). Structure of sodium carboxymethyl cellulose aqueous solutions: A SANS and rheology study. *Journal of Polymer Science Part B: Polymer Physics*, 53(7), 492-501.
- Luna-Martinez, J., Hernández-Uresti, D., Reyes-Melo, M., Guerrero-Salazar, C., González-González, V., & Sepúlveda-Guzmán, S. (2011). Synthesis and optical characterization of ZnS–sodium carboxymethyl cellulose nanocomposite films. *Carbohydrate Polymers*, 84(1), 566-570.
- Lu, L., Pan, Z., Hao, N., & Peng, W. (2014). A novel acrylamide-free flocculant and its application for sludge dewatering. *Water Research*, 57, 304-312.
- Luo, L., Luan, W., Yuan, B., Zhang, C., & Jin, L. (2015). High efficient and stable solid solar cell: based on FeS<sub>2</sub> nanocrystals and P3HT: PCBM. *Energy Procedia*, 75, 2181-2186.
- Luque, A., & Hegedus, S. (2011). *Handbook of photovoltaic science and engineering*: John Wiley & Sons.
- Ma, F., Deng, Y., Ni, X., Hou, J., Liu, G., & Peng, S. (2021). Flexible CdS/CdSe quantum dots sensitized solar cells with high performance and durability. *Nano Select*.
- MacDiarmid, A. G. (2001). Synthetic metals: a novel role for organic polymers. *Synthetic Metals*, 125(1), 11-22.
- Magalhães, A. S. G., Almeida Neto, M. P., Bezerra, M. N., Ricardo, N. M., & Feitosa, J. (2012). Application of FTIR in the determination of acrylate content in poly (sodium acrylate-co-acrylamide) superabsorbent hydrogels. *Química Nova*, 35(7), 1464-1467.
- Martínez-Ferrero, E., Seró, I. M., Alberó, J., Giménez, S., Bisquert, J., & Palomares, E. (2010). Charge transfer kinetics in CdSe quantum dot sensitized solar cells. *Physical Chemistry Chemical Physics*, 12(12), 2819-2821.
- Meng, K., Suroliya, P. K., Byrne, O., & Thampi, K. R. (2015). Quantum dot and quantum dot-dye co-sensitized solar cells containing organic thiolate–disulfide redox electrolyte. *Journal of Power Sources*, 275, 681-687.
- Meshginqalam, B., Jameil, A. K., Ahmadi, M. T., & Centeno, A. (2015). Investigation on optical and electrical properties of bilayer graphene. *Diyala Journal of Engineering Sciences*, 8(4), 538-545.
- Mingsukang, M., Buraidah, M., Careem, M., Albinsson, I., Mellander, B., & Arof, A. (2017). Investigation of counter electrode materials for gel polymer electrolyte based quantum dot sensitized solar cells. *Electrochimica Acta*, 241, 487-496.
- Moniha, V., Alagar, M., Selvasekarapandian, S., Sundaresan, B., & Boopathi, G. (2018). Conductive bio-polymer electrolyte iota-carrageenan with ammonium



nitrate for application in electrochemical devices. *Journal of Non-Crystalline Solids*, 481, 424-434.

- Nagashima, S., Ando, S., Makino, K., Tsukamoto, T., & Ohshima, H. (1998). Size dependence of polymer composition in the surface layer of poly (acrylamide-co-acrylic acid) hydrogel microspheres. *Journal of colloid and interface science*, 197(2), 377-382.
- Nesrinne, S., & Djamel, A. (2017). Synthesis, characterization and rheological behavior of pH sensitive poly (acrylamide-co-acrylic acid) hydrogels. *Arabian Journal of Chemistry*, 10(4), 539-547.
- Nguyen, D., & Lehman, B. (2008). An adaptive solar photovoltaic array using model-based reconfiguration algorithm. *Industrial Electronics, IEEE Transactions on*, 55(7), 2644-2654.
- Ning, Z., Yuan, C., Tian, H., Fu, Y., Li, L., Sun, L., & Ågren, H. (2012). Type-II colloidal quantum dot sensitized solar cells with a thiourea based organic redox couple. *Journal of Materials Chemistry*, 22(13), 6032-6037.
- Nithya, V., & Selvan, R. K. (2011). Synthesis, electrical and dielectric properties of FeVO<sub>4</sub> nanoparticles. *Physica B: Condensed Matter*, 406(1), 24-29.
- Nozik, A. J. (2002). Quantum dot solar cells. *Physica E: Low-dimensional Systems and Nanostructures*, 14(1-2), 115-120.
- Nozik, A. (2005). Exciton multiplication and relaxation dynamics in quantum dots: applications to ultrahigh-efficiency solar photon conversion. *Inorganic chemistry*, 44(20), 6893-6899.
- O'Regan, B., & Gratzel, M. (1991). A low-cost, high-efficiency solar cell based on dye-sensitized colloidal TiO<sub>2</sub> films. *Nature*, 353(6346), 737-740.
- Okutan, M., & Şentürk, E. (2008).  $\beta$  Dielectric relaxation mode in side-chain liquid crystalline polymer film. *Journal of Non-Crystalline Solids*, 354(14), 1526-1530.
- Pan, Z., Mora-Seró, I. n., Shen, Q., Zhang, H., Li, Y., Zhao, K., Bisquert, J. (2014). High-efficiency "green" quantum dot solar cells. *Journal of the American Chemical Society*, 136(25), 9203-9210.
- Pan, Z., Rao, H., Mora-Seró, I., Bisquert, J., & Zhong, X. (2018). Quantum dot-sensitized solar cells. *Chemical Society Reviews*, 47(20), 7659-7702.
- Pan, Z., & Zhong, X. (2016). A ZnS and metal hydroxide composite passivation layer for recombination control in high efficiency quantum dot sensitized solar cells. *Journal of Materials Chemistry A*, 4(48), 18976-18982.

- Park, J. P., Heo, J. H., Im, S. H., & Kim, S.-W. (2016). Highly efficient solid-state mesoscopic PbS with embedded CuS quantum dot-sensitized solar cells. *Journal of Materials Chemistry A*, 4(3), 785-790.
- Park, K., Chen, J., & Park, H. (2001). Hydrogel composites and superporous hydrogel composites having fast swelling, high mechanical strength, and superabsorbent properties. U.S. Patent No. 6,271,278. Washington, DC: U.S. *Patent and Trademark Office*.
- Park, M., Zhang, X., Chung, M., Less, G. B., & Sastry, A. M. (2010). A review of conduction phenomena in Li-ion batteries. *Journal of Power Sources*, 195(24), 7904-7929.
- Patel, S. B., & Gohel, J. V. (2019). Quasi solid-state quantum dot-sensitized solar cells with polysulfide gel polymer electrolyte for superior stability. *Journal of Solid State Electrochemistry*, 23(9), 2657-2666.
- Pathan, H. M., & Lokhande, C. D. (2004). Deposition of metal chalcogenide thin films by successive ionic layer adsorption and reaction (SILAR) method. *Bulletin of Materials Science*, 27(2), 85-111
- Plass, R., Pelet, S., Krueger, J., Grätzel, M., & Bach, U. (2002). Quantum dot sensitization of organic-inorganic hybrid solar cells. *The Journal of Physical Chemistry B*, 106(31), 7578-7580.
- Pourjavadi, A., Mahdavinia, G., & Zohuriaan-Mehr, M. (2003). Modified chitosan. II. H-chitoPAN, a novel pH-responsive superabsorbent hydrogel. *Journal of Applied Polymer Science*, 90(11), 3115-3121.
- Raphael, E., Jara, D. H., & Schiavon, M. A. (2017). Optimizing photovoltaic performance in CuInS<sub>2</sub> and CdS quantum dot-sensitized solar cells by using an agar-based gel polymer electrolyte. *RSC advances*, 7(11), 6492-6500.
- Rahaman, M. D., Mia, M. D., Khan, M. N. I., & Hossain, A. A. (2016). Study the effect of sintering temperature on structural, microstructural and electromagnetic properties of 10% Ca-doped Mn<sub>0.6</sub>Zn<sub>0.4</sub>Fe<sub>2</sub>O<sub>4</sub>. *Journal of Magnetism and Magnetic Materials*, 404, 238-249.
- Rahman, M. Y. A., Ahmad, A., Lee, T. K., Farina, Y., & Dahlan, H. M. (2011). Effect of ethylene carbonate (EC) plasticizer on poly (vinyl chloride)-liquid 50% epoxidized natural rubber (LENR50) based polymer electrolyte. *Materials Sciences and Applications*, 2(07), 817.
- Ramesh, S., & Arof, A. (2001). Ionic conductivity studies of plasticized poly (vinyl chloride) polymer electrolytes. *Materials Science and Engineering: B*, 85(1), 11-15.

- Ramesh, S., & Ling, O. P. (2010). Effect of ethylene carbonate on the ionic conduction in poly (vinylidene fluoride-hexafluoropropylene) based solid polymer electrolytes. *Polymer Chemistry*, 1(5), 702-707.
- Razykov, T., Ferekides, C., Morel, D., Stefanakos, E., Ullal, H., & Upadhyaya, H. (2011). Solar photovoltaic electricity: Current status and future prospects. *Solar Energy*, 85(8), 1580-1608.
- Ren, F., Li, S., & He, C. (2015). Electrolyte for quantum dot-sensitized solar cells assessed with cyclic voltammetry. *Science China Materials*, 58(6), 490-495.
- Ren, Z., Wang, J., Pan, Z., Zhao, K., Zhang, H., Li, Y., Zhong, X. (2015). Amorphous TiO<sub>2</sub> buffer layer boosts efficiency of quantum dot sensitized solar cells to over 9%. *Chemistry of Materials*, 27(24), 8398-8405.
- Robel, I., Subramanian, V., Kuno, M., & Kamat, P. V. (2006). Quantum dot solar cells. Harvesting light energy with CdSe nanocrystals molecularly linked to mesoscopic TiO<sub>2</sub> films. *Journal of the American Chemical Society*, 128(7), 2385-2393.
- Roy, A., Ghosh, A., Datta, S., Das, S., Mohanraj, P., Deb, J., & Rao, M. B. (2009). Effects of plasticizers and surfactants on the film forming properties of hydroxypropyl methylcellulose for the coating of diclofenac sodium tablets. *Saudi pharmaceutical journal*, 17(3), 233-241.
- Rühle, S., Shalom, M., & Zaban, A. (2010). Quantum-dot-sensitized solar cells. *ChemPhysChem*, 11(11), 2290-2304.
- Samsudin, A. S., Lai, H. M., & Isa, M. I. N. (2014). Biopolymer materials based carboxymethyl cellulose as a proton conducting biopolymer electrolyte for application in rechargeable proton battery. *Electrochimica Acta*, 129, 1-13.
- Santra, P. K., & Kamat, P. V. (2012). Mn-doped quantum dot sensitized solar cells: a strategy to boost efficiency over 5%. *Journal of the American Chemical Society*, 134(5), 2508-2511.
- Semonin, O. E., Luther, J. M., & Beard, M. C. (2012). Quantum dots for next-generation photovoltaics. *Materials today*, 15(11), 508-515.
- Semonin, O. E., Luther, J. M., Choi, S., Chen, H.-Y., Gao, J., Nozik, A. J., & Beard, M. C. (2011). Peak external photocurrent quantum efficiency exceeding 100% via MEG in a quantum dot solar cell. *Science*, 334(6062), 1530-1533.
- Seol, M., Kim, H., Tak, Y., & Yong, K. (2010). Novel nanowire array based highly efficient quantum dot sensitized solar cell. *Chemical Communications*, 46(30), 5521-5523.
- Selvakumar, K., Kalaiselvarany, J., Rajendran, S., & Prabhu, M. R. (2016). Novel proton-conducting polymer electrolytes based on poly (vinylidene fluoride-co-

hexafluoropropylene)-ammonium thiocyanate. *Polymer-Plastics Technology and Engineering*, 55(18), 1940-1948.

- Serpone, N., Borgarello, E., & Grätzel, M. (1984). Visible light induced generation of hydrogen from H<sub>2</sub>S in mixed semiconductor dispersions; improved efficiency through inter-particle electron transfer. *Journal of the Chemical Society, Chemical Communications*(6), 342-344.
- Shalom, M., Dor, S., Ruhle, S., Grinis, L., & Zaban, A. (2009). Core/CdS quantum dot/shell mesoporous solar cells with improved stability and efficiency using an amorphous TiO<sub>2</sub> coating. *The Journal of Physical Chemistry C*, 113(9), 3895-3898.
- Sharma, D., Jha, R., & Kumar, S. (2016). Quantum dot sensitized solar cell: recent advances and future perspectives in photoanode. *Solar Energy Materials and Solar Cells*, 155, 294-322.
- Sheldon, M. H., Glasse, M. D., Latham, R. J., & Linford, R. G. (1989). The effect of plasticiser on zinc polymer electrolytes. *Solid State Ionics*, 34(1-2), 135-138.
- Shen, M., Zhang, K., Koettig, P., Welch, W. C., & Dawson, J. M. (2011). In vivo biostability of polymeric spine implants: retrieval analyses from a United States investigational device exemption study. *European Spine Journal*, 20(11), 1837.
- Shen, Q., Yamada, A., Tamura, S., & Toyoda, T. (2010). CdSe quantum dot-sensitized solar cell employing TiO<sub>2</sub> nanotube working-electrode and Cu<sub>2</sub>S counter-electrode. *Applied Physics Letters*, 97(12), 123107.
- Shaheen, S. E., Brabec, C. J., Sariciftci, N. S., Padinger, F., Fromherz, T., & Hummelen, J. C. (2001). 2.5% efficient organic plastic solar cells. *Applied Physics Letters*, 78(6), 841-843.
- Sikkanthar, S., Karthikeyan, S., Selvasekarapandian, S., Arunkumar, D., Nithya, H., & Junichi, K. (2016). Structural, electrical conductivity, and transport analysis of PAN-NH 4 Cl polymer electrolyte system. *Ionics*, 22(7), 1085-1094.
- Şolpan, D., Duran, S., Saraydin, D., & Güven, O. (2003). Adsorption of methyl violet in aqueous solutions by poly (acrylamide-co-acrylic acid) hydrogels. *Radiation Physics and Chemistry*, 66(2), 117-127.
- Sonmez, G., Meng, H., Zhang, Q., & Wudl, F. (2003). A Highly Stable, New Electrochromic Polymer: Poly (1, 4-bis (2-(3', 4'-ethylenedioxy) thienyl)-2-methoxy-5-2 "-ethylhexyloxybenzene). *Advanced Functional Materials*, 13(9), 726-731.
- Srivastava, N., Chandra, A., & Chandra, S. (1995). Dense branched growth of (SCN) x and ion transport in the poly (ethyleneoxide) NH<sub>4</sub>SCN polymer electrolyte. *Physical Review B*, 52(1), 225.

- Sunardi, S. (2017). Preparation of carboxymethyl cellulose produced from purun tikus (*Eleocharis dulcis*). In AIP Conference Proceedings 1868, 020008 (2017) (Vol. 1868).
- Suo, A., Qian, J., Yao, Y., & Zhang, W. (2007). Synthesis and properties of carboxymethyl cellulose-graft-poly (acrylic acid-co-acrylamide) as a novel cellulose-based superabsorbent. *Journal of Applied Polymer Science*, 103(3), 1382-1388.
- Surana, K., & Mehra, R. (2018). Quantum Dot Sensitized Solar Cells (QDSSCs), *Nanomaterials and Their Applications* (pp. 315-321), Springer.
- Tamilselvi, P., & Hema, M. (2014). Conductivity studies of LiCF<sub>3</sub>SO<sub>3</sub> doped PVA: PVdF blend polymer electrolyte. *Physica B: Condensed Matter*, 437, 53-57.
- Tang, C.-Y., Huang, S.-M., & Lee, W. (2011). Electrical properties of nematic liquid crystals doped with anatase TiO<sub>2</sub> nanoparticles. *Journal of Physics D: Applied Physics*, 44(35), 355102.
- Tao, M. (2008). Inorganic photovoltaic solar cells: silicon and beyond. *The Electrochemical Society Interface*, 17(4), 30-35.
- Theerthagiri, J., Senthil, R., Buraidah, M., Madhavan, J., & Arof, A. (2015). Effect of tetrabutylammonium iodide content on PVDF-PMMA polymer blend electrolytes for dye-sensitized solar cells. *Ionics*, 21(10), 2889-2896.
- Trausel, F., De Jong, A.J., & Cuypers, R. (2014). A review on the properties of salt hydrates for thermochemical storage. *Energy Procedia*, 48, 447-452.
- Varaprasad, K., Jayaramudu, T., & Sādiku, E. R. (2017). Removal of dye by carboxymethyl cellulose, acrylamide and graphene oxide via a free radical polymerization process. *Carbohydrate Polymers*, 164, 186-194.
- Vázquez, C. I., Baruzzi, A. M., & Iglesias, R. A. (2016). Charge extraction from TiO<sub>2</sub> nanotubes sensitized with CdS quantum dots by SILAR method. *IEEE Journal of Photovoltaics*, 6(6), 1515-1521.
- Vlachy, N., Jagoda-Cwiklik, B., Vácha, R., Touraud, D., Jungwirth, P., & Kunz, W. (2009). Hofmeister series and specific interactions of charged headgroups with aqueous ions. *Advances in colloid and interface science*, 146(1-2), 42-47.
- Vogel, R., Hoyer, P., & Weller, H. (2002). Quantum-sized PbS, CdS, Ag<sub>2</sub>S, Sb<sub>2</sub>S<sub>3</sub>, and Bi<sub>2</sub>S<sub>3</sub> particles as sensitizers for various nanoporous wide-bandgap semiconductors. *The Journal of Physical Chemistry*, 98(12), 3183-3188.
- Vogel, R., Pohl, K., & Weller, H. (1990). Sensitization of highly porous, polycrystalline TiO<sub>2</sub> electrodes by quantum sized CdS. *Chemical Physics Letters*, 174(3-4), 241-246.

- Wang, J., Mora-Seró, I., Pan, Z., Zhao, K., Zhang, H., Feng, Y., Bisquert, J. (2013). Core/shell colloidal quantum dot exciplex states for the development of highly efficient quantum-dot-sensitized solar cells. *Journal of the American Chemical Society*, 135(42), 15913-15922.
- Wang, W., Feng, W., Du, J., Xue, W., Zhang, L., Zhao, L., Zhong, X. (2018). Cosensitized quantum dot solar cells with conversion efficiency over 12%. *Advanced Materials*, 30(11), 1705746.
- Wang, W., Jiang, G., Yu, J., Wang, W., Pan, Z., Nakazawa, N., & Zhong, X. (2017). High efficiency quantum dot sensitized solar cells based on direct adsorption of quantum dots on photoanodes. *ACS applied materials & interfaces*, 9(27), 22549-22559.
- Wei, H., Wang, G., Shi, J., Wu, H., Luo, Y., Li, D., & Meng, Q. (2016). Fumed SiO<sub>2</sub> modified electrolytes for quantum dot sensitized solar cells with efficiency exceeding 11% and better stability. *Journal of Materials Chemistry A*, 4(37), 14194-14203.
- Wieczorek, W., Such, K., Florjanczyk, Z., & Stevens, J. R. (1995). Polyacrylamide based composite polymeric electrolytes. *Electrochimica acta*, 40(13-14), 2417-2420.
- Williams, K. J., Nelson, C. A., Yan, X., Li, L.-S., & Zhu, X. (2013). Hot electron injection from graphene quantum dots to TiO<sub>2</sub>. *Acs Nano*, 7(2), 1388-1394.
- Wu, D., Wang, Y., Ma, N., Cao, K., Zhang, W., Chen, J., Jiang, K. (2019). Single-crystal-like ZnO mesoporous spheres derived from metal organic framework delivering high electron mobility for enhanced energy conversion and storage performances. *Electrochimica Acta*, 305, 474-483.
- Wu, M., Lin, X., Wang, Y., & Ma, T. (2015). Counter electrode materials combined with redox couples in dye-and quantum dot-sensitized solar cells. *Journal of Materials Chemistry A*, 3(39), 19638-19656.
- Xu, J., Yang, X., Wang, H., Chen, X., Luan, C., Xu, Z., Lee, C.-S. (2011). Arrays of ZnO/Zn<sub>x</sub>Cd<sub>1-x</sub>Se Nanocables: Band Gap Engineering and Photovoltaic Applications. *Nano letters*, 11(10), 4138-4143.
- Yamamoto, T., Inami, M., & Kanbara, T. (1994). Preparation and properties of polymer solid electrolytes using poly (vinyl alcohol) and thermally resistive poly [arylene (1, 3-imidazolidine-2, 4, 5-trione-1, 3-diyl)] as matrix polymers. *Chemistry of materials*, 6(1), 44-50.
- Yang, H., Huq, R., & Farrington, G. (1990). Conductivity in PEO-based Zn (II) polymer electrolytes. *Solid State Ionics*, 40, 663-665.
- Yang, Y., & Wang, W. (2015). A new polymer electrolyte for solid-state quantum dot sensitized solar cells. *Journal of Power Sources*, 285, 70-75.

- Ye, M., Liu, X., Iocozzia, J., Liu, X., & Lin, Z. (2016). Nanostructured materials for high efficiency perovskite solar cells. *Nanomaterials for Sustainable Energy* (pp. 1-39): Springer.
- Yella, A., Lee, H.-W., Tsao, H. N., Yi, C., Chandiran, A. K., Nazeeruddin, M. K., Grätzel, M. (2011). Porphyrin-sensitized solar cells with cobalt (II/III)-based redox electrolyte exceed 12 percent efficiency. *Science*, *334*(6056), 629-634.
- Yu, P., Zhu, K., Norman, A. G., Ferrere, S., Frank, A. J., & Nozik, A. J. (2006). Nanocrystalline TiO<sub>2</sub> solar cells sensitized with InAs quantum dots. *The Journal of Physical Chemistry B*, *110*(50), 25451-25454.
- Yu, X., Yi, B., Liu, F., & Wang, X. (2008). Prediction of the dielectric dissipation factor  $\tan \delta$  of polymers with an ANN model based on the DFT calculation. *Reactive and Functional Polymers*, *68*(11), 1557-1562.
- Yu, X. Y., Liao, J. Y., Qiu, K. Q., Kuang, D. B., & Su, C. Y. (2011). Dynamic study of highly efficient CdS/CdSe quantum dot-sensitized solar cells fabricated by electrodeposition. *Acs Nano*, *5*(12), 9494-9500.
- Zaban, A., Mičić, O., Gregg, B., & Nozik, A. (1998). Photosensitization of nanoporous TiO<sub>2</sub> electrodes with InP quantum dots. *Langmuir*, *14*(12), 3153-3156.
- Zhang, H., Cheng, K., Hou, Y., Fang, Z., Pan, Z., Wu, W., Zhong, X. (2012). Efficient CdSe quantum dot-sensitized solar cells prepared by a postsynthesis assembly approach. *Chemical Communications*, *48*(91), 11235-11237.
- Zhang, K., Cui, Z., Xing, G., Feng, Y., & Meng, S. (2016). Improved performance of dye-sensitized solar cells based on modified kaolin/PVDF-HFP composite gel electrolytes. *RSC Advances*, *6*(102), 100079-100089.
- Zhang, Q., Guo, X., Huang, X., Huang, S., Li, D., Luo, Y., Meng, Q. (2011). Highly efficient CdS/CdSe-sensitized solar cells controlled by the structural properties of compact porous TiO<sub>2</sub> photoelectrodes. *Physical Chemistry Chemical Physics*, *13*(10), 4659-4667.
- Zhang, W., Dahbi, M., & Komaba, S. (2016). Polymer binder: a key component in negative electrodes for high-energy Na-ion batteries. *Current Opinion in Chemical Engineering*, *13*, 36-44.
- Zhao, K., Pan, Z., Mora-Seró, I., Cánovas, E., Wang, H., Song, Y., & Zhong, X. (2015). Boosting power conversion efficiencies of quantum-dot-sensitized solar cells beyond 8% by recombination control. *Journal of the American Chemical Society*, *137*(16), 5602-5609.

## LIST OF PUBLICATIONS

### Journal Publications:

- i. **Iraj Alaei, Yap Chen Lee, Mohd Hamdi Bin Ali Buraidah, Iis Sopyan, Yose Fachmi Buys (2020), “Optical and Electrical Properties of Polymer Blend Electrolyte Containing Sodium Carboxyl Methylcellulose, Poly (acrylamide-co-acrylic acid), and Sodium Sulfide”, *International Journal of Advanced Science and Technology* Vol. 29, No. 7, pp. 12241 – 12247.**
  
- ii. **Alaei, I., Al-Bat’hi, S. A., & Sopyan, I., (2015), “Fabrication and Characterization of Poly (Ethylene Oxide) for Photo-Electronic Device”, *Asian Research Publishing Network (ARPN)* Vol.10, No 22. P (17239-17241).**